Involvement of Polyamines in Ribosome Biogenesis and Identification of Potential Genes Associated with Spermine Resistance in *Arabidopsis thaliana*

Ester Murillo Villuendas

UNIVERSITAT DE BARCELONA

FACULTAT DE FARMÀCIA I CIÈNCIES DE L'ALIMENTACIÓ

Involvement of Polyamines in Ribosome Biogenesis and Identification of Potential Genes Associated with Spermine Resistance in *Arabidopsis thaliana*.

Ester Murillo Villuendas

2023

UNIVERSITAT DE BARCELONA

FACULTAT DE FARMÀCIA I CIÈNCIES DE L'ALIMENTACIÓ

DOCTORAT EN BIOTECNOLOGIA

Involvement of Polyamines in Ribosome Biogenesis and Identification of Potential Genes Associated with Spermine Resistance in *Arabidopsis thaliana*

Memòria presentada per Ester Murillo Villuendas per optar al títol de doctor per la universitat de Barcelona

Rubén Alcázar Hernández

Director i Tutor

Ester Murillo Villuendas

doctoranda

2023

A mis padres, Fer y Lor.

AGRADECIMIENTOS

Al Ministerio de Ciencia e Innovación, por el proyecto BFU2017-87742-R en el marco del cual he podido realizar mis estudios de doctorado con la beca para la Formación de Personal Investigador PRE2018-083289.

A mi director y tutor de tesis, el Dr. Rubén Alcázar Hernández, por brindarme su confianza y por haber hecho posible el alcanzar uno de mis sueños. Por sus comentarios, que me impulsaron a pensar de manera diferente y llevaron mi investigación a otro nivel, lo cual me será beneficioso en mi vida profesional.

Al personal del Servicio de los Campos Experimentales de la Universidad de Barcelona, Francesc, Josep, Susana y Xavier, por su cercanía y profesionalidad.

A la secretaria de la Sección de Fisiología Vegetal de la Facultad de Farmacia y Ciencias de la Alimentación, Mari Carmen Molina, por su ayuda y disponibilidad.

A mis compañeros de la Sección de Fisiología Vegetal, Diego, Luciana, Ana Belén y Ainoa por su ayuda y consejos y, en especial, a Edgar y Miguel, con los que empecé y termino esta aventura. Por todos los momentos vividos dentro y fuera de laboratorio.

A todos los compañeros con los que he coincidido en el grupo de poliaminas: Kostadin, Changxin, Nazanin, Ana Fleitas, Chi, Lucía, Cristina, Jiaqui, Anna Valls. Por facilitar un buen ambiente de trabajo, por enseñarme y por estar siempre dispuestos a ayudar. En especial a Chi, Cristina, y Lucía porque no sólo han sido un valioso apoyo en el ámbito académico, sino que también han estado ahí para mí en lo personal.

Al Dr. Joachim Kopka y a su grupo del Instituto Max Planck de Fisiología Molecular de Plantas, por acogerme como a un miembro más. A Dione y Alex, por ayudarme y enseñarme, y, en especial, a Federico, por todo lo aprendido, por aconsejarme, por guiarme y sobre todo por transmitirme su pasión por los ribosomas. Gracias por hacer que fuera una experiencia tan enriquecedora.

A mis padres, porque siempre antepusieron mi educación e invirtieron en ella, dejando otras cosas en el camino. Por apoyarme, aconsejarme, consolarme y escucharme siempre. Porque sin vosotros no habría llegado hasta aquí.

A Cristian, mi compañero de vida, por dejar su vida en Zaragoza y venirse a Barcelona. Por estar siempre ahí y hacerme la vida más fácil, especialmente estos últimos meses.

A mi familia, por su preocupación y su cariño durante todo este tiempo.

A mis amigas de Épila, por todos esos momentos de desconexión en los que he vuelto con las pilas cargadas, por su interés en mi tesis y, sobre todo, por su apoyo.

A mis dos grupos de amigas de la carrera, mis "Biotecs", Henar, Gema, Carmen y Bea, y mis "Amebas", Ana, Ester Antón, Inés, Luis, Marta y Vicky. Porque con vosotras siempre me he sentido comprendida y arropada. Porque a pesar de la distancia y de no vernos todo lo que nos gustaría, siempre estáis en lo importante.

A las amigas que me ha traído Barcelona, Mireia y María, por los planes, las charlas terapéuticas y el apoyo que siempre me han brindado.

A mis compañeras de piso, Rosa y Silvia, por acogerme cuando llegué a Barcelona y enseñarme los lugares que sólo la gente que vive aquí conoce.

ABSTRACT

Polyamines are small polycationic molecules that contain amino groups and are found in all living organisms. This study is aimed at acquiring a comprehensive understanding of the diverse roles of polyamines in plants, specifically in *A. thaliana*, in order to gain a better understanding of their mechanisms of action.

Studies have revealed that polyamines increase general proteins synthesis and are necessary for efficient translation. While some progress has been made regarding the participation of polyamines in ribosome biogenesis in bacteria and, recently, also in mammalians, little is known about their contribution and mode of action in plants. Given our interest on plant defense, the first part of this study was focused on analyzing the ribosome complexes of plants treated with the polyamines putrescine (Put) and spermine (Spm) in combination or not with the purified pathogen associated molecular pattern (PAMP) flagellin22 (flg22). Our results evidenced that treatments with polyamines and flg22 lead to increases in polysome abundance, resulting in a global enhancement of translational activity. Riboproteomic analyses revealed the accumulation of specific ribosomal proteins in response to Put, but not to Spm. Put was also found in polysome fractions where Spm was absent, suggesting a specific effect for Put on ribosome function. Additionally, when analyzing mutants deficient in Put and Spm biosynthesis, we observed a differential accumulation of ribonucleoprotein complex binding proteins. The data suggests a new role for Put in plants and provide valuable information for future investigations on how polyamines may have modulatory and functional effects on the ribosome machinery.

The second part of the study was focused on identifying mutants insensitive to Spm. For this, two strategies were followed: forward genetics through random EMS mutagenesis and reverse genetics through loss-of-function analyses. As part of our screening process, we administered exogenous Spm supplementation to identify mutants that display insensitivity to Spm. This is possible because exogenously supplied Spm inhibits the growth of *A. thaliana* seedlings *in vitro*, enabling us to pinpoint mutants that display resistance to Spm. The mutagenesis screen identified the *Ammonium Transporter 2* (*AMT2*), the *Putative Laccase 9* (*LAC9*), and a hypothetical protein (*At5g28090*) as candidate genes responsible for Spm tolerance in roots. Such tolerance was associated with reduced ROS production under Spm treatment. In addition, *Copper-Amine Oxidase γ2* (*CuAOγ2*) and mutations in ethylene pathway genes, *EIN1*, *EIN2*, *EIN3*, and *EIN3EIL1*, were identified as candidates underlying Spm tolerance in roots through reverse genetics. *CuAOγ2*

mutation might be related to reduced ROS production. The lack of rescue using ethylene inhibitors and lack of reconstitution of the triple response by Spm feeding suggests an effect of Spm on ethylene signaling.

Last, we conducted an RNA-seq experiment that revealed a correlation between exogenous Spm supplementation and responses to Fe deficiency. This correlation was further validated through qRT-PCR analysis, and the fact that Fe supplementation restored growth in photosynthetic tissues under Spm supplementation, along with the induction of coumarin production by exogenous Spm. Additionally, we observed more severe Fe deficiency symptoms in *spms* mutants, indicating that Spm homeostasis can significantly impact the availability of Fe. The observed interaction between Spm and Fe deficiency holds promising implications in the modulation of the nutritional status of plants by polyamines.

Overall, these studies open new frontiers of exploration and underscores the significance of polyamines in shaping various fundamental aspects of plant biology with potential applications in agriculture.

LIST OF ABBREVIATIONS

$^1O_2$	Singlet oxygen
A site	Aminoacyl site
ABA	Abscisic acid
ABC	Ammonium bicarbonate
ACC	1-aminocyclopropane-1-carboxylic acid
ACN	Acetonitrile
ACO	1-aminocyclopropane-1-carboxylic acid oxidase
ACS	1-aminocyclopropane-1-carboxylic acid synthase
ADC	Arginine decarboxylase
adc1-1	*Arginine decarboxylase 1-1* mutant
AdoMetDC	S-adenosylmethionine decarboxylase
AHP1	Histidine phosphotransfer protein 1
AIH	Agmatine deiminase/iminohydrolase
AMT2	Ammonium transporter 2
AVG	(S)-trans-2-Amino-4-(2-aminoethoxy)-3-butenoic acid hydrochloride
AZIN1	Antizyme inhibitor 1
BGLU42	β-Glucosidase 42
bHLH	Basic helix-loop-helix
Brij-35	Polyoxyethylene(23)lauryl ether
BTS	Brutus
BTSL	BTS-LIKE
C_2H_4	Ethylene
CEND	C-terminal domain
CO_2	Carbon dioxide
Col-0	Columbia-0
CTAB	Cetyl trimethyl ammonium bromide
CTR1	Constitutive triple response 1
CuAO	Copper-amine oxidase
DAP	1,3-diaminopropane
dcSAM	Decarboxylated S-adenosylmethionine
ddH_2O	Double-distilled water
DEPC	Diethyl pyrocarbonate
dH_2O	Distilled water
dNTP	Deoxynucleotide triphosphate
DOC	Sodium deoxycholate
DTT	Dithiothreitol

E site	Exit site
E. coli	*Escherichia coli*
EBF1	EIN3-binding F-box protein 1
EBF2	EIN3-binding F-box protein 2
ECIP1	EIN2 C-terminal interacting protein 1
EDTA	Ethylenediaminetetraacetic acid
EGTA	Ethylene glycol-bis (β-aminoethyl ether)-N,N,N´,N´-tetraacetic acid
EIL1	EIN3-like
ein	*Ethylene insensitive* mutant
EIN1	Ethylene insensitive 1
EIN2	Ethylene insensitive 2
EIN3	Ethylene insensitive 3
EMS	Ethyl methanesulfonate
ENAP1	EIN2 nuclear-associated protein 1
ER	Endoplasmic reticulum
ERS1	Ethylene response sensor 1
ERS2	Ethylene response sensor 2
ETP1	Ethylene targeting protein 1
ETP2	Ethylene targeting protein 2
ETR1	Ethylene response 1
ETR2	Ethylene response 2
f6´h1-1	*Feruloyl CoA 6´-hydroxylase 1* mutant
FA	Formic acid
Fe	Iron
FeNaEDTA	Ethylenediaminetetraacetic Acid, Ferric-Sodium Salt
FIT	FER-like iron deficiency-induced transcription factor
flg22	Flagelline 22
FRO2	Ferric reduction oxidase 2
FW	Fresh weight
GAF	cGMP phosphodiesterase/adenylyl cyclase/FhlA
GuHCl	Guanidine hydrochloride
H_2O_2	Hydrogen peroxide
HCl	Hydrochloric acid
$HO^{\cdot}$	Hydroxyl radical
HR	Hypersensitive response
HTD	1,7-diaminoheptane
IAA	Iodoacetamide

Igepal CA 630	Octylphenoxy poly(ethyleneoxy)ethanol
IMA/FEP	Iron man/Fe-uptake-inducing peptide
IRT1	Iron-regulated transporter 1
ITS1	Internal transcribed spacer 1
KCl	Potassium chloride
KOH	Potassium hydroxide
LAC9	Laccase 9
Lys	Lysine
MES	2-(N-morpholino)ethanesulfonic acid
Met	Methionine
Met-tRNA$^{Met}_{i}$	Methionyl-tRNA initiation
$MgCl_2$	Magnesium chloride
mORF	Main genic open reading frame
MS	Murashige and Skoog medium
$Na_2S_2O_3$	Sodium thiosulfate
NaCl	Sodium chloride
NADPH	Nicotinamide adenine dinucleotide phosphate
NCPAH	N-carbamoylputrescine amidase/amidohydrolase
NH_3	Ammonia
NO	Nitric oxide
O_2^-	Superoxide
OAZ	Antizyme
ODC	Ornithine decarboxylase
P site	Peptidyl site
PAMP	Pathogen-associated molecular pattern
PAO	Flavin-containing polyamine oxidases
P-body	processing body
PBS	Phosphate buffered saline
PCA	Perchloric acid
PCD	Programmed cell death
PI	Protease inhibitor cocktail
PIC	Preinitiation complex
PMSF	Phenylmethylsulfonyl fluoride
POL I	RNA polymerase I
POL II	RNA polymerase II
POL III	RNA polymerase III
PTE	Polyoxyethylene 10 tridecyl ether

PTS1	Peroxisomal targeting signal 1
Put	Putrescine
PVP-40	Polyvinylpyrrolidone-40
RAP	Ribosome associated protein
RB	Ribosome factor
RBOH	Respiratory burst oxidase homologue
rDNA	Ribosomal DNA
REB	Ribosome extraction buffer
RNA-seq	RNA sequencing
ROS	Reactive oxygen species
RP	Ribosomal protein
rRNA	Ribosomal RNA
RS	Resuspension buffer
RT	Room temperatura
S. aureus	*Staphylococcus aureus*
S8H	*Scopoletin 8-hydroxilase*
SAM	S-adenosylmethionine
SAMDC	S-adenosylmethionine decarboxylase
SD	Shine-Dalgarno
Ser	Serine
Spd	Spermidine
SPDS	Spermidine synthase
Spm	Spermine
Spmi	*Spermine insensitive* mutant
SPMS	Spermine synthase
spms	*Spermine synthase* mutant
TCA	Trichloroacetic acid
TCEP	Tris(2-carboxyethyl) phosphine hydrochloride
TEAB	Triethylammonium bicarbonate buffer
TF	Transcription factor
TFA	Trifluoroacetic acid
Thr	Threonine
$TiCl_4$	Titanium tetrachloride
Tris-HCl	Tris(hydroxymethyl)aminomethane hydrochloride
t-Spm	Thermospermine
uORF	Upstream open reading frames

CONTENTS

LIST OF FIGURES

LIST OF TABLES

Introduction

The field of agriculture faces significant challenges in today's world. Firstly, the population is growing at a rate that surpasses the available food and feed supply, and this trend is expected to persist in the future. Secondly, environmental pressures have a detrimental impact on plant growth and productivity. These environmental stresses, such as desertification, soil salinization, or increased atmospheric carbon dioxide (CO_2) levels, have brought substantial changes in the climate conditions and are the primary contributors to global crop losses (Singh et al., 2022).To address the existing challenges in agriculture, one possible approach is to consider the polyamine pathway and develop strategies accordingly.

The study of polyamines encompasses a wide range of processes across multiple disciplines, including plant sciences, human health, and microbiology (Alcázar & Tiburcio, 2014). Polyamines play a vital role in numerous physiological processes, such as the regulation of cell division and growth, the stabilization of nucleic acids and cell membranes, and the facilitation of transcription and translation. They also contribute to organogenesis, embryogenesis, leaf senescence, and the development of flowers and fruits. Furthermore, polyamines respond to both abiotic and biotic stressors (Alcázar et al., 2006). While significant advancements have been done in this field, there are still unexplored areas, particularly in plant science, making it an intriguing and captivating subject.

This study is aimed at acquiring a comprehensive understanding of the diverse roles of polyamines in plants, specifically in *Arabidopsis thaliana* (*A. thaliana*), in order to gain a better understanding of their mechanisms of action.

1. *Arabidopsis thaliana* as a model plant

The *A. thaliana* plant is a universal reference organism in plant sciences. It is a small, rosette plant that can be either annual or winter annual (**Figure 1**). It is a member of the Brassicaceae family in the eudicotyledonous group of angiosperm vascular plants, native from Europe, Asia, and northwest of Africa (Krämer, 2015).

A. thaliana was initially described in 1577, but it gained popularity in research during the 1980s, when researchers started integrating genetics with advanced molecular biology methods. In 2000, the Arabidopsis Columbia-0 (Col-0) genome sequence was released, marking it as the first nuclear genome sequenced in a flowering plant (source: http://www.arabidopsis.org/). This achievement was documented in the publication entitled "Analysis of the Genome Sequence of the flowering Plant *Arabidopsis thaliana*" (2000).

Figure 1. The different stages of the life cycle of *A. thaliana*, accession Columbia-0 (Col-0): seed stage (0 day), seedling stage (11 days), transitions to vegetative growth (39 days), and reproductive growth (45 days). Adapted from (Krämer, 2015).

A. thaliana possesses several traits that make it an attractive model plant. It has a short generation time, small size, and simple growth requirements, which facilitate its cultivation in laboratory conditions. The plant exhibits prolific seed production through self-pollination. Additionally, *A. thaliana* can be easily transformed. It has one of the smallest known genomes among flowering plants, and the presence of over 50,000 polymorphisms between the two most commonly used accessions has greatly aided at the identification of mutations through positional cloning. A substantial collection of characterized mutations and transgenic plants is also available, providing disruptions in various aspects of plant growth and development (Somerville & Koornneef, 2002).

Due to the availability and active development of genomic, proteomic, and metabolomic tools and resources, along with the accumulation of extensive knowledge about this plant, our study was focused on *A. thaliana*.

2. Polyamines

Polyamines are small polycationic molecules that contain amino groups and are found in all living organisms. In plants, the most abundant polyamines are the diamine putrescine (Put), the triamine spermidine (Spd) and the tetramine spermine (Spm). Polyamines can exist as free forms or be covalently conjugated to other small molecules such as phenolic acids, as well as to macromolecules such us proteins and nucleic acids (Alcázar et al., 2006).

Polyamine biosynthesis

The first step in plant polyamine biosynthesis pathway is the decarboxylation of ornithine or arginine, catalyzed by ornithine decarboxylase (ODC) or arginine decarboxylase (ADC), respectively. In *A. thaliana* plants, polyamines are exclusively produced via ADC (Hanfrey et al., 2001), which is encoded by two genes (*ADC1* and *ADC2*). These isoforms convert arginine to agmatine, which is subsequently converted into Put through two reactions involving agmatine deiminase/iminohydrolase (AIH) and *N*-carbamoylputrescine amidase/amidohydrolase (NCPAH) (Janowitz et al., 2003). Put is converted into Spd by spermidine synthase (SPDS) through the addition of an aminopropyl group donated from decarboxylated S-adenosylmethionine (dcSAM), which is synthesized from SAM (S-adenosylmethionine) by SAM decarboxylase (SAMDC). Similarly, Spd is converted into Spm by spermine synthase (SPMS) through the addition of another aminopropyl group from dcSAM (**Figure 2**) (Alcázar et al., 2006).

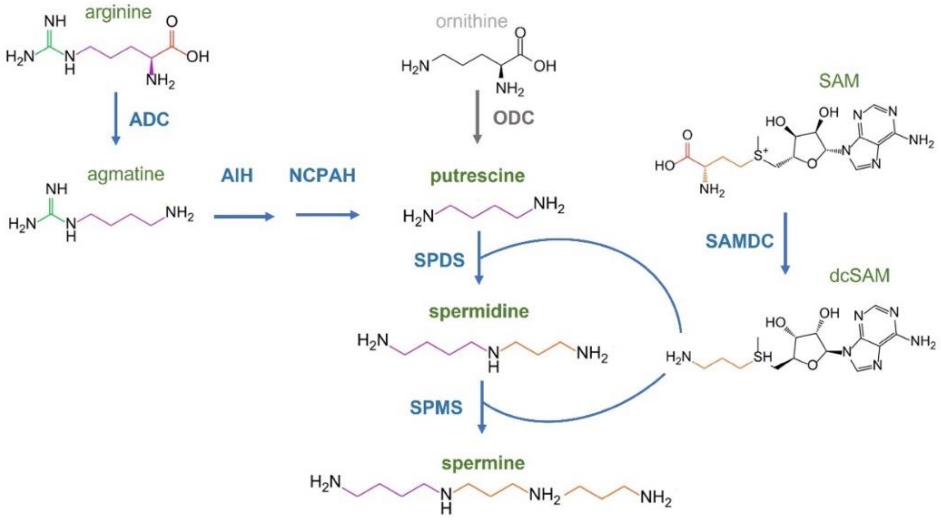

Figure 2. Polyamine biosynthesis pathway in plants. ODC: ornithine decarboxylase, ADC: arginine decarboxylase, AIH: agmatine deiminase/iminohydrolase, NCPAH: *N*-carbamoylputrescine amidase/amidohydrolase, SPDS: spermidine synthase, SPMS: spermine synthase, SAM: S-adenosylmethionine, SAMDC: S-adenosylmethionine decarboxylase, dcSAM: decarboxylated S-adenosylmethionine.

Polyamine catabolism

Polyamine catabolic processes are performed by two types of enzymes: copper-amine oxidases (CuAOs) and flavin-containing polyamine oxidases (PAOs) (**Figure 3**). These enzymes exhibit different substrate specificities, subcellular localizations, and functional roles.

CuAOs primarily oxidize diamines, such as Put at their primary amino groups (Tavladoraki et al., 2016). The oxidation results in the production of 4-aminobutanal, hydrogen peroxide (H_2O_2), and ammonia (NH_3) (**Figure 3**). Although CuAOs in *A. thaliana* mainly catalyze the oxidation of Put, it has been observed that certain CuAOs are also capable of oxidizing Spd (Planas-Portell et al., 2013).

In A. *thaliana* there are 10 *CuAO* genes, out of which eight encode putative functional CuAOs [*AtCuAOα1* (*At1g31670*); *AtCuAOα2* (*At1g31690*); *AtCuAOα3* (*At1g31710*; previously *AtCuAO2*); *AtCuAOβ* (*At4g14940*; previously *ATAO1* or *AtAO1*); *AtCuAOγ1* (*At1g62810*; previously *AtCuAO1*); *AtCuAOγ2* (*At3g43670*); *AtCuAOδ* (*At4g12290*, previously *AtCuAOδ2*); *AtCuAOζ* (*At2g42490*; previously *AtCuAO3* or *AtCuAO1*)]. The remaining two genes *AtCuAOε1* (*At4g12270*; previously *AtCuAOε*) and *AtCuAOε2* (*At4g12280*; previously *AtCuAOδ1*) represent sequential segments of a copy of *AtCuAOδ* gene (Tavladoraki et al., 2016).

CuAOs in plants can be classified into two groups based on their subcellular localization. The first group consists of CuAOs localized in the apoplast, which contain a N-terminal signal peptide. The second group includes CuAOs localized in peroxisomes, characterized by the presence of a C-terminal peroxisomal targeting signal 1 (PTS1) (Planas-Portell et al., 2013).

In contrast to CuAOs, PAOs show a strong affinity for Spd, Spm, and their acylated forms (Alcázar et al., 2010). *A. thaliana* possesses five PAOs (AtPAO1-AtPAO5), which are intracellularly located in the cytosol (AtPAO1 and AtPAO5) or peroxisomes (AtPAO2, and AtPAO3, and AtPAO4) ((Tavladoraki et al., 2016). Based on their roles in polyamine catabolism and subcellular localization, plant PAOs can be classified into two classes.

The first class of PAOs is involved in the terminal catabolism of Spd and Spm, leading to the production of H_2O_2, 1,3-diaminopropane (DAP), and 4-aminobutanal (in Spd catabolism) or *N*-(3-aminopropyl)-4- aminobutanal (in Spm catabolism). The second class includes PAOs that catalyze the back-conversion reactions, converting Spm to Spd and

Spd to Put. These reactions involve reverse reactions of polyamine synthesis and results in the production of 3-aminopropanal and H_2O_2 (**Figure 3**). All the five existing *PAO* genes in Arabidopsis (*AtPAO1–AtPAO5*) catalyze the polyamine back-conversion reactions although with different substrate specificities (Moschou, et al., 2008a).

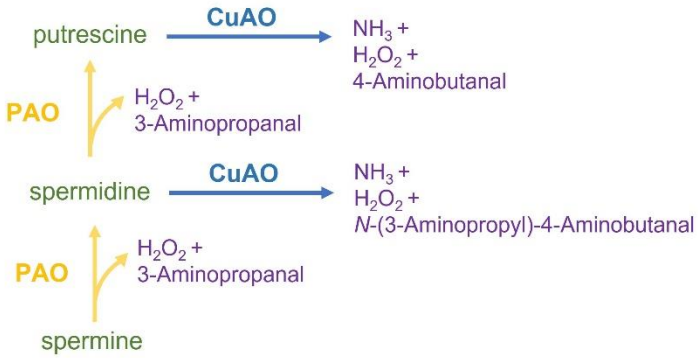

Figure 3. Catabolism pathway in *A. thaliana*. PAO: flavin-containing polyamine oxidase, CuAO: cupper-amine oxidase.

3. Ribosome biogenesis

Ribosomes are complex structures composed of ribosomal RNA (rRNA) molecules and ribosomal proteins (RPs). In plants, there exist three distinct types of ribosomes: cytosolic, chloroplastic and mitochondrial (Martinez-Seidel et al., 2020). For this study, our focus was on investigating the characteristics of cytosolic ribosomes.

In plants, as in other eukaryotes, the cytosolic ribosomes are composed of two subunits, a 40S small subunit (SSU) and a 60S large subunit (LSU), which play two distinct roles during translation. The 40S subunit contains the decoding center with binding sites for aminoacyl-tRNAs and the mRNA, whereas the 60S subunit contains the peptidyltransferase active site responsible for peptide bond formation of the newly synthesized proteins. The ribosome has three tRNA-binding sites, including the aminoacyl (A) site, the peptidyl (P) site, and the exit (E) site. The small subunit consists of an 18S rRNA and 33 RPs while the large subunit contains three rRNA species, 5S, 5.8S and 25S, which ranges between 25S and 26S, along with 47 RPs (Chang et al., 2005; Merchante et al., 2017). More than 80 RPs have been identified in *A. thaliana*, and each is encoded by two to seven gene paralogs, resulting in a total of 242 proteins encoded by the Arabidopsis genome. Notably, only one member of each RP gene family is present in a ribosome (Barakat et al., 2001; Browning & Bailey-Serres, 2015), except for a few cases, such as P-Stalk protein dimers (Santos & Ballestat, 1995; Uchiumi & Kominami, 1992).

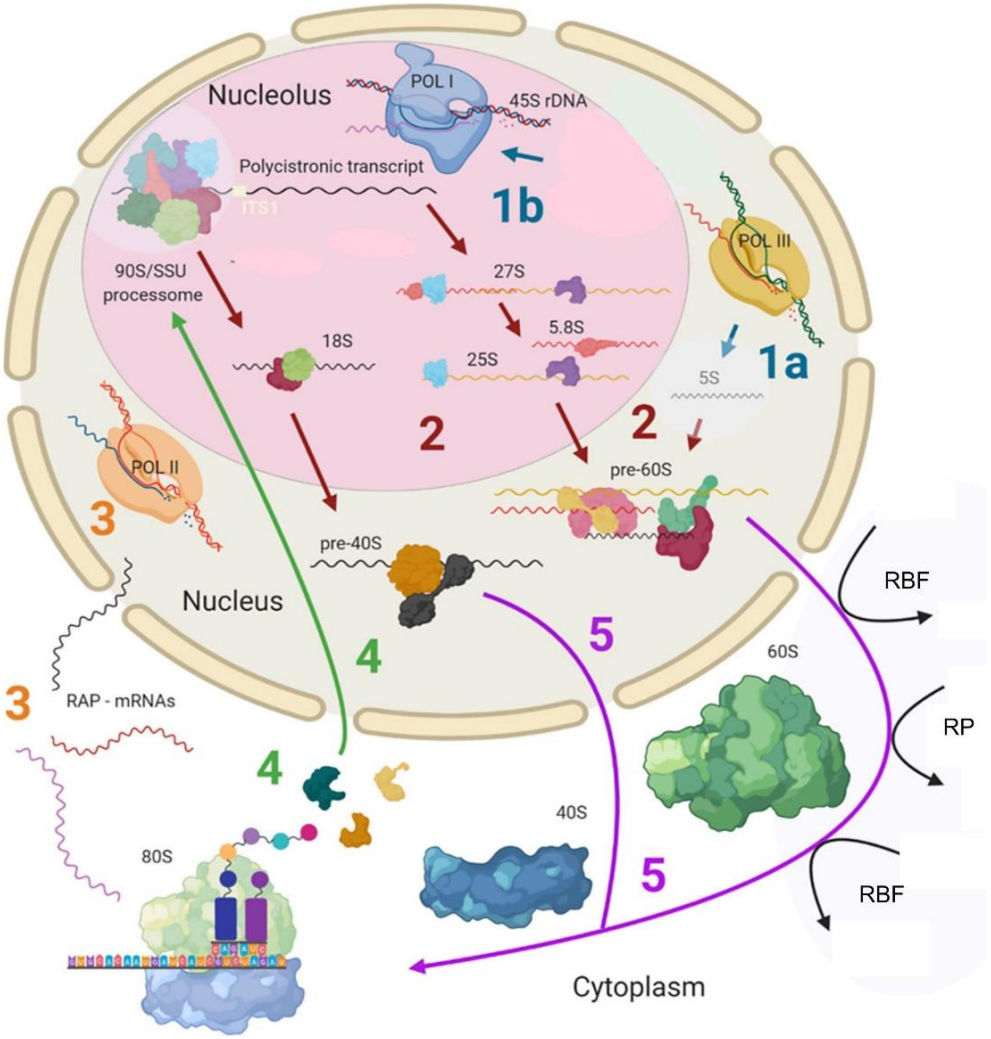

Figure 4. Cytosolic ribosome biogenesis steps in plants. Adapted from (Martinez-Seidel et al., 2020).

The process of cytosolic ribosome biogenesis begins in the nucleolus and ends in the cytoplasm where the last steps of maturation occur (**Figure 4**). The first step involves the synthesis of the different rRNA species. 5S rRNA is transcribed by RNA polymerase III (POL III) in the nucleus (step 1A) and 45S ribosomal DNA (rDNA) is transcribed by RNA polymerase I (POL I) into a polycistronic transcript containing 18S, 5.8S and 25S rRNAs in the nucleolus (step 1B). In the second step, the polycistronic transcript forms the 90S pre-ribosome/SSU processome, a large ribonucleoprotein complex, which is processed into pre-40S and pre-60S subunits after the splicing event on internal transcribed spacer 1 (ITS1). In the third step, genes coding for ribosome-associated proteins (RAPs) and RPs are transcribed by RNA polymerase II (POL II) and spliced in the nucleus. In the fourth step, the transcribed mRNAs corresponding to RAPs and RPs are exported and translated in the cytoplasm and then, most of the RAPs and RPs are imported back into the nucleus and nucleolus to assist in ribosome assembly. Finally, the nuclear ribosomal pre-subunits

are exported to the cytoplasm for the final maturation steps that make the functional subunits translationally competent. The usage of different rRNAs sequences, RPs and RAPs, as well as posttranscriptional or posttranslational modifications of all components, may result in heterogeneity in ribosomal populations that may arise during (from scratch) or after ribosome biogenesis (e.g., ribosome remodeling (Martinez-Seidel et al., 2022)) in plants. Plant-specific ribosome factors (RBFs) are involved in rRNA processing, indicating that plant ribosome biogenesis has specialized features. (Martinez-Seidel et al., 2020).

Translation

As previously mentioned, ribosomes are responsible for decoding the information contained in mRNA and translating it into amino acid sequences of proteins. However, not all RNAs are successfully translated, as translation can be influenced by structural features within the RNA molecule. These regulatory mechanisms, such as hairpins and upstream open reading frames (uORFs), often inhibit translation of the main genic open reading frames (mORFs). By default, mRNAs are typically translationally active, but regulatory mechanisms can restrict or control this translation process. For example, transcripts with non-optimal codons in their sequences are actively repressed and protein abundances diminished by ribosome surveillance mechanisms (Barrington et al., 2022; Narula et al., 2019). Additionally, not all non-repressed mRNAs are actively engaged with ribosomes due to limitations in translation-initiation factors, especially those involved in initiating translation by recruiting ribosomal complexes. As a result, most mRNAs are distributed between translated and non-translated pools in the cytoplasm, and alterations in the activity of these limiting translation factors can impact global protein synthesis (Gebauer & Hentze, 2004).

The protein synthesis pathway can be divided into four steps: initiation, elongation, termination, and ribosome recycling. During the initiation, the initiator methionyl-tRNA (Met-tRNA$^{Met}_{i}$) attaches to the P site of the ribosome, creating a complex in which its anticodon is paired with the start codon of the mRNA (**Figure 5**). The eukaryotic translation initiation factor eIF2 binds GTP and Met-tRNA$^{Met}_{i}$ to form a ternary complex, which then binds to the 40S subunit along with other translation initiation factors (eIF1, eIF1A, and eIF5) forming the preinitiation complex (PIC). The PIC binds near the 5′end of an mRNA with the assistance of the cap-binding complex eIF4F, composed of the eIF4E and eIF4G proteins, and other associated factors (eIF4a and eIF4b). The PIC then scans the mRNA towards the 3′direction searching for a start codon. Once the base-

pairing interaction between the anticodon of the Met-tRNA$^{Met}_{i}$ and an AUG codon in the mRNA is established, a series of events is triggered. These events include the hydrolysis of GTP by eIF2, structural changes in the ribosome to strengthen the binding of Met-tRNA$^{Met}_{i}$, and the subsequent release eIF2–GDP. The eIF2-GDP is then replaced by eIF5B, which, along with eIF1A, assists in the recruitment of 60S ribosome subunit, as other eIFs dissociate. Subsequently, the 60S subunit joins the complex, forming an 80S ribosome. The GTP associated with eIF5B is hydrolyzed, and the complex becomes ready for translation elongation. After subunits are assembled, all the translation initiation factors have dissociated from the ribosome (Dever & Ivanov, 2018; Merchante et al., 2017).

The eukaryotic translation elongation process consists of several steps. First, the eukaryotic translation elongation factor eEF1A binds to GTP and an aminoacyl-tRNA to form a ternary complex. Once this complex attaches to the A site of the ribosome and the anticodon of the aminoacyl-tRNA base pairs with the mRNA codon present in the A site, eEF1A prompts the hydrolysis of GTP. Once, eEF1A–GDP complex is released, the aminoacyl-tRNA is accommodated into the A site, promoting peptide bond formation by positioning it near the peptidyl-tRNA in the P site (Dever & Ivanov, 2018). After peptide bond formation, the factor eEF2 facilitates the translocation of the tRNAs from the P and A sites to E and P sites, respectively, and the mRNA is translocated with the tRNAs. Once eEF2 is released, the A site becomes available to receive the next aminoacyl-tRNA and the translation elongation will continue until a stop codon enters the A site (Dever & Ivanov, 2018).

Of relevance when discussing the roles of polyamines in translation, the translation factor eIF5A, which is post-translationally modified by Spd, binds to the E site, and further promotes peptide bond formation (Park & Wolff, 2018). eIF5A is the only cellular protein that contains the amino acid hypusine, and Spd is the source of the n-butylamine moiety for hypusine formation (Chattopadhyay et al., 2003).

Termination of protein synthesis is controlled by the release of factors eRF1 and eRF3, which form a ternary complex along with a GTP molecule. This complex enters the A site of the ribosome and promotes the release of the polypeptide chain and tRNA. The 80S ribosome dissociates into its subunits and can then be used for new rounds of translation (Merchante et al., 2017). Recent studies have shown that eIF5A, in addition to its role in elongation, is also involved in termination (Schuller et al., 2017).

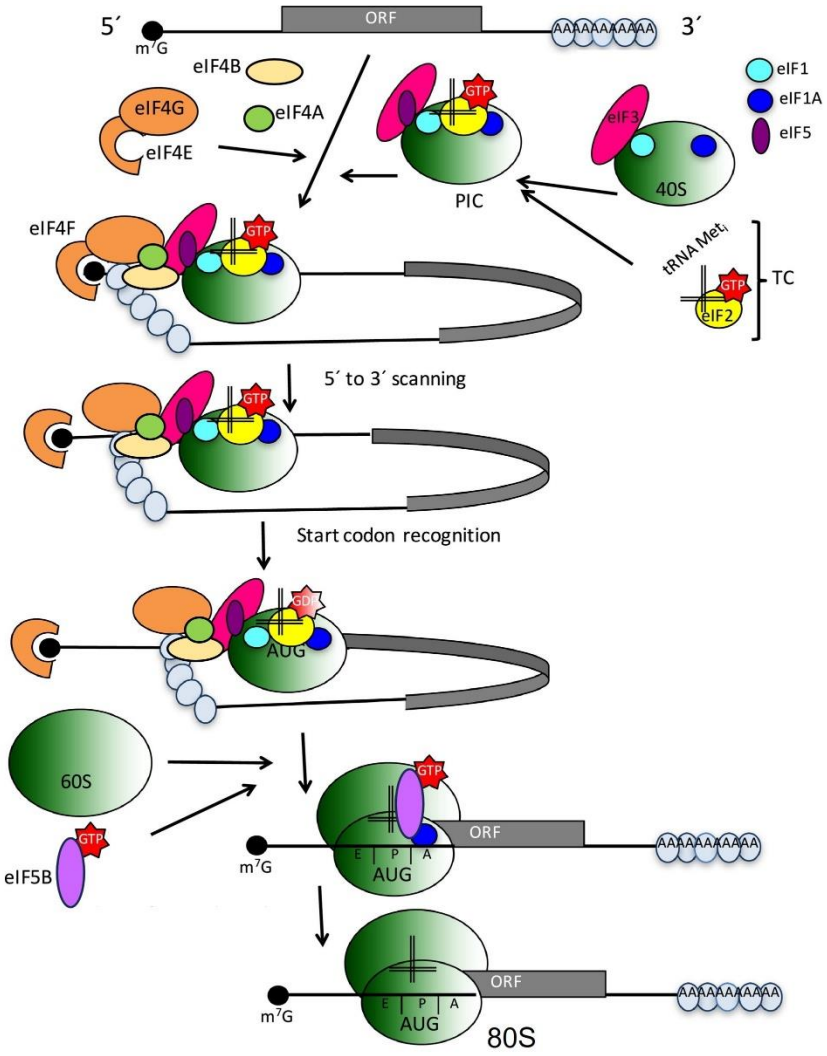

Figure 5. The process of translation initiation in plants. ORF: Open reading frame, TC: ternary complex, PIC: preinitiation complex. Adapted from (Merchante et al., 2017).

Polyamines in translation

The association between polyamines and protein synthesis was initially discovered in a study by (Cohen & Lichtenstein, 1960) when they found a consistent link between polyamines Put and Spd and ribosomes in *Escherichia coli* (*E. coli*) cells. Another study conducted in a fractionated mammalian cell-free protein system demonstrated that the addition of polyamines stimulated protein synthesis independently of the utilized mRNA, suggesting that polyamines likely act on the translational machinery (Atkins et al., 1975).

In the context of plant translation, only a single study conducted in a wheat-germ cell-free system has been performed (Hunter et al., 1977). The study showed that polyamines had a stimulatory effect on the incorporation of amino acids into elongating polypeptides, suggesting that polyamines enhance translation elongation. The researchers also confirmed

that the addition of polyamines resulted in a lower Mg^{2+} optimum for protein synthesis. These finding align with others *in vitro* studies conducted in bacteria or mammalian cells (Ogasawara et al., 1989; Takeda, 1969) that support the notion of polyamines playing a role in translation elongation.

Moreover, a separate study (Park & Wolff, 2018) supports the involvement of eIF5A in translation elongation, further strengthening the connection between polyamines and this process. However, it is important to note that polyamines also appear to be essential for cell growth, as observed through the inhibition of cell growth upon reduction of polyamines prior to a significant decrease in hypusinated eIF5A (Nishimura et al., 2005).

In contrast, a study conducted in mammalian cells under *in vivo* conditions (Mandal et al., 2013) revealed that inhibiting polyamines led to a disruption in translation initiation, characterized by a loss of large polysomes and an increase in 80S monosomes. This finding contradicts the *in vitro* studies suggesting a more prominent role for polyamines in translation elongation.

Furthermore, it has been identified that polyamines enhance the expression of 20 types of proteins in *E. coli* and 4 types of proteins in mammalians cells at the level of translation. The genes encoding these proteins have been termed the "polyamine modulon" (Igarashi & Kashiwagi, 2018). In plants, it has been shown that polyamines regulate the expression of *SAMDC* mRNA at the level of translation, suggesting the existence of a similar modulon (Hanfrey et al., 2005).

These findings suggest that polyamines regulate translation in a specific and global manner at both the initiation and elongation stages of mRNA translation, although their direct and indirect effects on protein synthesis have yet to be fully elucidated. While both *in vitro* and *in vivo* studies have demonstrated the implication of polyamines in translation, no studies have been conducted on the effect of polyamines on plant translation *in vivo*.

A recent study from our research group investigated the differential effect of Put and Spm application on the modulation of flg22-triggered responses, by determination of the global changes in expression at 24 h of 100 μM Put, 100 μM Spm, 1 μM flg22, 100 μM Put + 1 μM flg22, 100 μM Spm + 1 μM flg22 and mock (H_2O) treatments in *A. thaliana* wild type plants. These analyses suggested a transcriptional effect of Put and flg22 on increase of ribosome biogenesis that was not evidenced in the Spm treatment (C. Zhang et al., 2023).

4. Reactive oxygen species production

The activation or reduction of oxygen can result in the generation of reactive oxygen species (ROS) such as singlet oxygen ($^1O_2$), superoxide (O_2^-), H_2O_2 and hydroxyl radical ($HO^\cdot$). Plants and other living organisms continuously produce ROS in an oxidizing environment as part of their metabolic processes occurring in chloroplasts, mitochondria, peroxisomes, and other cellular sites (Tripathy & Oelmüller, 2012). When ROS levels exceed the physiological range required for normal redox reactions and cell signaling, it leads to oxidative stress (Gerlin et al., 2021).

Polyamines and H_2O_2 production

In plants, there is substantial evidence supporting the involvement of polyamine catabolism and the resulting ROS in cell differentiation. For example, when the maize ZmPAO1 enzyme is overexpressed, it leads to early xylem differentiation and has a strong impact on root development in transgenic tobacco plants. This effect is correlated with increased production of H_2O_2 and an elevated rate of cell death (Tisi, Federico, et al., 2011). Additionally, H_2O_2 generated through polyamine catabolism plays a role in the cross-linking of cell wall polysaccharides during cell wall maturation (Cona et al., 2006; Liu, et al., 2014a; Tisi, Federico, et al., 2011). Moreover, external polyamines also influence the growth of pollen tubes by regulating ROS generation (Benkő et al., 2020; Do et al., 2019; Scholz et al., 2020; Wu et al., 2010).

During leaf senescence, there is an observed increase in the transcription and activity of polyamine catabolic enzymes in barley leaves undergoing dark-induced senescence (Ioannidis et al., 2014; Sobieszczuk-Nowicka et al., 2016). Consistently, the *Arabidopsis pao4* mutant shows delayed senescence, which is correlated with elevated levels of Spm but reduced ROS accumulation (Sequera-Mutiozabal et al., 2016). Moreover, H_2O_2 generated by polyamine catabolism contributes to programmed cell death (PCD) during xylem differentiation ((Tisi, Angelini, et al., 2011a; Tisi, Federico, et al., 2011b). Additionally, tobacco cells secrete Spd into the apoplast, where it is oxidized by PAOs, resulting in the generation of H_2O_2. This H_2O_2 level promotes PCD (Moschou, et al., 2008b; Moschou, et al., 2008c).

Polyamine catabolism also play a significant role in various abiotic stress responses. For instance, in citrus, the apoplastic CsPAO4 produces H_2O_2 leading to oxidative damages under salt stress (W. Wang & Liu, 2016). Reducing the expression of PAO-coding genes enhances the thermotolerance of tobacco, likely due to a decrease in heat-induced

H_2O_2 generation (Mellidou et al., 2017). PAO activity contributes to oxidative stress induced by aluminum or selenium, further emphasizing its pro-oxidant role during severe stresses (Y. Wang et al., 2019; Yu et al., 2018). Interestingly, some studies also highlight the importance of polyamine catabolism in antioxidant defense signaling. For example, it contributes to salt tolerance in transgenic tobacco plants that overproduce polyamines (Moschou, et al., 2008b; Seo et al., 2019). Additionally, the contrasting salt stress tolerance observed in different maize genotypes correlates with polyamine catabolism dependent H_2O_2 production during salt stress (Freitas et al., 2018). In *A. thaliana*, *pao5* mutant displays salt stress tolerance, although this is not correlated with reduced ROS production but increased level of thermospermine (t-Spm) (Zarza et al., 2017). However, the salt-tolerant in *pao1 pao5* double mutant, lacking cytoplasmic PAOs, exhibits reduced ROS production under NaCl stress (Sagor et al., 2016). These observations highlight the diverse contributions of various PAOs with different activities and intracellular localizations to stress tolerance.

PAO-generated H_2O_2 may also contribute to pathogen defense. For example, in response to the biotrophic pathogen *Pseudomonas syringae*, PAO activity is increased in tobacco, and the infection induces Spm secretion, resulting in significant H_2O_2 accumulation in the apoplast (Moschou et al., 2009). While the catabolism of polyamines and the production of H_2O_2 might beneficially regulate the hypersensitive response (HR) in biotrophic host–pathogen interactions (Cowley & Walters, 2002; Yoda et al., 2003), it may have detrimental effects in the case of infection by necrotrophic pathogens (Marina et al., 2008).

Polyamine catabolism and RBOHs (respiratory burst oxidase homologues) enzymes, which are NADPH (nicotinamide adenine dinucleotide phosphate) oxidases, are involved in various cellular processes, indicating a potential functional link in the regulation of ROS homeostasis (Agurla et al., 2018; Desikan et al., 2006; Wu et al., 2010). However, the precise interconnection between PAO and RBOH activities remains unclear due to inconsistent experimental data obtained from different species and experimental systems. Some studies suggest that polyamines influence the transcription of RBOH genes and/or the activity of the RBOH enzymes (Cuevas et al., 2004; Shen et al., 2000; Xu et al., 2021; C. Zhang et al., 2023) while other investigations support the hypothesis that RBOH activity is involved in modulating polyamine metabolism (Demiralay et al., 2022).

In summary, the H_2O_2 generated by PAO serves as a double-edged sword. On one hand, it is necessary for normal development and can improve stress adaptation. However, on

the other hand, if its levels surpass a certain threshold, it can become detrimental and result in cell death.

5. Ethylene Pathway

Ethylene (C_2H_4) is a gaseous plant hormone that plays a crucial role in regulating various growth and developmental processes in plants. Although its most well-known function is the stimulation of fruit ripening, ethylene is involved in many other physiological processes including the regulation of plant responses to both biotic and abiotic stress (Zhao et al., 2021).

Ethylene biosynthesis

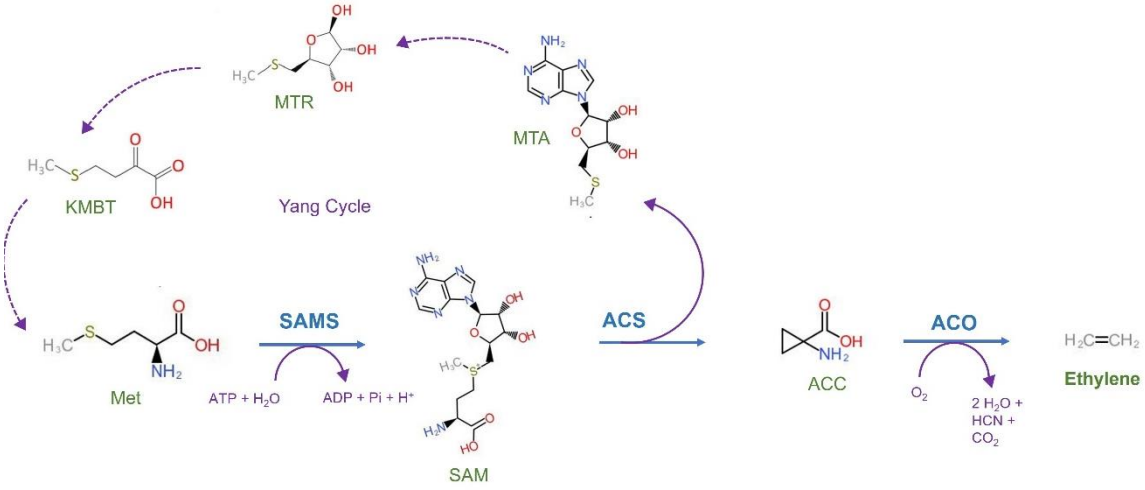

Figure 6. Representation of the ethylene biosynthesis pathway. Met: methionine, SAMS: S-adenosyl-L-methionine synthetase SAM: S-adenosyl-L-methionine, ACS: 1-aminocyclopropane-1-carboxylic acid synthase, ACC: 1-aminocyclopropane-1-carboxylic acid, ACO: 1-aminocyclopropane-1-carboxylic acid oxidase, MTA: methylthioadenosine, MTR: 5′-methylthioribose, KMBT: 2-keto-4-methylthiobutyrate. Yang cycle recycles sulfur moiety from MTA back to methionine.

Ethylene is synthesized from SAM, the active form of methionine (Met), in two enzymatic steps. The first step converts SAM to 1-aminocyclopropane-1-carboxylic acid (ACC) through the action of 1-aminocyclopropane-1-carboxylic acid synthase (ACS). During this conversion, a byproduct called 5′-methylthioadenosine (MTA) is released. MTA is a metabolite that is recycled in the Met salvage cycle, also known as the Yang cycle (Alonso et al., 2003; Merchante & Stepanova, 2017). SAM serves as precursor not only for ethylene biosynthesis, but also for the polyamine synthesis pathway, where it serves as a source of aminopropyl groups (Alcázar et al., 2006). ACC, the product of the ACS-mediated step, is then transformed into ethylene by 1-aminocyclopropane-1-carboxylic acid oxidase

(ACO). In plants, the ethylene levels are generally low but can increase in response to developmental cues and environmental signals, such as ripening (Tatsuki & Mori, 2001) or osmotic stress (Huang et al., 2004). The regulation of ethylene levels is tightly controlled by transcriptional and post-transcriptional regulation, primarily focusing on the regulation of ACS and, to some extent, ACO (**Figure 6**) (Bakshi et al., 2015).

Ethylene signaling

Ethylene perception involves a family of receptors primarily located in the endoplasmic reticulum (ER) membrane. These receptors have an ethylene-binding domain lying within the ER membrane and the GAF (cGMP phosphodiesterase/adenylyl cyclase/FhlA) and histidine kinase domain in the cytosol (Y. F. Chen et al., 2002). In *A. thaliana*, there are five ET receptors: ethylene response 1 (ETR1/EIN1), ethylene response sensor 1 (ERS1), ethylene response 2 (ETR2), ethylene response sensor 2 (ERS2), and ethylene insensitive 4 (EIN4) (Bleecker, 1999).

Based on their structural characteristics, the receptors can be classified into two subfamilies. Subfamily I, which includes ETR1 and ESR1, has three transmembrane domains and a functional histidine kinase domain (Ju & Chang, 2015). The subfamily II, consisting of ETR2, ERS2 and EIN4, carry some additional amino acids at the N-terminus which are of unknown function, and a divergent histidine kinase domain (Moussatche & Klee, 2004). Consequently, it has been suggested that receptors in this subfamily may exhibit Serine (Ser)/Threonine (Thr) kinase activity (Zhao et al., 2021).

Downstream of ethylene receptors acts constitutive triple response 1 (CTR1). CTR1 is a Raf - like Ser/Thr kinase protein that contains an N-terminal regulatory domain and a C-terminal kinase domain and negatively regulates ethylene signaling (Kieber et al., 1993).

In the absence of ethylene (**Figure 7A**), the receptors interact with CTR1 leading to the activation of its kinase activity. Consequently, CTR1 phosphorylates the C-terminal domain (CEND) of ethylene insensitive 2 (EIN2), thereby inhibiting it signaling function. EIN2 is a protein located in the ER membrane, featuring an N-terminal transmembrane domain and a CEND exposed to the cytosol. The phosphorylated EIN2-CEND is then subjected to degradation by the F-box protein ETP1 (EIN2 targeting protein 1) and ETP2 through the 26 proteasome pathway. As a result, within the nucleus, EBF1 (F-box proteins EIN3-binding F-box protein 1) and EBF2 target the ethylene insensitive 3 (EIN3)/EIN3-like (EIL1) transcription factors for degradation via 26 proteasome, preventing the

activation of ethylene-responsive genes (Bakshi et al., 2015; Benavente & Alonso, 2006; Zhao et al., 2021).

In the presence of ethylene (**Figure 7B**), the receptors bind to ethylene, resulting in the inactivation of CTR1 and the subsequent dephosphorylation of EIN2. The EIN2-CEND portion is then cleaved from the ER membrane and translocated to the nucleus. In the nucleus, it interacts with the histone-binding protein EIN2 nuclear-associated protein 1 (ENAP1), facilitating histone acetylation. This interaction promotes the binding of EIN3 to the target DNA sites, initiating transcriptional activation. Additionally, apart from its role in the nucleus, EIN2-CEND can migrate to the cytoplasmic processing body (P-body). In the P-body, it aids at the translational repression of EBF1 and EBF2, resulting in the stabilization of EIN3/EIL1. Subsequently, the EIN3/EIL1 proteins activate ethylene responses by initiating the expression of downstream genes (Bakshi et al., 2015; Benavente & Alonso, 2006; Zhao et al., 2021).

Besides the conserved signaling components, novel regulators have been identified that play a role in modulating the function EIN2. For instance, ER membrane-localized MHL proteins have been found to interact with the N-terminal domain of EIN2, contributing to its stabilization. Another set of regulators are the EIN2 C-terminal interacting protein 1 (ECIP1) proteins, which interact with EIN2-CEND and influence its function. Additionally, it has been observed that ETR1 may interact with histidine phosphor-transfer protein 1 (AHP1) through its C-terminus domain, although the downstream events of this pathway have not yet been determined (Zhao et al., 2021).

A recently proposed pathway suggests the existence of a CTR1-independent, EIN2-dependent mechanism. In this pathway, the receptors regulate EIN2 function through an unknown mechanism that is independent of CTR1. When ethylene binds to the receptors, it leads to the release of EIN2 inhibition, allowing the full-length EIN2 protein to translocate to the nucleus and activate the ethylene response. However, further investigation is needed to fully understand this mechanism (J. Zhang et al., 2020).

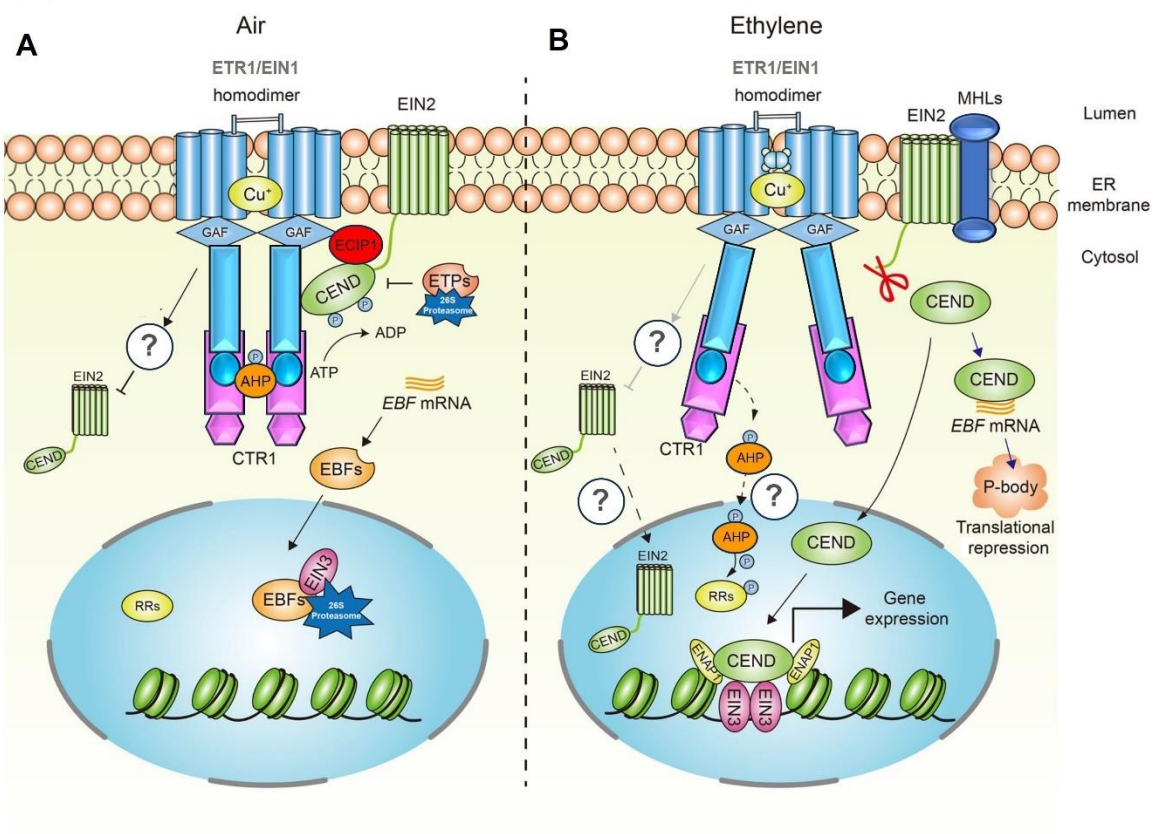

Figure 7. Ethylene signaling pathway in *A. thaliana*. (**A**) Signaling pathway in absence of ethylene. (**B**) Signaling pathway in presence of ethylene. Adapted from (Zhao et al., 2021).

Triple response

The triple response is a distinctive phenotype observed in plants as a result of ethylene's significant impact on plant morphogenesis. This response is specifically observed in seedlings that are germinated in the dark and exposed to high concentrations of ethylene. In *A. thaliana*, the triple response encompasses the shortening and thickening of hypocotyls and roots, along with an intensified curvature of the apical hook. By studying mutants that do not exhibit the triple response phenotype in the presence of ethylene or, conversely, display the triple response in the absence of the externally supplied hormone, researchers have gained insights into the molecular mechanisms involved (Benavente & Alonso, 2006; Merchante & Stepanova, 2017). For instance, *ethylene insensitive* (*ein*) mutants show a lack of triple response phenotype even when exposed to ethylene (Bakshi et al., 2015). These findings highlight the importance of these mutants in elucidating the functions of specific genes and their role in ethylene signaling pathways. Interestingly, not only classical mutants associated with ethylene biosynthesis and signaling show abnormal triple response, but also mutants with defects in downstream ethylene-regulated processes demonstrate

mild alterations in ethylene sensitivity. This is evident in mutants with deficiencies in auxin transport, signaling, or response, which display reduced responsiveness to ethylene specifically in roots (Alonso et al., 2003).

Relation between polyamines and ethylene

Polyamines and ethylene have inhibitory effects on each other´s synthesis. *In vitro* studies in tomato have shown that Spd and Spm inhibit ACS activity and, consequently, ethylene production (N. Li et al., 1992). Additionally, in peas, ethylene effectively inhibits SAMDC and ADC, which are key enzymes in the polyamine biosynthesis (Apelbaum & Goldlust, 1985). While the biosynthetic interaction between polyamines and ethylene is commonly viewed as competitive (S. Pandey et al., 2000), it has been found that the availability of SAM is not a limiting factor *in vivo* for the biosynthesis of ethylene or Spd/Spm. In fact, both pathways can operate concurrently (Mehta et al., 2002). Interestingly, in *A. thaliana,* exogenous ethylene increases the content of polyamines (Put, Spd, and Spm) but this effect is observed only at concentrations that stimulate abscisic acid (ABA) accumulation (Rakitin et al., 2009).

Ethylene is known for promoting senescence, while polyamines have a suppressive effect on senescence by slowing down membrane deterioration, chlorophyll loss, and enhancing protease and RNase activities (S. Pandey et al., 2000). A recent study in *A. thaliana* shows that Spd delays the process of leaf senescence by primarily interfering with the ethylene signaling pathway, suggesting that Spd reduces the levels of EIN3 protein by suppressing the degradation of EBF1/2 protein (Liebsch et al., 2022).

Ethylene also plays a crucial role in fruit ripening process. In contrast, fruits stored in controlled atmosphere undergo slower ripening and exhibit higher levels of polyamines (Kushand & Dumbroff, 1991). Similarly, external application of Spd to immature peach fruits inhibits ripening by disrupting ethylene metabolism and signaling pathways associated with the ripening process (Torrigiani et al., 2012). Moreover, overexpression of ODC leads to increased levels of Put, Spd, and Spm, which is correlated with decreased levels of ethylene, leading to a delay in fruit ripening (R. Pandey et al., 2015). Interestingly, in strawberries, which are non-climacteric fruits that ripen independently of ethylene, FaPAO5 enzyme has a negative effect on fruit ripening, while Spm/Spd (spermine/spermidine) act as positive regulators (Mo et al., 2020).

In stressed leaves, polyamines reduce ROS levels and inhibit ethylene production, while ethylene promotes the activities of CuAOs and PAO by increasing ROS levels, thereby

reducing Put, Spd and Spm levels (C. Li et al., 2004). Silicon treatment restricted gummosis development in peach shoots by activating polyamine biosynthesis and inhibiting ethylene synthesis in peach (Gao et al., 2022).

During germination, the presence of salt leads to a decrease in ethylene production and in the ratio [(Spm + Spd) /Put] in *Brassica napu*s (Lechowska et al., 2022). In contrast, in *Lactuca sativa*, the presence of salt increased the polyamine ratio and the ethylene production (Zapata et al., 2003).

In general, polyamines and ethylene exhibit antagonistic roles, although their relationship is not always clear and depends on the tissue and physiological stage of development. Further investigations are required to fully understand the intricate cross-regulation between these two pathways.

6. Iron deficiency

Iron (Fe) is a vital micronutrient for most living organisms. Despite the abundant presence of iron in the soil, plants often face iron deficiency due to the limited bioavailability of this element. In the presence of oxygen, iron primarily exists as Fe^{3+} in its oxidized form, whereas in the organisms, it is required in the reduced form Fe^{2+}, highlighting the need for a reduction step. Furthermore, because Fe^{3+} exhibits low solubility in oxygenated fluids at neutral pH, the transport of iron under physiological conditions requires a preliminary step involving the chelation of Fe^{3+} or acidification of the rhizosphere. Although iron is essential for the growth of plants and other organisms, excessive iron can be toxic and lead to yield losses in crops. Consequently, plants have developed tight regulatory mechanisms to maintain iron homeostasis (Curie & Briat, 2003; Kobayashi, 2019; López-Millán et al., 2013).

Plants employ two major mechanisms for iron uptake: strategy I, also known as the reduction mechanism, is utilized by dicot and non-graminaceous monocot species, while strategy II, known as the chelation mechanism, is employed by graminaceous species (Romheld & Marschner, 1986).

Strategy I in *A. thaliana* involves several steps for iron uptake. Firstly, it includes rhizosphere acidification through the release of protons by the P-type H^+-ATPase AHA2, which promotes the solubilization of Fe^{3+} (Santi & Schmidt, 2009). Small metabolites such as coumarins and flavins are also secreted to mobilize Fe^{3+} (Mladěnka et al., 2010; Romheld & Marschner, 1983). Ferric reduction oxidase 2 (FRO2) reduces Fe^{3+} to Fe^{2+} (Robinson

et al., 1999), and the iron-regulated transporter 1 (IRT1) facilitates the uptake of Fe^{2+} into root cells (Vert et al., 2002). The expression of these protein genes involved in Fe uptake is induced at the transcriptional level under Fe deficiency. Transcription factors (TFs) form a regulatory network that controls the expression of these Fe-deficiency responsive genes in roots. The master regulator, *FER-like iron deficiency-induced transcription factor* (*FIT*), a basic helix-loop-helix (bHLH) TF, regulates the expression of *AHA2*, *FRO2* and *IRT1* (Colangelo & Guerinot, 2004). FIT forms heterodimers with one of the four subgroup Ib bHLH TFs (bHLH038, bHLH039, bHLH100, or bHLH101) to exert its function. The expression of *FIT* and Ib subgroup bHLH TFs is induced by IVb subgroup bHLH TFs (*bHLH121/URI*) and IVc subgroup bHLH TFs (*bHLH34, bHLH104, bHLH105/ILR3 and bHLH115*) (Kobayashi, 2019). Additionally, the BRUTUS (BTS) and BTS-LIKE (BTSL) proteins, which act as ubiquitin E3 ligases, interact with IVc subgroup bHLH TFs and FIT, targeting them for proteasomal degradation. Therefore, BTS/BTSL negatively regulates Fe-deficiency responses by degrading IVc subgroup bHLH TFs and FIT (Tabata, 2023).

Furthermore, recent studies have highlighted the role of ironman/Fe-uptake-inducing peptides (IMA/FEPs) in positively regulating plant responses to iron deficiency (**Figure 8**) (Grillet et al., 2018). The expression of all *A. thaliana IMA/FEP* genes is triggered in response to Fe-starvation, and each individual *IMA/FEP* genes, except *IMA5* and *IMA8*, stimulates Fe uptake (Y. Li et al., 2021). When plants experience Fe-deficiency conditions, IMA/FEP peptides compete with IVc subgroup bHLH TFs for interaction with BTS/BTSL (**Figure 8A**). This competition inhibits the degradation of IVc subgroup bHLH TFs by BTS/BTSL (Y. Li et al., 2021). The induction of *IMA/FEP* leads to the activation of several genes, including Ib subgroup bHLH TFs (*bHLH38, bHLH39, bHLH100* and *bHLH101*), *FRO2* and *IRT1,* which are involved in Fe reduction and uptake. It also promotes the expression of *scopoletin 8-hydroxilase* (*S8H*), a gene involved in coumarin biosynthesis, and cytochrome *CYP82C4*, a gene related to Fe chelation (**Figure 8B**) (Okada et al., 2022). Despite recent advancements in this field, the primary event that triggers this signaling cascade in response to iron deficiency has not been identified (Tabata, 2023).

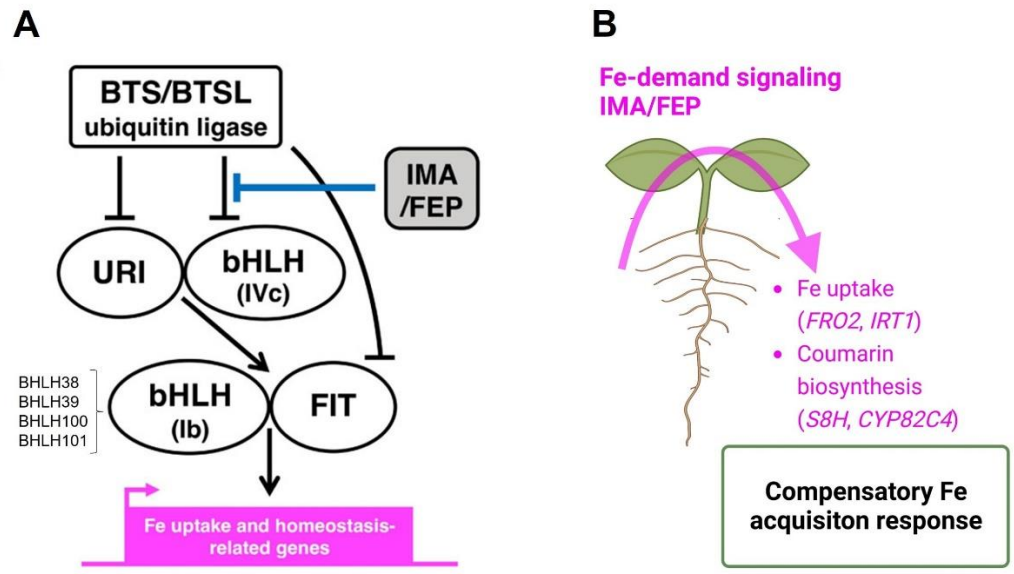

Figure 8. Model for IMA/FEP-mediated Fe-signaling response and under Fe deficiency conditions in plants. (**A**) IMA/FEP-mediated intracellular signaling of the local Fe-deficiency response. (**B**) Detection of Fe deficiency in the roots is transduced by an as-yet unknown mechanism, resulting in the upregulation of IMA/FEP peptide expression as a descending signal to roots (pink arrow: Fe-demand signaling). Adapted from (Tabata, 2023).

Relation between polyamines and Fe deficiency

Fe deficiency triggers the production of nitric oxide (NO) in roots, which acts as a positive regulator of the Fe-uptake machinery (W. W. Chen et al., 2010; Graziano & Lamattina, 2007). Hemicellulose-bound Fe represents the largest pool of Fe in the cell wall (Lei et al., 2014). Under Fe deficiency conditions, modifications such as methylation can alter the immobilization of Fe in the cell walls (Zhu et al., 2012). The dynamic changes in Fe distribution within the cell wall are regulated by NO. Additionally, Put, which is overproduced under Fe deficiency, is involved in this signaling pathway (Zhu et al., 2016). The application of exogenous Put has been shown to alleviate Fe-deficiency symptoms, but this effect is not observed in mutants lacking NO synthesis or in mutants impaired the hemicellulose production (Zhu et al., 2016). However, the specific mechanisms by which Put regulates the reutilization of Fe from the cell wall require further experimental investigation.

Spm and Spd exhibit Fe chelating properties by forming ternary complexes between Fe^{2+} ions and phosphate groups of membrane lipids. This chelation process inhibits Fe^{2+} auto-oxidation and, consequently, the generation of hydroxyl radicals (Mozdzan et al., 2006). In the context of *Staphylococcus aureus* (*S. aureus*) bacteria, exposure to high doses of Spm resulted in a significant increase in the expression of genes involved in Fe acquisition

and regulation. This suggests a specific connection between Spm and Fe depletion in bacteria (Yao & Lu, 2014).

Additionally, a recent study conducted in *E. coli* proposed that an excessive amount of Spd, stimulates the production of O_2^- radicals, leading to toxic levels. Spd directly interacts with Fe^{2+}, causing an increase in the Fe^{3+}/Fe^{2+} ratio (Kumar et al., 2022). This interaction can potentially abstract iron from certain iron-sulfur clusters, resulting in the inactivation of specific proteins. However, when Spd levels are optimal, most of it remains in a bound form with biomolecules, which slows down Fe oxidation and subsequent O_2^- production. Consequently, a deficiency in Spd would accelerate the rate of Fe oxidation, leading to ROS production (Kumar et al., 2022).

In summary, Spm and Spd exhibit a dual role, acting as both beneficial and detrimental factors. In excess, they can stimulate O_2^- production and Fe oxidation. Conversely, in scarcity, they contribute to higher levels of ROS with increased Fe oxidation.

Objectives

1. Involvement of polyamines in plant ribosome biogenesis in *A. thaliana*.

   1.1. To determine the effect of polyamines on the abundance of ribosome complexes.

   1.2. To investigate whether polyamines induce changes in the RPs bound to the polysome complexes.

   1.3. To check whether changes in the abundance of RPs produced by polyamines are confined to specific regions of the ribosome.

   1.4. To explore the presence of polyamines in the ribosome complexes.

   1.5. To perform and compare the proteome of polyamine deficient mutants *adc1-1* and *spms.*

2. Identification of potential mutations associated with Spm tolerance in *A. thaliana.*

   2.1. To generate a mutant population collection through EMS mutagenesis in *A. thaliana* to identify mutants insensitive to Spm (*spmi*).

   2.2. To map the identified mutations using state-of-the-art genomic tools.

   2.3. To confirm the causality of the identified mutations through different phenotyping approaches, including root length measurement and H_2O_2 quantification in loss-of-function mutants, and to infer the biological significance of the genes by GO enrichment analysis of co-expressed networks.

   2.4. To screen mutants insensitive to Spm in a collection of 6,000 homozygous T-DNA insertion mutants from SALK.

3. Identification of a relationship between Fe deficiency signaling pathway and Spm in *A. thaliana*.

   3.1. To confirm the activation of the Fe deficiency signaling pathway after exogenous spermine treatment, as observed in RNA-seq analyses.

   3.2. To determine whether Fe supplementation ameliorates the inhibitory effect of exogenous Spm on growth.

   3.3. To investigate whether exogenous Spm treatment induces coumarin production as observed in Fe deficiency conditions.

   3.4. To compare the gene expression of wild type and *spms* seedlings under Fe deficiency conditions.

Materials and Methods

1. Plant material and growth conditions

1.1 Plant Material

Seeds of *A. thaliana* accessions used in this study were obtained from the Nottingham Arabidopsis Stock Center (https://arabidopsis.info) or, in the case of *spmi* (*spermine insensitive*) mutants, obtained by the author.

1.2 Plant growth on soil

Seeds from *A. thaliana* (Col-0) were directly sown on soil containing perlite (10%), peat moss (40%) and vermiculite (50%). The seeds were vernalized for 2 days to stimulate germination. Germination and growth were conducted at 20-22 ºC under 12 h light / 12 h dark cycles, with a light intensity of 100-125 μmol photons m^{-2} s^{-1} and a relative humidity of 60-70 %.

1.3 Plant *in vitro* culture

To sterilize the seeds, a vapor-phase chlorine method was performed. Approximately 30 seeds per mutant were placed in 1.5 mL microcentrifuge tubes. A 250 mL beaker containing 100 mL of commercial bleach was placed inside a desiccator jar located in a fume hood. The seeds were placed into the desiccator jar. Just before sealing the desiccator jar, 4 mL of 37% (v/v) HCl (hydrochloric acid) were carefully added to the bleach. After 2 h, the seeds were transferred to a sterile laminar hood for an additional hour to remove any remaining vapors. Once the vapors were eliminated, the microcentrifuge tubes were closed, and the sterilized seeds were ready to use.

We also sterilized seeds using liquid-phase commercial bleach method, which resulted in better inhibition of fungal growth. The method involved placing approximately 30 seeds per mutant in 1.5 mL microcentrifuge tubes. In a laminar hood, 1 mL of a previously prepared 50% (v/v) bleach solution was added to each microcentrifuge tube, which was then closed and shaken for 10 min. The 50% (v/v) bleach solution was prepared by diluting commercial bleach with distilled water (dH_2O) and adding 0.05% (v/v) Tween 20 detergent. After 10 min, the bleach solution was removed from the microcentrifuge tubes using a micropipette, and 1 mL of sterile dH_2O was added to each tube to rinse away the bleach. The tubes were closed and inverted to mix the contents. Once the seeds had settled to the bottom of the microcentrifuge tube, the solution was carefully removed by pipetting. This process was repeated six times to ensure complete removal of the bleach. Finally, 1 mL of 0.1% (w/v) sterile agarose solution was added to each tube, and the sterilized seeds were ready to use.

Sterilized seeds were then sown on ½ Murashige and Skoog medium (MS) supplemented with vitamins and including MES (2-(N-morpholino)ethanesulfonic acid) buffer (500 mg/L) (Duchefa Biochemie, cat. No. M0255), 1 % (w/v) plant agar (Duchefa Biochemie, cat. No. P1001) and adjusted to pH 5.7 with 1 M KOH (potassium hydroxide). To synchronize germination, the seeds were stratified in the dark at 4° C for 2–3 days. Plates were incubated in 16 h light / 8 h dark cycles at 20-22 °C with a light intensity of 100–125 µmol photons m^{-2} s^{-1}. For root measurement assays and coumarin production analysis, the seedlings were grown in vertical plates.

Culture media

To assess coumarin production, the MS medium was supplemented with 1% (w/v) sucrose. However, when the seedlings were transferred to the different treatments, sucrose was removed.

For Fe deficiency treatment, the MS medium was prepared by adding the reagents one by one, excluding FeNaEDTA (ethylenediaminetetraacetic acid, ferric-sodium Salt), which corresponds to the Fe supply (**Table 1**).

Table 1. Murashige and Skoog (MS) composition for Fe deficiency treatments.

	mg/l	µM		mg/l	µM
Micro Elements					
$CoCl_2.6H_2O$	0.025	0.11	KI	0.83	5
$CuSO_4.5H_2O$	0.025	0.1	$MnSO_4.H_2O$	16.9	100
FeNaEDTA	0	0	$Na_2MoO_4.2H_2O$	0.25	1.03
H_3BO_3	6.2	100.27	$ZnSO_4.7H_2O$	8.6	29.91
Macro Elements					
$CaCl_2$	332.02	2.99	$MgSO_4$	180.54	1.5
KH_2PO_4	170	1.25	NH_4NO_3	1650	20.61
KNO_3	1900	18.79			
Vitamins					
Glycine	2	26.64	Pyridoxine HCl	0.5	2.43
myo-Inositol	100	554.94	Thiamine HCl	0.1	0.3
Nicotinic acid	0.5	4.06			
Buffer					
MES	500	2.35			

Stock solutions

The MS medium was supplemented with different treatments depending on the experiment. For treatments involving Spm, a stock solution of 100 mM Spm dissolved in 5 mM MES buffer at pH 5.7 was prepared. In treatments related to Fe supplementation, a stock solution of 10 mM Sequestrene 138 Fe G100 (Syngenta), dissolved in dH_2O, was prepared. Additionally, we prepared a stock solution of 10 mM AVG ((S)-trans-2-Amino-

4-(2-aminoethoxy)-3-butenoic acid hydrochloride) (Sigma-Aldrich, cat. No. A6685), dissolved in dH_2O, for ethylene synthesis inhibition assay.

2. Analysis of ribosome profiles

Ribosome fractions from infiltrated *A. thaliana* (Col-0) wild type were prepared as described in (Firmino et al., 2020).

2.1. Buffers and Solutions

Pre-ribosome extraction buffer (REB) and stock solutions that are required for the final, ready to use REB (**Table 2**) were prepared in DEPC (diethylpyrocarbonate)-H_2O. All solutions were sterilized in the autoclave and stored at room temperature.

The stock solutions required for REB buffer were the following: 1 M Tris-HCl (tris(hydroxymethyl)aminomethane hydrochloride) pH 9.0, 2 M KCl (potassium chloride), 0.5 M EGTA (ethylene glycol-bis (β-aminoethyl ether)-N,N,N´,N´-tetraacetic acid) pH 8.0, 1 M $MgCl_2$ (magnesium chloride), 20% (v/v) PTE (polyoxyethylene 10 tridecyl ether), and 10% (w/v) DOC (sodium deoxycholate). Detergent mix consisted of 20% (w/v) Brij-35 (polyoxyethylene(23)lauryl ether), 20% (v/v) Triton X-100, 20% (v/v) Igepal CA 630 (octylphenoxy poly(ethyleneoxy)ethanol), and 20% (v/v) Tween 20. This mixture was heated to dissolve it completely.

The above-described stock solutions were combined to obtain pre-REB using volumes and temperatures reported in **Table 2**. Pre-REB was stored at -20 ºC until further use. On the day of extraction, final REB was freshly prepared by adding the following stock solutions: 50 mg/mL cycloheximide dissolved in ethanol, 1 M DTT (dithiothreitol), 0.2 M PMSF (phenylmethylsulfonyl fluoride) dissolved in isopropanol, and 100X PI (protease inhibitor cocktail) (Sigma-Aldrich cat. No. P9559). These solutions were stored at -20 ºC.

The treatments used to infiltrate *A. thaliana* leaves were: 100 μM Put, 100 μM Spm, 1 μM flg22, its combinations (flg22 + Put, flg22 + Spm) and mock (H_2O).

For treatments involving Put and Spm, stock solutions of 100 mM for each polyamine, dissolved in 5 mM MES buffer at pH 5.7 were prepared. In treatments related to flg22 a stock solution of 1 mM dissolved in dH_2O was prepared. These stock solutions were later diluted in dH_2O to achieve the required concentrations for leaf infiltrations.

Table 2. Preparation of ribosome extraction buffer (REB).

Ribosome Extraction Buffer	Chemical Components (Final Concentration)	Stock Solutions (Concentration)	Volume Required for 10 mL	Volume Required for 50 mL	Temperature Conditions
Pre-REB Prepare 10 mL aliquots and store less than 6 months at -20 °C.	DEPC-H_2O	-	-	adjutst to 50 mL	RT
	200 Mm Tris-HCl	1 M	-	10 mL	RT
	200 mM KCl	2 M	-	5 mL	RT
	25 mM EGTA	0.5 M	-	2.5 mL	RT
	35 mM $MgCl_2$	1 M	-	1.75 mL	RT
	1% (*v/v*) PTE	20% (*v/v*)	-	2.5 mL	RT
	1% (*v/v*) DOC	10% (*v/v*)	-	5 mL	RT
	1% (*v/v*) Detergent mix	20% (*v/v*) DEPC-H_2O 20% (*v/v*) Brij-35 20% (*v/v*) Triton X-100 20% (*v/v*) Igepal CA 630 20% (*v/v*) Tween 20	-	2.5 mL	45ºC
Final REB Prepare freshly at day of use	50 µg/mL Cyclohexamide	50 mg/mL	10 µL	-	4 °C
	5 mM M DTT	1 M	50 µL	-	4 °C
	1 mM PMSF	0.2 M	50 µL	-	4 °C
	1X PI	100X	100 µL	-	4 °C

2.2. Extraction of Ribosome Complexes

5-week-old wild type leaves of *A. thaliana* were infiltrated with 100 µM Put, 100 Spm µM, 1 µM flg22, its combinations (flg22 + Put, flg22 + Spm) and mock (H_2O). After 24 h, leaves were harvested, shock-frozen in liquid nitrogen and homogenized.

~100 mg FW (fresh weight) of frozen and grinded plant tissue was mixed with pre-cooled, freshly prepared final REB (1.4 mL) by pipetting. This and all the following steps were performed on ice at 4 °C. The samples were incubated for 20 min with periodic resuspension by pipetting. To separate the debris, the supernatant was centrifuged for 20 min at maximum speed and 4 °C. The supernatant was loaded onto a lilac QI shredder mini spin column (Qiagen, Hilden, Germany), and centrifuged again 2 min at maximum speed and 4 °C. Since the supernatant volume was bigger than the column capacity, two columns were used per replicate. The eluate was loaded on previously prepared sucrose gradients.

2.3. Preparation of Sucrose Gradient Solutions

Sucrose density gradients were (**Table 3**) preserved at -80 °C until use. To prepare the sucrose gradient solutions, the following stock-solutions (convenient stock-volumes in square brackets) were necessary: a 10X salt and buffer solution [100 mL] that contained 20 mL of 2 M Tris-HCl, 10 mL of 2 M KCl, and 20 mL of 1 M $MgCl_2$ (**Table 2**). Once the pH was adjusted to 8.4 with 1 M HCl, the final volume of 100 mL was reached by the addition of ddH_2O (double-distilled water). The solution was then autoclaved and stored at room temperature.

Sucrose (2 M) was dissolved in water by heating below 50 °C. The resulting solution was then filtered using a 0.22 µm pore sterile filtration unit (Neolab, Heidelberg, Germany)

and stored at room temperature. Prior to gradient assembly, four gradient solutions were prepared, each with a different concentration of sucrose: 15% (w/v), 30% (w/v), 45% (w/v), and 60% (w/v). The volumes required of the 2 M sucrose stock-solution, the 10X salt and buffer solution, ddH_2O, and cycloheximide for each of the different sucrose gradient solutions are listed in **Table 3**. These volumes are sufficient to make 3.6 mL of sucrose gradient.

Table 3. Preparation of 15% to 60% (w/v) sucrose gradients in ultracentrifugation tubes.

Number of tubes (n)	Sucrose gradient solution (%)	2 M Sucrose (mL)	10X Salt and Buffer Solution (mL)	ddH_2O (mL)	Cycloheximide (µL)	Final Volume (mL)	Pipetting Order	Tube volume (mL)
1	60	0.655	0.075	0.02	0.075	0.825	1	0.6
	45	0.985	0.15	0.365	0.15	1.65	2	1.2
	30	0.655	0.15	0.695	0.15	1.65	3	1.2
	15	0.165	0.075	0.51	0.075	0.825	4	0.6

2.4. Assembly of Sucrose Gradients

Sucrose gradients were assembled in 5 mL thin-wall polypropylene ultracentrifugation tubes (Beckman Coulter, Krefeld, Germany, cat. No. 326819). Gradient assembly is the critical step for reproducible separation of ribosome complexes. As the quality of gradient assembly plays a crucial role in the reproducibility of ribosome complex separation, it is important to ensure that the gradients are assembled correctly. To achieve this, all the ultracentrifugation tubes employed were prepared in parallel, using the same 15%, 30%, 45%, and 60% (w/v) sucrose gradient solutions that are best prepared in large volumes.

The four sucrose concentrations steps were pipetted in ascending order, starting with the 60% sucrose gradient solution. The volumes for ultracentrifugation tubes are reported within **Table 3**. After the 60% step, the ultracentrifugation tubes were pre-cooled at -80 °C, transferred to the cold room for subsequent pipetting, and re-frozen 1 h at -80 °C before adding the next concentration step. To ensure accurate and reproducible volume dispensing of the highly viscous solutions, a pre-moistened pipette for each concentration step was used. The first volume from each non-wetted pipette was discarded to achieve consistency. It is important to pipette each concentration step continuously without interruption, while avoiding intermittent thawing of frozen material and hoarfrost deposition between pipetting steps.

2.5. Sample Loading and Ultracentrifugation

The extract of ribosome complexes, that is, the eluate of QI shredder mini spin columns (1.2 mL), was immediately loaded on the prepared sucrose gradients. Prior to loading, the prepared sucrose gradients were taken from -80 °C storage, transferred for 1 h at 37 °C and kept cold at 4 °C to allow diffusion and formation of a continuous gradient. Any abrupt movement or vibration while handling the thawing and thawed tubes was avoided to minimize gradient perturbation. The extracts of ribosome complexes or 1.2 mL REB non-sample controls, that is, blanks, were loaded by pipetting onto the top of the thawed sucrose gradients by letting the liquid run slowly down the tube walls. The surface of the sucrose gradients must not be perturbed by rapid, vigorous pipetting. All sample tubes of a run were equally balanced using REB. Ultracentrifugation was done using a SW55Ti rotor (Beckman Coulter, Krefeld, Germany) of 5.0 mL nominal tube capacity. The rotor was swinging-bucket and operated by an Optima L80-XP ultracentrifuge (Beckman Coulter, Krefeld, Germany). The rotor is limited to six buckets per ultracentrifugation run. Each run involved a non-sample gradient overlaid with 1.2 mL REB to ensure that any observed effects can be attributed to the treatments rather than technical artifacts. Since the total number of samples was 24, consisting of four biological replicates of six treatments, and each run could accommodate only six buckets, it was necessary to perform five runs to complete the analysis of all the samples. The first four runs included one biological replicate of each of the five treatments (mock, 100 μM Put, 100 μM Spm, 1 μM flg22, and 1 μM flg22 + 100 μM Spm) and a blank control, while the fifth run included two blank controls and the four biological replicates of the 1 μM flg22 + 100 μM Put treatment. Ultracentrifugation was performed for 1.5 h at 48,000 RPM and 4 °C.

2.6. Fractionation of Sucrose Gradients

After ultracentrifugation, sucrose gradients with separated ribosome complexes were retrieved from the top of bottom-pierced ultracentrifugation tubes. Approximately 250 μL fractions were collected at 0.75 mL min^{-1} flow rate with continuous absorbance measurement at λ= 254 nm using a Brandel BR-188 density gradient fractionation system (Alpha Biotech Ltd, Glasgow, UK). Considering the solvent delay between the UV-detector and fractionator, ~100 s equivalent to 1.25 mL, up to 25 fractions were collected. After completion of fractionation, the collected ~250 μL fractions were stored at -80 °C until further use.

In detail, prior to the sampling of each of the six 15-60% sucrose gradients from a rotor set, the fractionation system was equilibrated. Firstly, a clean ultracentrifugation tube was mounted and filled to about 80% of its volume with a 15% sucrose gradient solution. The tube was pierced at the bottom and the solution was pumped through the system to record an absorbance baseline. Next, a 15-60% sucrose gradient tube was mounted, pierced at the bottom and a high-density chase solution was used to push and empty the gradient from bottom to top. The chase solution, containing 62% (w/v) sucrose in 1X salt and buffer solution, ddH_2O, and 1 μg/mL bromophenol blue, was filtered and stored at 4 °C. Care was taken to avoid air bubbles when mounting the tubes and preparing the fractionation system. Before and after fractionation of each gradient, it was best to clean the system by flushing it in both forward and backward flow mode with at least 10 mL of DEPC-H_2O, without any sucrose.

2.7. Data analysis

The absorbance profiles of 18 samples in total (3 biological replicates per treatment) were exported from the acquisition system, aligned and background subtracted using the blank sample of each centrifugation run. The absorbance profiles were then normalized by the sample weight to obtain the abundances of ribosome fractions, which were measured as background-subtracted peak areas. Finally, the peak areas, the total sum of all peak areas including the 60S, 80S, and polysome fractions, and the 2-way ANOVA statistical test, were determined using RStudio software (https://github.com/MSeidelFed/RandodiStats_package) (Supplementary Information 1).

2.8. Ribosome Fraction Identification

Total RNA extraction of samples was conducted on each of the ribosome fractions that were obtained.

250 μL of TRIzol reagent (Thermo Scientific™ cat. No. 15596026) was added to 20 μL of a single collected fraction, then incubated at room temperature for 10 min. Then 50 μL of chloroform was mixed with the samples by vortex for 10 s and incubated at room temperature for 10 min with subsequent centrifugation at 12,000 *g* at 4 °C for 15 min. During centrifugation time, to improve RNA precipitation, 1 μL of RNase-free glycogen (Thermo Scientific™ cat. No. R0551) was added to new tubes. After centrifugation, the aqueous phase was transferred to the new tubes and, also 200 μL of isopropanol. The samples were thoroughly mixed and incubated at 4 °C overnight. Next day, samples were centrifugated at 12,000 *g* at 4 °C for 15 min. The supernatant was discarded. The pellet

was washed twice with 1 mL of pre-cooled 70% (v/v) ethanol, followed by centrifugation at 12,000 *g* at 4 °C for 5 min.

The extracted RNA samples were loaded onto an agarose gel and analyzed using an Agilent 2100 Bioanalyzer and RNA 6000 nano kit, according to the instructions of the manufacturer (Agilent Technologies, Santa Clara, CA, USA) and previously described in (Firmino et al., 2020). The microfluidic UV-traces were single-sample scaled to assess rRNA composition of each fraction. This process does not support the comparison of rRNA abundances between fractions.

3. Riboproteomic analysis of polysome fractions

The polysome fractions of all samples were used to perform riboproteomic analysis.

3.1. Pelleting of the polysome fractions

The polysome fractions, which had been stored at -80 °C, were thawed on ice. The fractions corresponding to the same sample were then combined in 2 mL Eppendorf tubes and resuspended. Half of the resulting volume (650 µL) was stored at -80 °C for polyamine analysis, while the other half (650 µL) was transferred to ultracentrifugation tubes (1 mL Open-Top Thickwall Polycarbonate Tube, Beckman Coulter, cat. No. 343778). After transferring the polysome fractions to the ultracentrifugation tubes, 350 µL of resuspension buffer (RS) was added to each tube.

To prepare RS buffer, a combination of stock solutions is required. The necessary volumes and temperatures for each stock solution are reported in **Table 4**. Pre-RS buffer was prepared by combining the following stock solutions: 1 M Tris-HCl pH 9.0, 2 M KCl, 0.5 M EGTA pH 8.0, and 1 M $MgCl_2$. The buffer was then stored at -20 °C until further use. On the day of extraction, the final RS buffer was prepared freshly by adding 1 M DTT and 50 mg/mL cycloheximide to the pre-RS aliquots. Due to the number of samples (18), one aliquots of pre-RS were required.

The mixture was then resuspended by gentle pipetting to decrease the concentration of the 60% sucrose gradient. This step allows all polysomes to pellet after ultracentrifugation. Samples were centrifuged at 110,000 *g* at 4 °C for 2 h in an MLA-130 fixed angle rotor (Beckman Coulter, Krefeld, Germany) and an Optima MAX-XP ultracentrifuge (Beckman Coulter, Krefeld, Germany). The rotor is limited to ten buckets per ultracentrifugation run. Since the total number of samples was 18, consisting of three biological replicates of six treatments, it was necessary to perform two runs to complete

the analysis of all samples. After centrifugation, the supernatant was carefully poured down. Briefly, the pellets were dried to remove most of the supernatant by placing them upside down over clean absorbent paper for 30 s to 1 min. To get better dry efficiency, absorbent paper was introduced inside the tubes without reaching the bottom. The polysome pellet has a flat jelly-like appearance at the bottom of the tube. Immediately after tubes were transferred to ice and finally, stored at -80 ºC to further use.

Table 4. Preparation of resuspension buffer (RS).

Resuspension Buffer	Chemical Components (Final Concentration)	Stock Solutions (Concentration)	Volume Required for 10 mL	Volume Required for 50 mL	Temperature Conditions
Pre-RS Prepare 10 mL aliquots and store less than 6 months at -20 ºC.	DEPC-H_2O	-	-	adjutst to 50 mL	RT
	200 Mm Tris-HCl	1 M	-	10 mL	RT
	200 mM KCl	2 M	-	5 mL	RT
	25 mM EGTA	0.5 M	-	2.5 mL	RT
	35 mM $MgCl_2$	1 M	-	1.75 mL	RT
Final RS Prepare freshly at day of use	50 µg/mL Cyclohexamide	50 mg/mL	10 µL	-	4 ºC
	5 mM M DTT	1 M	50 µL	-	4 ºC

3.2. Resuspension for riboprotein dissociation

Centrifuge tubes with RP pellets, which had been stored at -80 ºC, were placed on ice. 60 µL of 6M GuHCl (guanidine hydrochloride), was added to each pellet, resuspended by pipetting, and transferred to 2 mL Eppendorf tubes. Then 1.2 µL of 50% (v/v) TFA (trifluoroacetic acid) was added, and the mix was vortexed. Both 6M GuHCl and 50% TFA were freshly prepared. Samples were centrifuged at maximum speed for 20 min to precipitate and remove the RNA. After centrifugation the supernatant was transferred to a new 2 mL Eppendorf tube and kept at 4 ºC.

3.3. Determination of riboprotein concentration for beads and protease requirements

The determination of RP concentration in each sample was made according to the Pierce™ BCA Protein Assay protocol (Thermo Scientific™, cat. No. 23225). 6 µL from each sample was diluted 1X with RNase-free H_2O to reach a 3M GuHCl concentration and allow compatibility with the Pierce™ BCA Protein Assay. 10 µL of diluted BSA (bovine serum albumin) standards were prepared in triplicate as the blank (3M GuHCl), and H_2O.

Diluted samples were layered in 96 well plates with 200 µL of the working reagent, which had been prepared following the Pierce™ BCA Protein Assay protocol, that was added to each well. Subsequently, the plate was mixed thoroughly on a plate shaker for 30 s. The

plate was then covered with aluminum foil and incubated at 37 °C for 30 min. After cooling to room temperature for 10 min, the absorbance at 562 nm was measured using a plate reader. The average absorbance measurement of the blank replicates was subtracted from all standard and unknown sample replicates. A standard linear regression was fitted by plotting the average blank-corrected 562 nm measurement for each BSA standard against its concentration in μg/mL and it was used to determine the protein concentration of each unknown sample.

The volume of each sample required to obtain 10 μg of protein was calculated and transferred to new 2 mL Eppendorf tubes using a pipette. To standardize protein concentrations across all samples, a mixture of 6M GuHCl and 1% (v/v) TFA was added to each tube up to a final volume of 50 μL. The pH of each sample was then adjusted to 8 by adding 10 μL of 1M TEAB (triethylammonium bicarbonate buffer) (Sigma-Aldrich, cat. No. 15715-58-9) to each tube, and the pH was monitored using pH strips after adding 1 μL of the sample to the strips.

3.4. Reduction, alkylation, and digestion of the riboprotein

To disrupt the tertiary structure of the RPs 1.2 μL of 0.5 M TCEP (tris(2-carboxyethyl) phosphine hydrochloride) (ThermoScientific™, cat. No. H51864) was added to each sample and agitated with an incubator at 800 *g* and 37 °C for 45 min. To perform alkylation, 60 μL of freshly prepared 55 mM IAA (Iodoacetamide) (in 25 mM TEAB) was added and agitated again with an incubator at 800 *g* and 37 °C for 45 min. Since IAA is sensitive to light, the final incubation was performed in the dark.

To prepare for the next step, a working solution of 20 μg/mL SP3 beads (Sera-MagTM SpeedBad Carboxilated-Modified magnetic particles, GE Healthcare, cat. No. 45152105050250 (hydrophilic); 65152105050250 (hydrophobic)) was created following the steps outlined in **Box 1.** Next, 160 μL of neat ACN (acetonitrile) was added to each sample, followed by the addition of the SP3 bead working solution at a 10:1 ratio of beads to protein. Since 10 μg of protein were used, 5 μL of the SP3 bead working solution were added to each sample. The samples were then left to sit for 10 min, mixed by pipetting, and left to sit for an additional 10 min.

Box 1. SP3 bead working solution preparation.

- Remove the beads from the cold room and let them to reach to RT for 10 min, mix to homogenize beads solution.
- Mix 100 µL of hydrophilic beads with 100 µL of hydrophobic beads and add 800 µL of Mili-Q H_2O.
- Wash the beads 3 times with 1mL of Mili-Q H_2O, using a magnetic rack to separate the beads from the supernatant each time. Mix and place the beads back on the rack between washes.
- Add 500 µL of Mili-Q H_2O to the beads and store at a concentration of 20 µg/mL at 4 ºC for up to one month.

Before starting the digestion, the Eppendorf tubes containing the samples were placed on a magnetic rack (DynaMag-2, Life Technologies, cat. No. 12321D,) and allowed to separate for 30 s. Subsequent washing steps were performed quicky without removing the tubes from magnetic rack. Once the protein was bound to the magnetic rack, the supernatant was removed and discarded using a pipette tip with vacuum suction. Next, 1 mL of neat ACN was added to each tube, left to sit for 10 s, and then removed and discarded using a pipette tip with vacuum suction. Finally, 1 mL of 70% (v/v) ethanol was added to each tube, left to sit 10 s, and then removed and discarded using a pipette tip with vacuum suction.

Digestion buffer solution at a 10:1 ratio of digestion buffer (µL) to protein (µg) was added to each sample. Since 10 µg of protein were used, 100 µL of the digestion buffer was added to each sample. The digestion buffer contained Lys-C protease (New England Biolabs, cat. No. P8109S) at a 1:20 ratio of protease (µg) to protein (µg) diluted in 25 mM TEAB. Since 10 µg of protein were used, 0.5 µg of protease were added to each sample. Finally, the samples were incubated at 37 °C by shaking at 200 RPM overnight.

3.5. Peptide wash

2 µL of 50% TFA to reach 1% concentration was added to the samples, mixed and spined for 3 s in a microcentrifuge. Next, magnetics beads were removed by transferring the tubes to the magnetic rack, allowed to separate for 60 s and the supernatant was then transferred to new 2 mL Eppendorf tubes. This step was repeated by transferring the tubes with the supernatant back to the magnetic rack, allowed to separate for 60 s and the supernatant was then transferred to new 1.5 mL Eppendorf tubes. To get rid any residual beads, a centrifugation at maximum speed for 10 min was performed and 80% of the supernatant (80 µL) was transferred to new 1.5 mL Eppendorf tubes. To corroborate that pH was below 3, 1 µL of each sample was added to a pH strip.

To perform the washes, SPE cartridges (Waters, cat. No. 186000383) were mounted (one per sample) in a vertical manner with the help of a stander and glue tape. First, the SPE cartridges were washed with 1 mL of 80% of ACN (v/v) with 0.1% (v/v) TFA and the flow through was allowed to be release by gravity and discarded. Two more washes were performed with 1.2 mL of 0.1% TFA and the flow through was discarded. Samples were loaded to bind the peptides to the membrane. The bound peptides were washed with 1.5 mL of 0.1% TFA. 1.5 mL Eppendorf tubes were mounted below each SPE cartridge, and the peptides were collected by eluting with 800 μL of ACN with 0.1% TFA. To evaporate all the ACN, speed-vac at room temperature was performed, this was when the volume was approximately 160 μL (20% of initial volume). The samples were frozen at -80 °C for one hour and then freeze-dried for 3 hours or until tubes are dry.

3.6. Data Analysis

LC-MS/MS (liquid chromatography–mass spectrometry) analysis was performed at the Department of Agriculture and Water Resources of The University of Melbourne (Australia) with Spectronaut software version 16.2.220903.53000. We analyzed intensity based absolute quantification peptide values (IBAQ) across all samples. Peptides were annotated with *A. thaliana* FASTA files obtained from the UniProt database that contained 15,893 proteins reviewed in the Swiss-Prot subsection. Peptides that were identified as contaminants, those identified solely by site, and those identified from the redundant and reversed database were removed and an IBAQ matrix was created using RStudio software. All subsequent analyses were performed with RStudio software (**Supplementary Information 2**). The IBAQ abundance of each 40S SSU RP was normalized to the sum of abundances of all 40S SSU proteins and the IBAQ abundance of each 60S LSU RP was normalized to the sum of abundances of all 60S LSU proteins in order to be able to analyze RP sub-stoichiometries in the ribosomal complex. After normalization, a new matrix was generated by combining the normalized abundance values of 40S SSU RPs and 60S LSU RPs. To test for significant varying RPs within the treatments, ANOVA test was applied. The resulting data was visualized using volcano plots, which enabled a rapid and easy identification of the statistically significant RPs.

3.7. Spatial analysis

Structural work was done as described in (Martinez-Seidel et al., 2021) using the COSNet$_i$ Python module. The methodology was divided into four steps: (1) initial structural data preprocessing, (2) proximity network building, (3) structural region sampling and definition, and (4) statistical testing of enriched relative changes within structural regions and has been compiled in the GitHub repository COSNet$_i$ (https://github.com/MSeidelFed/COSNet_i).

To further explain the methodology: as preprocessing steps "Hetero atoms" (HETATMs) and duplicate atoms were removed from all proteins. Subsequently, the RP sequences were blasted to verify the correct annotation and renamed according to the last naming scheme (Ban et al., 2014). Next, a proximity network was constructed of protein–protein interactions (based on structural proximity) omitting the rRNA and based on a distance threshold of 8 Å between individual amino acids coarse-grained to their center of gravity. Weights of this network's edges were calculated as the proportion of inter-amino acid residue contacts between two proteins. A higher weight indicated a larger contact surface between two proteins. Networks were visualized using Cytoscape software (**Figure S1**). We sampled random regions from the proximity network defining a walk length and an iteration number. The weight of edges was used as transit probability. A consensus walk from the iteration was calculated and pre-regions defined for every start node. Finally, we calculated the minimum set cover that spans the whole edge universe while minimizing the number of overlapping regions. The Fisher exact test allowed us to test if the selected regions were significantly enriched as compared to the entire ribosome (**Supplemantary Information 3**).

To conclude the methodology, structural visualization of the ribosome was enabled via PyMol software version 2.5.4.

4. Polyamine analysis

Polyamines were analyzed by high-performance liquid chromatography (HPLC) separation of dansyl chloride-derivatized polyamines as described previously (Marce et al., 1995) with some modifications.

4.1. Polyamine extraction

Polyamines were extracted from different types of samples: total tissue, ribosome fractions corresponding to 60S subunit and 80S subunit, and pelleted ribosome fractions

corresponding to polysomes. Since we had 6 treatments and 3 biological replicates per treatment, the total number of samples in each case was 18.

Total tissue

Frozen and ground plant tissue (~100 mg FW) was mixed with pre-cooled 5% (v/v) PCA (perchloric acid) and vortexed for 30 s. To adjust the volume of 5% PCA to the sample weight, a ratio of 500 µL of 5% PCA per 100 mg of sample was considered. Samples were then incubated on ice for 30 min with the subsequent centrifugation at 12,000 *g* at 4 ºC for 10 min. Next, 100 µL of supernatant was transferred to new 1.5 mL tubes. This step is repeated twice to obtain two technical replications.

To derivatize the samples the following solutions were added: 40 µL of 0.05 mM HTD (1,7-diaminoheptane), used as an internal standard, 140 µL of a saturated solution of calcium carbonate and 300 µL of 5 mg/mL dansyl chloride (in acetone and protected from light). We also derivatized a standard in this step, which contained 100 µL of 5% PCA, 40 µL of 0.05 mM HTD as an internal standard, and 40 µL of 0.05 mM polyamines (Put, Spd, and Spm) to be analyzed, along with 140 µL of a saturated solution of calcium carbonate and 300 µL of 5 mg/mL dansyl chloride. After thoroughly mixing the samples and standard, we incubated them in the dark overnight.

The following day, we extracted the polyamines by adding 500 µL of toluene to each sample, vortexing for 30 s, and spinning at 12,000 *g* at room temperature for 1 min. The mixture was then separated into two phases, and 400 µL of the organic phase (upper phase) was transferred to new 1.5 mL tubes.

The tubes were dried in a speed vacuum system for 2 h and re-dissolved in 800 µL of ACN. We then centrifuged the samples at 12,000 *g* at room temperature for 5 min to eliminate any residual material. Finally, we transferred 750 µL of the supernatant to HPLC vials for analysis.

60S and 80S subunit fractions

Ribosome fractions containing the 60S and 80S subunits, which had been stored at -80 ºC, were selected for polyamine analysis. The polyamine extraction protocol performed in this type of samples was based on the total tissue samples extraction method with some modifications.

Derivatization of fractions for polyamine analysis

Since the fractions were already in solution form, only the standard sample required 5% PCA, with a volume of 250 µL. To derivatize the fractions, the volumes of the previously used solutions were adjusted to match the 250 µL volume of each fraction. This involved adding 40 µL of 0.05 mM HTD, 280 µL of a saturated solution of calcium carbonate, and 450 µL of 5 mg/mL dansyl chloride to each fraction.

Re-dissolving ribosome fractions in ACN

The subsequent steps were carried out in the same manner as previously described for total tissue samples, until the point where the samples needed to be re-dissolved in ACN. If the ribosome subunit was obtained in two fractions, the first dried fraction was resuspended in 800 µL of ACN, and the resulting solution was transferred to the second dried fraction. This ensured that all the subunits were finally diluted in the same volume in one tube.

Pelleted polysome fractions

The samples containing half of the volume (650 µL) of the mixture of polysome fractions, which had been stored at -80 °C, were selected to determine for polyamine analysis.

The samples were thawed on ice and 350 µL of RS buffer was added. The mix was resuspended by gentle pipetting and each sample was transferred to 1 mL ultracentrifugation tubes to pelleting. The pelleting protocol was the same as the one described before (see section 3.1). The pellets were stored at -80 °C until further use.

On the day of the polyamine extraction, the samples were kept on ice and 300 µL of 5% PCA was gradually added to ensure complete dissolution of the pellet. The polyamine extraction protocol was then continued, following the same procedure as described for total tissue samples.

4.2. Polyamine levels determination

The free Put, Spd and Spm levels were determined by high-performance liquid chromatography (HPLC) separation of dansyl chloride-derivatized polyamines. The fluorescence detection was performed at 252 nm. 20 µL Samples were injected into the column (BRISA-LC2, C18) that was previously eluted with 100% ACN and HPLC H_2O. The initial condition was 70% ACN and 30% HPLC H_2O for 4 min. At min 4, the concentration of ACN was elevated up to 100% for 10 min. High concentration of ACN was optimized for Spd and Spm elution, which were strongly retained on the column.

This concentration of ACN returned to the initial condition at minute 10. The column was re-equilibrated during the remaining time.

Polyamine values for each sample were calculated based on the data obtained from the HPLC chromatographs. The formula used for each polyamine can be found in **Table 5.**

Table 5. Formulas used for the calculation of polyamines values.

Polyamine	Formula Calculation	Unit
Put	$44.3085 \times \frac{Area\ Put}{Area\ HTD}$	nmol/g (FW)
Spd	$27.4505 \times \frac{Area\ Spd}{Area\ HTD}$	nmol/g (FW)
Spm	$22.9089 \times \frac{Area\ Spd}{Area\ HTD}$	nmol/g (FW)

4.3. Statistical analysis

Statistical comparisons were conducted for each polyamine (Put, Spd, Spm) in every sample type (total tissue, 60S subunit, 80S subunit, and polysomes) between the treatments. To determine if there were any significant differences, a two-way ANOVA was performed using GraphPad Prism version 8.0.2.

5. Proteomic analysis

Proteomic analysis was performed on 5-week-old leaves of *A. thaliana* (Col-0) wild type and the mutants, *adc1-1* and *spms.*

5.1. Protein extraction

Total protein was extracted from the samples as described in (Y. J. Kim et al., 2013)with some modifications.

We transferred frozen and ground leaves (~200 mg FW) to 2 mL Eppendorf tubes and analyzed 4 biological replicates per genotype, resulting in a total of 12 samples. Next, we added 1 mL of pre-cooled Tris-Mg/NP-40 extraction buffer and 15 µL of 100X PI to each sample. The Tris-Mg/NP-40 extraction buffer was composed of 500 mM Tris-HCl pH 8.3, 2% (v/v) NP-40 detergent, and 20 mM $MgCl_2$. Samples were then centrifuged at 12,000 *g* at 4 °C for 10 min. The supernatant was transferred to new 2 mL tubes, and to eliminate any residual debris, the centrifugation was repeated. The resulting supernatant was transferred to new 2 mL tubes. To precipitate the protein, the clear supernatant was divided into two 2 mL tubes (600 µL + 600 µL), and 1.4 mL of pre-cooled 12.5% (w/v) TCA (trichloroacetic acid) (in acetone) was added. The mixture was thoroughly mixed

and incubated at -20 ºC overnight. The following day, the samples were centrifuged at 12,000 *g* at 4 ºC for 15 min, and the supernatant was discarded. The precipitated protein pellets were washed three times with 2 mL of pre-cooled 80% (v/v) acetone, with subsequent centrifugation at 12,000 *g* at 4 ºC for 5 min. The protein pellets were then resuspended in 100 µL of 7 M urea, and the samples that had been divided were combined again, resulting in a total volume of 200 µL for each sample.

5.2. Determination of protein concentration

The determination of protein concentration in each sample was made according to the Qubit Protein Assay protocol (Thermo Scientific™, cat. No. A50668). 10 µL of Qubit standards and 1 µL of samples were combined with either 190 µL or 199 µL of working solution, resulting in a total of 200 µL solution, and incubated at room temperature for 15 min. Working solution was prepared following Qubit Protein Assay protocol. Then, Qubit 4 fluorimeter (Thermo Scientific™) was used to read the standards and generate a calibration curve. This allowed the protein concentration of the samples to be directly obtained upon reading.

5.3. Protein digestion

20 µg of proteins from each sample were in solution digested as follows: samples were reduced with 200 mM DTT in 50 mM ABC (ammonium bicarbonate) at 32 ºC for 90 min. The samples were then alkylated using 300 mM of IAA in 50 mM ABC and incubated in the dark at room temperature for 30 min. Another round of 200 mM DTT was added to do the quenching, and an appropriate amount of 50 mM ABC was added to dilute the urea to a final concentration of 1M. Digestion was done in two steps: an initial digestion with 1:20 (w/w) trypsin 0.1 µg/µL (Sequence grade modified trypsin, Promega) at 32 ºC for 2 h followed by a digestion with 1:20 (w/w) trypsin 0.1 µg/µL at 32 ºC for 16 h. Finally, the resulting peptide mixtures were acidified with FA (formic acid) and concentrated in a SpeedVac vacuum system (Eppendorf). Peptides were cleaned up with C18 tips (P200 top tip, PolyLC Inc.). Briefly, peptides were loaded in the tip columns (previously washed with 70% (v/v) ACN in 0.1 % (v/v) FA and equilibrated with 0.1% FA) by centrifugation (350 *g* for 2 min). Columns were washed twice with 100 µL 0.1% FA by centrifugation (350 *g* for 2 min) and then peptides were eluted in 2 x 80 µL of 50% ACN / 0.1% FA by centrifugation (350 *g* for 2 min and 900 *g* for 1 min). The peptides were dried-down in Speed Vacuum (Eppendorf) and delivered to IRB Mass Spectrometry and Proteomics Core Facility to perform LC-MS/MS analysis.

5.4. Data analysis

Label-Free Quantification and Database search

Raw data obtained at the IRB Mass Spectrometry and Proteomics Core Facility (Barcelona, Spain) and were processed with MaxQuant software version 1.6.6.0. The spectra were searched using its built-in Andromeda search engine, against the SwissProt *A. thaliana* database (v_220419) including contaminants. The following parameters were used: fixed modifications: carbamidomethylation of cysteins (C); variable modifications: methionine (M) oxidation and deamidation of asparagine and glutamine (NQ); enzyme: trypsin; maximum allowed missed cleavage: 2; match between runs and alignment time window were set to 0.7 and 20 min, respectively. Other non-specified parameters were left as default. For label-free quantification (LFQ), minimum ratio count was set to 1 and both razor and unique peptides were used for quantitation. False discovery rate (FDR) was set to 1% for both protein and peptide spectrum match (PSMs) levels.

Data processing and statistical analysis

Label-free quantitative data was processed using Perseus open software version 1.6.15.0. Perseus was used to obtain the curated protein dataset, which was built by removing from the list of identified proteins, those proteins identified as contaminants, proteins identified only by site, and proteins identified from the redundant and reversed databases. In addition, data were base 2 log transformed, and missing values were excluded unless 3 valid values were present in at least one group. Finally, imputation was done using normal distribution method. To test for significant varying proteins within the study groups, Student's T-test was applied to the curated proteins dataset and absolute fold-changes values calculated.

6. EMS mutagenesis

Seeds of *A. thaliana* (Col-0) wild type were soaked in 1 mg/mL KCl solution shaking at 4°C overnight. After seed imbibition, the solution was discarded, and the seeds were washed with dH_2O. Next, the solution was replaced with a 0.2% (v/v) EMS (ethyl methanesulfonate) solution (Sigma, cat. No. M0880), prepared immediately before use, and incubated on a rocking table for 16 h. Due to its toxicity, steps involving EMS were performed in a fume hood. After 16 hours, the seeds were washed with a 100 mM $Na_2S_2O_3$ (sodium thiosulfate) solution on the rocking table for 15 min. This step was repeated 8 times. Subsequent washes with dH_2O were performed in the same manner as for $Na_2S_2O_3$, and the seeds were then suspended in a 0.1% (w/v) agarose solution for sowing on soil. Approximately 3,000 M1 plants were allowed to self. M2 seeds were collected from a total

of 2,784 M1 plants. M2 plants were grown *in vitro* on ½ MS medium supplemented with 1% (w/v) sucrose and 1% (w/v) plant agar in the presence of 300 μM Spm. The seedlings were then grown under 16 h light / 8 h dark cycles at 20-22 ºC for three weeks to identify mutants that were insensitive to Spm.

7. Whole-Genome sequencing

Genomic DNA from ten selected *spmi* mutants (M4 generation) was extracted from leaves of 5-week-old plants grown on soil at 20-22 ºC under 12 h light / 12 h dark cycles using the CTAB (cetyl trimethyl ammonium bromide) method (Doyle & Hortorium, 1991).

The following solutions necessary for CTAB preparation (**Table 6**) were prepared: 1 M Tris-HCl pH 8.0, 5 M NaCl (sodium chloride), and 0.5 M EDTA (ethylenediaminetetraacetic acid) pH 8.0.

Table 6. Composition of CTAB solution.

	Chemical Components (Final Concentration)	Stock Solutions (Concentration)	Volume Required for 100 mL
CTAB solution	HPLC-H_2O	-	Adjust to 100 mL
	100 mM Tris-HCl, pH 8.0	1 M	10 mL
	140 mM NaCl	5 M	28 mL
	20 mM EDTA, pH 8.0	0.5 M	4 mL
	2 g CTAB	-	-
	1 g PVP-40	-	-

100 mg FW of frozen and ground plant tissue were mixed with 300 μL of CTAB solution in 1.5 mL Eppendorf tubes. To digest RNA, 4 μL of RNase DNase-free (Roche, cat. No. 11119915001) were also added to each sample. The samples were then agitated using an incubator at 1,000 *g* at 65 ºC for 15 min. Next, 300 μL of a phenol- chloroform-isoamyl alcohol mixture (25:24:1 v/v/v) (Sigma, cat. No. 77617) were added to each sample, followed by vortexing and subsequent centrifugation at 12,000 *g* at room temperature for 10 min. The upper aqueous phase of each sample was transferred to new 1.5 mL Eppendorf tubes and combined with 400 μL of 96% (v/v) ethanol and 60 μL of 3 M sodium acetate pH 5.2. The solution was mixed by inverting and incubated at -20 ºC overnight. The next day, the samples were centrifuged at 12,000 *g* at 4ºC for 15 min to precipitate de DNA. The supernatant was then discarded, and 1 mL of pre-cooled 70% (v/v) ethanol was added in each sample, followed by centrifugation at 12,000 *g* at 4ºC for 10 min. The washing step was repeated, and the pellets were air-dried and resuspended in 30 μL of ultrapure H_2O.

DNA quality of each sample was checked on 1% (w/v) agarose gel electrophoresis stained with ethidium bromide. DNA concentration in each sample was determined according to the Qubit dsDNA HS Assay protocol (Thermo Scientific™, cat. No. Q32851) using a Qubit fluorometer (Thermo Scientific™).

Whole-genome sequencing was performed at the Centro Nacional de Análisis Genómico (CNAG, Spain) using Illumina platform. The reads obtained were mapped to the Col-0 reference genome of *A. thaliana* using the CLC Genomics Workbench 21 version 21.0.5 (Qiagen). Mutations were filtered to identify those that resulted in non-synonymous substitutions or alternative splicing. The reliability of these mutations was further assessed by considering parameters such as coverage (the number of reads that covered the region), count (the number of times the mutation appeared in the reads), sequencing quality, and the presence of the mutation in other mutants (**Table S1**). Based on these criteria, a total of 21 genes were identified as potential candidates responsible for Spm resistance.

8. Root growth assays

A. thaliana seeds of gene candidate mutants and wild type were germinated and grown *in vitro* on ½ MS growth medium supplemented with 1% (w/v) plant agar. The medium was further supplemented with different treatments, including Spm (300 µM or 400 µM), Sequestrene 138 Fe G100 (100 µM, 150 µM, or 250 µM final concentration of Fe), a combination of 400 µM Spm with the different Sequestrene 138 Fe G100 conditions, or a mock treatment. The seedlings were then vertically incubated in 16 h light / 8 h dark cycles at 20-22 ºC. After 15 days, pictures were taken using a Canon Rebel Xsi EOS camera with the same settings in manual modus, and the primary root length was measured using ImageJ software (https://imagej.nih.gov/ij/index.html).

To determine if there were any significant differences between the different genotypes, a two-way ANOVA was performed using GraphPad Prism version 8.0.2.

9. Dark growth assays

Seedlings of *A. thaliana* (Col-0) wild type, *ctr1* and *ein3eil1* mutants, were grown *in vitro* on ½ MS growth medium, supplemented with 1% (w/v) plant agar and under different conditions: control (0 µM Spd and 0 µM Spm), 100 µM Spd, 100 µM Spm, 300 µM Spm, or 400 µM Spm. The seeds were stratified in the dark at 4º C for 2–3 days, and the plates were covered with aluminum foil. The seedlings were then incubated in the dark at 20-

22 °C. After 15 days, pictures were taken using a Canon Rebel Xsi EOS camera with the same settings in manual modus.

To determine if there were any significant differences in the hypocotyl length between the different genotypes, a two-way ANOVA was performed using GraphPad Prism version 8.0.2.

10. Ethylene synthesis inhibition assays

Seedlings of *A. thaliana* (Col-0) wild type were grown *in vitro* on ½ MS growth medium, supplemented with 1% (w/v) plant agar and either 400 µM Spm, 10 µM AVG, a combination of both, or a mock treatment. The seedlings were then incubated under 16 h light / 8 h dark cycles at 20-22 °C. After 15 days, pictures were taken using a Canon Rebel Xsi EOS camera with the same settings in manual modus.

To determine if there were any significant differences in the main root length between the different treatments, a two-way ANOVA was performed using GraphPad Prism version 8.0.2.

11. Quantification of hydrogen peroxide

Seedlings of *A. thaliana* (Col-0) wild type and gene candidate mutants were grown *in vitro* on ½ MS growth medium supplemented with 1% (w/v) plant agar and either 300 µM Spm, 400 µM Spm, or a mock treatment. The seedlings were then incubated in 16 h light / 8 h dark cycles at 20-22 °C for 15 days.

Frozen and ground seedling tissue (~30 mg FW) was mixed with 1 mL of pre-cooled PBS (phosphate buffered saline) at pH 6.5 in 1.5 mL Eppendorf tubes. The mixture was then centrifuged at 10,000 *g* at 4 °C for 10 min. Next, 700 µL of supernatant was transferred to new 2 mL microcentrifuge tubes and combined with 700 µL of pre-cooled and light-protected 0.1% (w/v) titanium tetrachloride ($TiCl_4$) dissolved in 20% (v/v) of sulfuric acid. The solution was vortexed and centrifuged again at 10,000 *g* at 4 °C for 10 min. After centrifugation, 1 mL of supernatant was transferred to new 2 mL microcentrifuge tubes, and the absorbance at 410 nm was measured using a spectrophotometer. A blank was prepared containing 500 µL of PBS at pH 6.5 and 500 µL of 0.1% $TiCl_4$. A standard curve was generated by measuring the absorbance at 410 nm for different concentrations of H_2O_2. The different H_2O_2 concentrations were prepared by mixing different volumes of a 1mM H_2O_2 stock solution with 0.1% $TiCl_4$ to reach a final volume of 1 mL.

To determine if there were any significant differences between the different genotypes, a two-way ANOVA was performed using GraphPad Prism version 8.0.2.

12. RNA sequencing gene expression analyses

Seedlings of *A. thaliana* (Col-0) wild type and gene candidate mutants were grown *in vitro* on ½ MS growth medium supplemented with 1% (w/v) plant agar. The growth medium was further supplemented with 400 µM Spm, or a mock treatment. The seedlings were then incubated in 16 h light / 8 h dark cycles at 20-22 ºC. After 21 days of growth, three biological replicates per treatment were collected for total RNA extraction. Each biological replicate consisted of three seedlings.

Total RNA was extracted by adding 1 mL of TriZol (Thermo Scientific™, cat. No. 10296010) to ground tissue in 1.5 mL Eppendorf tubes. The mixture was vortexed and incubated at room temperature for 10 min. Next, 200 µL of chloroform were added to each sample, vigorously mixed by inverting the tubes, and intubated at room temperature for 5 min. After incubation, the samples were centrifuged at 12,000 *g* at 4 ºC for 15 min. The upper aqueous phase, containing the RNA, was transferred to new 1.5 mL Eppendorf tubes. Then, 500 µL of isopropyl alcohol were added to each sample, mixed by inverting the tubes, and incubated at room temperature for 10 min to precipitate the RNA. The samples were centrifuged again at 12,000 *g* at 4 ºC for 15 min, and the supernatant was discarded. Next, 1 mL of 75% ethanol (v/v) was added to each sample, followed by centrifugation at 7,500 *g* at 4 ºC for 5 min. The supernatant was discarded, and this washing step was repeated. Finally, the RNA samples were air-dried and resuspended in 30 µL DEPC-H_2O.

Total RNA of each sample was quantified according to the Qubit RNA HS Assay protocol (Thermo Scientific™, cat. No. Q32852) using a Qubit fluorometer (Thermo Scientific™). Purity and integrity of the total RNA samples was checked using an Agilent 2100 Bioanalyzer device (Agilent Technologies). Subsequently, RNA samples were further processed by Sequentia Biotech company for library preparation and RNA sequencing using Novaseq 6000. The libraries were prepared using the TruSeq mRNA library preparation kit following the manufacturer's instructions, and each library was paired-end sequenced (2 x 150 bp) on the Ilumina Novaseq platform. Read mapping and expression analyses were conducted using the CLC Genomics Workbench 21 version 21.0.5 (Qiagen). Only significant expression differences (fold-change ≥ 2; Bonferroni corrected $P \leq 0.05$) were considered. Gene ontology analyses were performed using Gene Ontology

resource (GO; http://geneontology.org) and annotations from Araport11 (Carbon et al., 2019; Cheng et al., 2017).

13. Biomass weight assay

A. thaliana seeds of wild type were germinated and grown *in vitro* on ½ MS growth medium supplemented with 1% (w/v) plant agar. The growth medium was further supplemented with different treatments, involving 400 µM Spm, Sequestrene 138 Fe G100 at final concentrations of 100 µM, 150 µM and 250 µM of Fe, combinations of Spm and Fe treatments, or a mock treatment. The seedlings were then incubated in 16 h light / 8 h dark cycles at 20-22 °C. After 15 days of growth, pictures were taken using a Canon Rebel Xsi EOS camera. The camera settings were kept consistent in manual mode to ensure uniformity across the images. Additionally, the seedlings were weighed using a precision balance to measure their weight accurately.

To determine if there were any significant differences between the different genotypes a two-way ANOVA was performed using GraphPad Prism version 8.0.2.

14. Coumarins detection assay

A. thaliana seeds of wild type, *spms*, and *f6'h1*, were germinated and grown *in vitro* on ½ MS growth medium supplemented with 1% (w/v) sucrose and 1% (w/v) plant agar. The seedlings were vertically incubated in a growth chamber under 16 h light / 8 h dark cycles at 20-22 °C. After 8 days, the seedlings were transferred to new plates containing ½ MS growth medium and 1% (w/v) plant agar, supplemented with different treatments: mock, 400 µM Spm, Fe deficiency, or a combination of 400 µM Spm and Fe deficiency.

After an additional 4 days, the presence of coumarins in the seedling roots was detected under UV light at a wavelength of 365 nm. Pictures were taken with a Canon Digital using a Canon Rebel Xsi EOS camera, maintaining the same settings in manual modus.

15. qRT-PCR gene expression analyses

Total RNA of *A. thaliana* tissue of different genotypes and treatments was extracted using 1 mL of TriZol following the previously described method (see section 14).

2 µg of RNA from each sample were treated with 1 µL of DNAse I (Thermo Scientific™, cat. No. EN0521), and 1 µL of DNAse I buffer to digest the DNA. The samples were then incubated at room temperature for 15 min. Following this, the samples were cooled on ice.

Next, 0.5 µL of OligoDT, 0.5 µL of Random Hexamers, and 1 µL of 10 mM dNTP (deoxynucleotide triphosphate) were added to the samples for hybridization. The samples were then incubated at 65 °C for 5 min. Subsequently, the samples were cooled ice.

To synthetize the first-strand cDNA, 4 µL of Superscript IV reverse transcriptase (Thermo Scientific™, cat. No. 18090010), 4 µL of Superscript IV reverse transcriptase buffer, and 1 µL of 100 mM DTT were added to the samples. The samples were then incubated at 50 °C for 20 min followed by an incubation at 80 °C for 10 min to inactivate the reverse transcriptase. The synthesized cDNA was then diluted (1/5) and ready to use.

Quantitative real-time PCR using SYBR Green I dye method was performed on Roche LightCycler 480 II detector system. The PCR conditions consisted of an initial step at 95 °C for 2 min, followed by 40 cycles of amplification (95 °C, 15 s; 60 °C, 30 s; 68 °C, 20 s). Standard curves were performed for quantification. To normalize gene expression *ACTIN2 (At3g18780)* was used as the housekeeping genes. The primer sequences used for gene expression analyses are listed in **Table S2**. qRT-PCR analyses were always performed on three biological replicates.

Results and Discussion

1. Involvement of Polyamines in Ribosome Biogenesis in *A. thaliana*

1.1. RESULTS

1.1.1. Polyamines produce an increase in the abundance of polysome complexes

To determine the effect of polyamines Put and Spm, the PAMP flg22 and its combinations on cytosolic translation, we performed ribosome profile analyses in 5-week-old *A. thaliana* (Col-0) wild type plants at 24 h of treatment with 100 µM Put, 100 µM Spm, 1 µM flg22, 1 µM flg22 + 100 µM Put, 1 µM flg22 + 100 µM Spm, and mock (H_2O).

The sucrose sedimentation gradient used was established to separate non-translating from translating ribosome fractions, and enabled to separate 60S LSU, 80S monosomes, and polysomes fractions. However, 40S SSU fractions remained unresolved. To reduce the presence of chloroplast ribosomes, chloramphenicol, which is typically used to inhibit organelle translation, was eliminated from the REB buffer (**Figure 9**).

Fractions F07 - F25 were selected for comparative UV absorbance analysis. The absorbance profiles were then normalized by the sample weight, aligned, and background corrected by a non-sample control to obtain the abundance of ribosome fractions. To determine any significant differences between the treatments and mock control, two-way ANOVA test was performed on the peak areas and the total sum of all peak areas, which included the 60S, 80S, and polysome fractions. The statistical analysis was conducted using RStudio, and the RandodiStats_package repository on GitHub (https://github.com/MSeidelFed/RandodiStats_package) was utilized (**Figure S2; Supplementary Information 1**).

Microfluidic analysis was conducted on fractions F08 - F22 (**Figure 9**) to assess the rRNA composition. Fractions F08 - F09 exhibited high intensity of 16S rRNA, indicating the presence of chloroplastic 30S SSU. 18S rRNA was also observed, but with lower intensity, indicating the presence of cytosolic 40S SSU. Fraction F10 predominantly contained 18S rRNA. In this fraction, 16S rRNA was still present but with lower intensity, and 23S rRNA began to elute. The rRNAs profiles suggested the presence of small ribosomal subunits that could not be resolved under the sucrose sedimentation gradient employed. Fraction F11 contained 23S rRNA, which indicated the presence of chloroplastic 50S LSU. Accordingly, we assigned fractions F12 - F13 and the respective UV peak to non-translating 60S SLU because of the high intensity of 25S rRNA. Fraction 14 and its corresponding UV peak showed high abundance of 80S monosomes, as evidenced by the presence of both 25 rRNA and 18 rRNA. The subsequent fractions were found to be enriched in polysomes, in which all rRNAs are present.

The analysis revealed no significant differences between the treatments (100 µM Put, 100 µM Spm, 1 µM flg22, 1 µM flg22 + 100 µM Put, 1 µM flg22 + 100 µM Spm) compared to the mock treatment in the abundance of 60S LSU. However, for 80S monosomes, the (flg22 + Spm) treatment showed a significant increase in the abundance compared to the mock treatment. The most pronounced effect was observed in the polysomes, for which all treatments produced a notable increase in their abundance compared to the mock. Among the treatments, the combination (flg22 + Put) and (flg22 + Spm) triggered the greatest increase in polysome abundance, followed by Spm and Put treatments. While flg22 also caused a likely increase in the quantity of polysomes, it was not statistically significant compared to the mock.

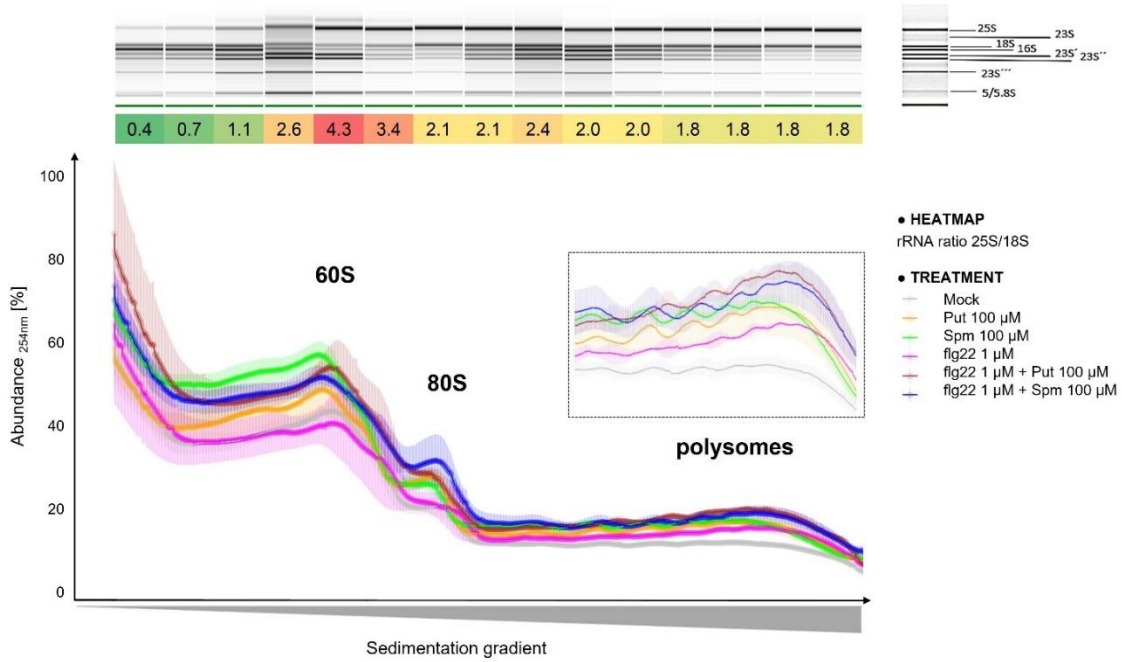

Figure 9. Sucrose density gradient analysis of ribosome complexes from *A. thaliana* leaves collected from plants grown on soil for 5 weeks at 22°C under 12 h light / 12 h dark cycles. Leaves were infiltrated with mock (H_2O), 100 µM Put, 100 µM Spm, 1 µM flg22, 1 µM flg22 + 100 µM Put, 1 µM flg22 + 100 µM Spm and samples collected at 24 h for ribosome profiling. Spectra was obtained by measurement of absorbance at 254 nm. The data was normalized, the peaks aligned, and the background corrected using a blank. The rRNA was examined and labeled using single-sample scaled microfluidic electrophoresis of total RNA, as described by (Firmino et al., 2020). Heatmap was generated to display the ratio of 25S rRNA to 18S rRNA. The eluting fractions of ribosomal 60S, 80S and polysomes are indicated.

According to the analysis, the abundance of polysomes increased in response to polyamines. An increase in polysomes typically implies a greater level of global translational activity, indicating that more translation processes are occurring. However, it is important

to note that the quantity of polysomes alone is not always a reliable indicator of translation efficiency. In certain contexts, the rise in polysomes can be attributed to translational stalling (Faye et al., 2014). In certain contexts, the rise in disomes or trisomes, can be attributed to ribosome collision as a product of stalling.

To determine whether the increase in polysomes was a result of increased translational activity or translational stalling, the rate of translation was calculated (**Figure 10**). The rate of translation is measured using the polysome-to-monosome (P/M) ratio, which is expected to decrease with translation initiation defects and increase with defects in elongation (Pospísek & Valásek, 2013).

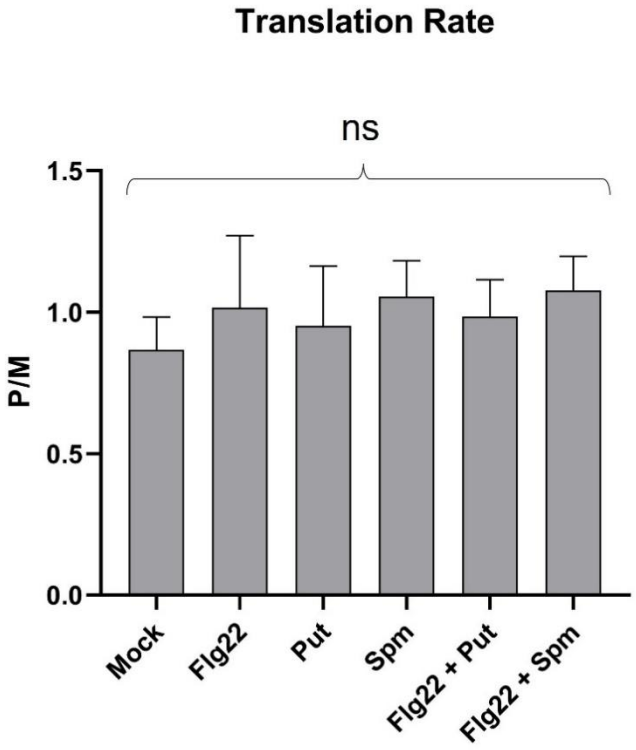

Figure 10. Quantification of translation rate by calculation of the polysome to 80S monosome ratio (P/M) in leaves of *A. thaliana* plants grown on soil for 5 weeks at 22ºC under 12 h light / 12 h dark cycles. Leaves were infiltrated with mock (H_2O), 100 µM Put, 100 µM Spm, 1 µM flg22, 1 µM flg22 + 100 µM Put, 1 µM flg22 + 100 µM Spm and samples collected at 24 h. The data are presented as mean ± SD, with $N = 3$ replicates. Statistical analysis was performed using a one-way ANOVA test against the mock conditions, denoted as follows: * $P \leq 0.05$, ns = non-significant.

The results showed no significant difference in the rate of translation among the treatments (Put, Spm, flg22, (flg22 + Put), and (flg22 + Spm) compared to the mock, indicating that the observed increase in polysomes was associated with enhanced global translational activity rather than elongation inhibition. Additionally, when elongation inhibition occurs, it is commonly observed that an increase in the polysome-to-monosome (P/M) ratio is

accompanied by a decrease in 80S ribosome abundance. However, in our study, (flg22 + Spm) treatment not only did not decrease the abundance of 80S monosomes but also significantly increased it (**Figure 10**). This finding suggested that (flg22 + Spm) treatment had a particularly strong impact on enhancing translational activity compared to the other treatments (Put, Spm, flg22, (flg22+Put)).

Collectively, these findings revealed that polyamines increased the global translational activity, especially the (flg22+Spm) treatment.

1.1.2. Polyamines induce changes in riboproteins binding to polysome complexes

To determine whether polyamines caused changes in the abundance of RPs, we conducted a riboproteomic analysis using the fractions enriched in polysome complexes.

Using LC-MS/MS technique, a total of 148 RPs was detected, of which 111 (75%) corresponded to cytosolic RPs, 35 (24%) to chloroplast RPs and only two (1%) mitochondrial RPs (**Table 7**).

Table 7. Overview of detected RPs in polysome complexes of *A. thaliana* leaves at 24 h of treatment (mock, 100 µM Put, 100 µM Spm, 1 µM flg22, 1 µM flg22 + 100 µM Put, 1 µM flg22 + 100 µM Spm).

	Eukaryotic				Chloroplast			Mitochondrial		
	Total RPs	60S	40s	Total	50S	30S	Total	mtSSU	mtLSU	Total
Identified RPs	148	66	45	111	21	14	35	1	1	2

To identify cytosolic RPs differentially accumulating between the different treatments, we generated a matrix containing the abundance of 60S LSU and 40S SSU proteins in each of the treatments. For this, the abundance of each RP was normalized either to the sum of the abundance of all 60S LSU, or to the sum of the abundance of all 40S SSU RPs, respectively, in order to avoid biases product from differential subunit abundances across experimental conditions. Based on the matrix, a volcano plot was generated for each treatment, which highlighted the proteins showing differential accumulation (**Supplementary Information 2**). Subsequently, we selected the significant RPs that displayed $\log_2$ fold differences in abundance of 0.6 or greater for increased abundance and -0.6 or lesser for decreased abundance.

Among the 45 RPs quantified in 40S SSU, the treatment with Put showed the greatest increase in the abundance of RPs compared to the mock treatment, affecting seven RPs. It exhibited significant differences in two paralogs of eS12 RPs and two paralogs of eS1 RPs, suggesting the importance of these RPs as targets of Put treatment. Put treatment

also increased the abundance of eS7, uS4, and eS17 RPs. The treatments with (flg22 + Spm) and (flg22+ Put) significantly increased the abundance of five RPs compared to the mock. Specifically, (flg22 + Spm) treatment increased eS10, eS30, eS12, eS19, and eS17 RPs, while (flg22 + Put) treatment increased uS17, eS19, eS12, eS17, and eS7 RPs. Flg22 treatment produced significant increases in the abundance of three RPs (uS17, uS10, and eS7). In contrast, no significant changes were observed in RPs of 40S SSU following the treatment with Spm (**Table 8**).

Out of the 66 RPs quantified in 60S LSU, the treatments with Spm, flg22, (flg22 + Put), and (flg22 + Spm) showed a significant decrease in the abundance of eL13 RP compared to the mock treatment. This was the only RP that exhibited a decrease under these treatments. Furthermore, Put, flg22, and (flg22 + Put) treatments increased the abundance of certain RPs compared to the mock treatment. Specifically, Put treatment increased the abundance of three RPs (uL10, eL28 and uL4), while flg22 treatment increased uL3, eL21 and uL13 RPs. The (flg22 + Put) treatment showed a significant increase in the abundance of uL22 RP. However, no significant increases in the RPs of 60S LSU were observed following the treatments with Spm and (flg22 + Spm) (**Table 8**).

Table 8. Detailed list of identified RPs in the polysome complexes which abundance is significantly increased (log2 fold change > 0.6) or decreased (log2 fold change < -0.6) compared to the mock treatment at 24 h of treatment with 100 µM Put, 100 µM Spm, 1 µM flg22, 1 µM flg22 + 100 µM Put, 1 µM flg22 + 100 µM Spm. The list includes the gene identifier (TAIR), subunit origin, ribosomal protein nomenclature, log2 of fold change and *P* value for each treatment relative to the mock. New and old RPs nomenclature was established according to (Ban et al., 2014) The heat map color scale ranges from log2 fold change +3.124 to (red) to -1.397 (blue).

Gene code	Ribosome	Subunit	New RP names	Old RP names	log2 Fold change Put vs Mock	p value Put vs Mock	log2 Fold change Spm vs Mock	p value Spm vs Mock	log2 Fold change flg22 vs Mock	p value Flg22 vs Mock	log2 Fold change flg22 + Put vs Mock	p value Flg22 + Put vs Mock	log2 Fold change flg22 + Spm vs Mock	p value Flg22 + Spm vs Mock
AT2G32060	cytosolic	40S	**eS12**	RPS12C	**1.883**	**0.017**	1.423	0.109	1.376	0.126	**1.753**	**0.031**	**1.976**	**0.011**
AT5G61170	cytosolic	40S	**eS19**	RPS19C	1.277	0.175	1.186	0.220	1.357	0.139	**1.871**	**0.019**	**1.802**	**0.027**
AT2G19750	cytosolic	40S	**eS30**	RPS30A	1.915	0.078	1.607	0.181	0.795	0.619	1.918	0.078	**2.183**	**0.030**
AT5G52650	cytosolic	40S	**eS10**	RPS10C	1.910	0.248	2.093	0.198	0.140	0.947	2.404	0.127	**3.124**	**0.032**
AT2G04390	cytosolic	40S	**eS17**	RPS17A	**0.864**	**0.015**	0.596	0.103	0.367	0.336	**1.118**	**0.002**	**0.751**	**0.036**
AT4G30800	cytosolic	40S	**uS17**	RPS11B	1.477	0.228	1.783	0.108	**2.619**	**0.003**	**2.050**	**0.045**	1.989	0.056
AT5G16130	cytosolic	40S	**eS7**	RPS7C	**1.240**	**0.014**	0.912	0.089	**1.554**	**0.002**	**1.043**	**0.046**	0.983	0.063
AT1G15930	cytosolic	40S	**eS12**	RPS12A	**2.468**	**0.030**	1.877	0.173	1.556	0.313	2.134	0.091	2.231	0.068
AT4G34670	cytosolic	40S	**eS1**	RPS3aB	**1.252**	**0.043**	1.025	0.100	0.899	0.160	1.102	0.073	1.073	0.083
AT5G15200	cytosolic	40S	**uS4**	RPS9B	**0.984**	**0.035**	0.479	0.359	0.488	0.349	0.614	0.223	0.630	0.209
AT3G04840	cytosolic	40S	**eS1**	RPS3aA	**1.280**	**0.015**	0.583	0.344	0.345	0.603	0.653	0.280	0.652	0.281
AT5G62300	cytosolic	40S	**uS10**	RPS20C	1.042	0.127	0.498	0.416	**1.938**	**0.026**	0.569	0.357	0.537	0.382
AT5G23900	cytosolic	60S	**eL13**	RPL13D	-0.546	0.066	**-1.019**	**0.026**	**-1.171**	**0.017**	**-1.397**	**0.009**	**-1.000**	**0.028**
AT3G09630	cytosolic	60S	**uL4**	RPL4A	**0.789**	**0.048**	0.717	0.075	-0.281	0.602	0.723	0.072	0.619	0.131
AT1G61580	cytosolic	60S	**uL3**	RPL3B	0.903	0.148	0.863	0.171	**1.393**	**0.014**	0.692	0.295	0.862	0.171
AT2G19730	cytosolic	60S	**eL28**	RPL28A	**0.818**	**0.042**	0.445	0.303	0.691	0.092	0.532	0.209	0.563	0.180
AT1G27400	cytosolic	60S	**uL22**	RPL17A	0.420	0.386	0.528	0.279	0.803	0.105	**1.007**	**0.044**	0.519	0.287
AT5G48760	cytosolic	60S	**uL13**	RPL13aD	0.896	0.054	0.548	0.274	**1.100**	**0.015**	0.368	0.484	0.531	0.291
AT3G09200	cytosolic	60S	**uL10**	RPP0B	**1.468**	**0.032**	0.919	0.245	0.570	0.519	0.513	0.569	0.846	0.295
AT1G57660	cytosolic	60S	**eL21**	RPL21E	0.605	0.285	0.400	0.465	**1.380**	**0.044**	0.539	0.335	0.569	0.311

Overall, the results indicated that polyamines generally enriched the RPs within the polysome complexes. However, there was an exception with eL13 RP located in 60S LSU, which exhibited a significant decrease in abundance under the treatments with Spm, flg22, (flg22+Put), and (flg22 + Spm) compared to the mock treatment. This decrease

suggested that eL13 could be an important target of these treatments. Furthermore, most of the increases induced by the treatments were observed in 40S SSU, with the (flg22+Spm) treatment specifically affecting RPs belonging to 40S SSU. While Put and (flg22 + Put) treatments increased RPs in both 60S SLU and 40S SSU, the majority of the affected RPs belonged to 40S SSU. In contrast, flg22 treatment showed a more heterogeneous effect, modifying the same number of RPs in both subunits. Finally, Spm treatment was the least effective, as it did not produce any significant increase in RPs.

To determine the overlap and specificity of the identified RPs among the treatments, Venn diagrams were generated for the 40S SSU RPs and the 60S LSU RPs (**Figure 11**). The results indicated that certain RPs exhibited increased abundance and were shared between different treatments in the 40S SSU. For example, eS12 and eS17 were increased in abundance in Put, (flg22 + Put), and (flg22 + Spm) treatments; eS19 was increased in (flg22 + Put) and (flg22 + Spm) treatments; eS7 was increased in Put, flg22, and (flg22 + Put); and uS17 was increased in flg22 and (flg22 + Put) treatments. In contrast, specific increases in RPs were observed in certain treatments, such as eS1 and uS4 in Put treatment, eS30 and eS10 in (flg22 + Spm) treatment, and eS10 in flg22 treatment.

In the 60S LSU, all increases in RPs were specific to individual treatments (**Figure 11**). For instance, uL4, eL28 and uL10 were enriched under Put treatment, uL3, uL13 and eL21 under flg22 treatment, and uL22 under (flg22 + Put) treatment. However, it is worth noting that eL13 RP, which exhibited a decrease in abundance, was the only RP that overlapped among the Spm, flg22, (flg22+Put), and (flg22 + Spm) treatments compared to the mock in 60S LSU.

Overall, the results indicated that affected RPs in the 40S SSU showed either overlap between certain treatments or were induced by individual treatments. In contrast, all the affected RPs in the 60S SLU, except for eL13, were induced by individual treatments. Interestingly, the treatment flg22 had a greater individual effect on the affected RPs compared to other treatments. This could be attributed to the fact that 60S SLU had a higher number of RPs affected by individual treatments, and flg22 treatment influenced more RPs in the 60S LSU compared to other treatments (Put, (flg22+Put), flg22+Spm)). As mentioned before, while other treatments (Put, (flg22+Put), flg22+Spm)) predominantly affected RPs in the 40S SSU, flg22 treatment had an equal impact on both subunits.

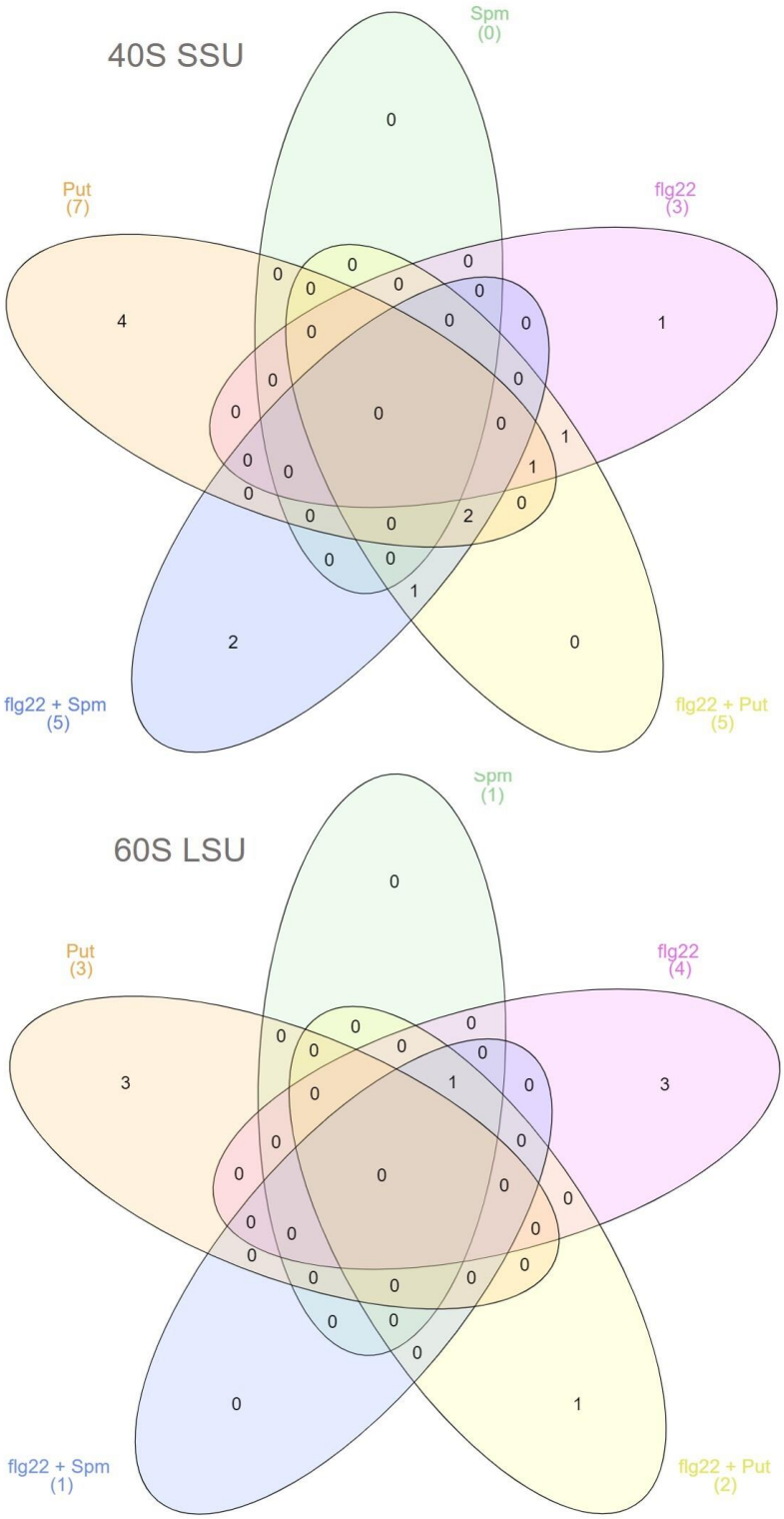

Figure 11. Venn diagrams of RPs of polysome complexes differentially expressed in 100 mg of *A. thaliana* leaves collected from plants grown on soil for 5 weeks at 22ºC under 12 h light / 12 h dark cycles at 24 h of treatment (mock, 100 µM Put, 100 µM Spm, 1 µM flg22, flg22 + Put, flg22 + Spm). The above Venn diagram corresponds to RPs belonging to 40S SSU and the below Venn diagram to the ones belonging to 60S LSU.

Collectively, these findings demonstrated that polyamines generally enriched RPs predominately located in 40S SSU, with Put treatment being the most effective and the Spm treatment being the least effective compared to the mock treatment. Additionally, the affected RPs can be induced by either several or individual treatments, with the flg22 treatment having a greater individual effect. Finally, it is worth noting that eL13 RP was the only RP that exhibited a decrease in abundance under the Spm, flg22, (flg22 + Put), and (flg22 + Spm) treatments, suggesting that it could be an important target for these treatments.

1.1.3. Increases in RP abundance induced by polyamines are confined to specific regions of the ribosome

To investigate whether the changes in RPs identified in the polysome complexes at 24 h of treatment were confined to specific ribosomal regions, we utilized the methodology described in the GitHub repository COSNet$_i$ (https://github.com/MSeidelFed/COSNet_i). The test employs a random walk algorithm to identify coherent ribosomal regions based on protein-protein interactions within a certain distance and assesses whether the proportion of significantly changed RPs in these regions is different from that of the entire ribosome. The null hypothesis assumes that the significant changes are randomly distributed across the ribosome structure. Thus, the method uses the Fisher's exact test to detect significant differences in the proportion of RPs (**Supplementary Information 3**).

The results evidenced that only treatments with Put and the combination of (flg22 + Spm) led to significant changes of protein abundance in confined regions of the ribosomes (**Figure 12**). Notably, Put modified the protein abundance of RPs at a single region of the 40S SSU, whereas changes in RP abundance triggered by (flg22 + Spm) treatment mapped to two different regions, both of which also located to the 40S SSU, in close proximity to the tRNA and mRNA. This finding was consistent with riboproteomic analysis, which indicated that most of the increased RPs were located to the 40S SSU. Furthermore, (flg22 + Spm) treatment significantly increased RPs belonging to the 40S SSU, and most of the increased RPs in Put treatment were also from this subunit, which explains why these two treatments were observed to modulate specific regions of 40S SSU. While the Put treatment led to an increase in the abundance of seven 40S SSU RPs, affecting a greater number of RPs compared to the (flg22 + Spm) treatment, which affected five RPs (Figure S2), it was observed that the latter treatment had a stronger impact by modifying two regions of the ribosome. In contrast, the Put treatment only affected one region.

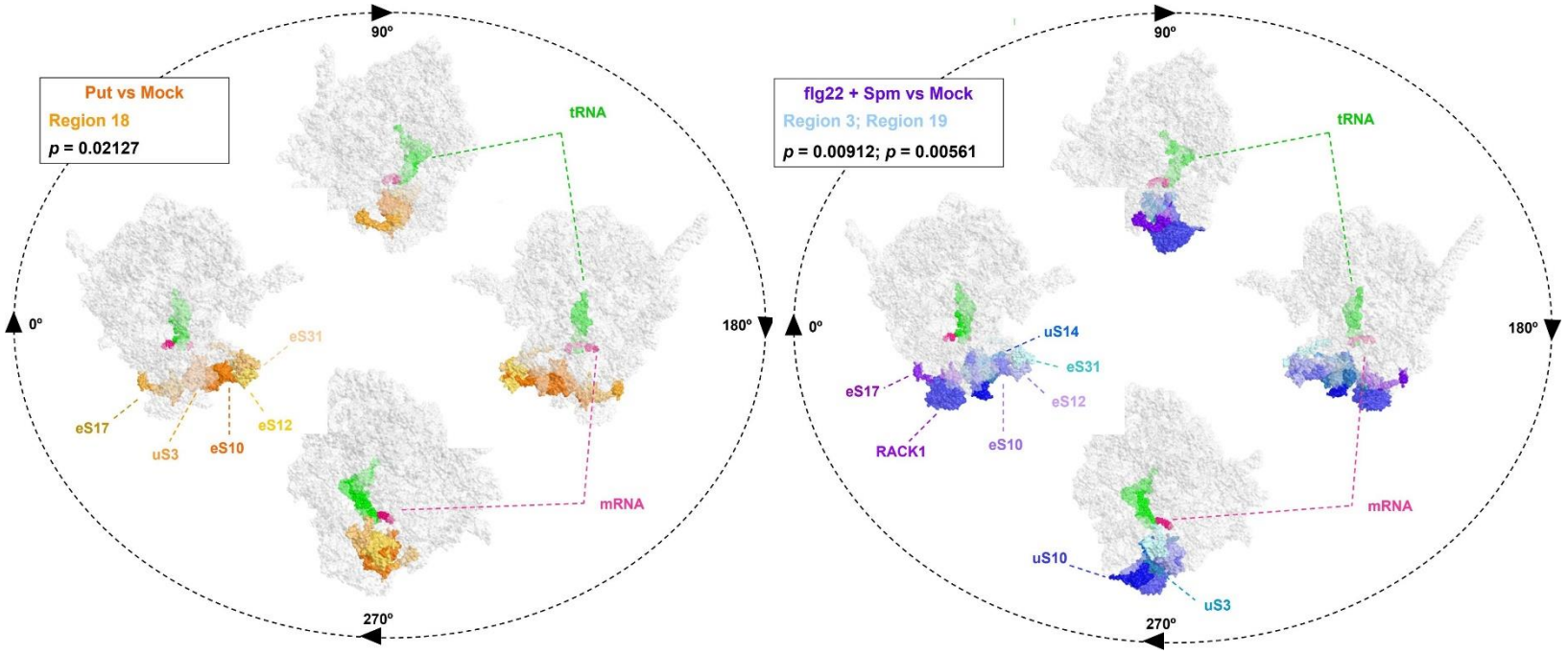

Figure 12. Significantly altered ribosomal regions in the polysome complexes of 5-week-old *A. thaliana* leaves at 24 h of treatment with 100 µM Put (on the left) and 1 µM flg22 + 100 µM Spm (on the right) compared to the mock. These changes were measured in three biological replicates. The figure is a visualization of the random walk sampling results and tested regions of interest detailed in the GitHub repository COSNet$_i$ (https://github.com/MSeidelFed/COSNet_i). Regions with a significantly increased proportion of RP changes, (colored in orange shades for Put and blue shades for flg22 + Spm), as determined by Fisher's exact test (P <0.05) were located in the 40S SSU. The mRNA has been colored pink and the tRNA green to outline its relative location as compared to the region enriched in proteins. Ribosomal structures in the figure are rotated 90◦ in the y-axis at a time to highlight the boundaries of significantly changed regions.

1.1.4. Polyamines are present in the ribosome complexes

In order to investigate whether polyamines bind to ribosome complexes, and if there were differences in the treatments (mock, 100 µM Put, 100 µM Spm, 1 µM flg22, flg22 + Put, flg22 + Spm), we measured polyamine levels (Put, Spd, and Spm) in the 60 SLU, 80S monosomes, and polysome complexes.

First, to determine the effect of the treatments in the cell polyamine concentrations, we analyzed the levels of Put, Spd and Spm in *A. thaliana* leaves at 24 h of inoculation with mock, 100 µM Put, 100 µM Spm, 1 µM flg22, 1 µM flg22 + 100 µM Put, 1 µM flg22 + 100 µM Spm. We detected significant increases in Put levels in Put treatment ($P = 0.05$) compared to the mock, while significant increases in Spm levels were observed in Spm and (flg22 + Spm) treatments, with the latter showing the most significant increase ($P = 0.0140$ and $P = 0.0003$, respectively). No changes in Spd levels were detected in any of the treatments (**Figure 13**). Overall, the results indicated that infiltration with Spm and (flg22 + Spm) resulted in mild increases in Spm levels, leading to physiological concentration increases. Similarly, infiltration with Put also resulted in mild increases in Put levels, although to a lesser extent compared to Spm.

The analysis of polyamines in different ribosome complexes, including 60S SLU, 80S monosomes, and polysomes, revealed distinct patterns. Put was found in all ribosome complexes, while Spm was only detectable in 60S SLU and 80S monosomes. Although Spm was two-fold more abundant than Put in the bulk tissue, the levels of Put were 20-fold higher than Spm specifically in 60S LSU and 80S monosomes. This indicated that ribosome complexes were enriched in Put (**Figure 13**). Spd, the most abundant polyamine in the bulk tissue, was in all ribosome complexes, with comparable levels to Put in 60S LSU and similar levels to Spm in 80S monosomes. However, the amount of Spd detected in polysomes was lower than that of Put.

Among the treatments, the level of Put was significantly higher in 60S LSU in the case of (flg22 + Put) ($P = 0.0346$) and (flg22 + Spm) ($P = 0.0038$) treatments, whereas the level of Spm was significantly higher in 60S LSU in the case of (flg22 + Spm) ($P = 0.0067$) treatment and in 80S monosomes in the case of Spm ($P = 0.0089$) treatment. For Spd levels, Put ($P = 0.0003$), (flg22 + Put) ($P = 0.0001$), and (flg22 + Spm) ($P = 0.0021$) also presented a significant increase in 60S LSU (**Figure 13**).

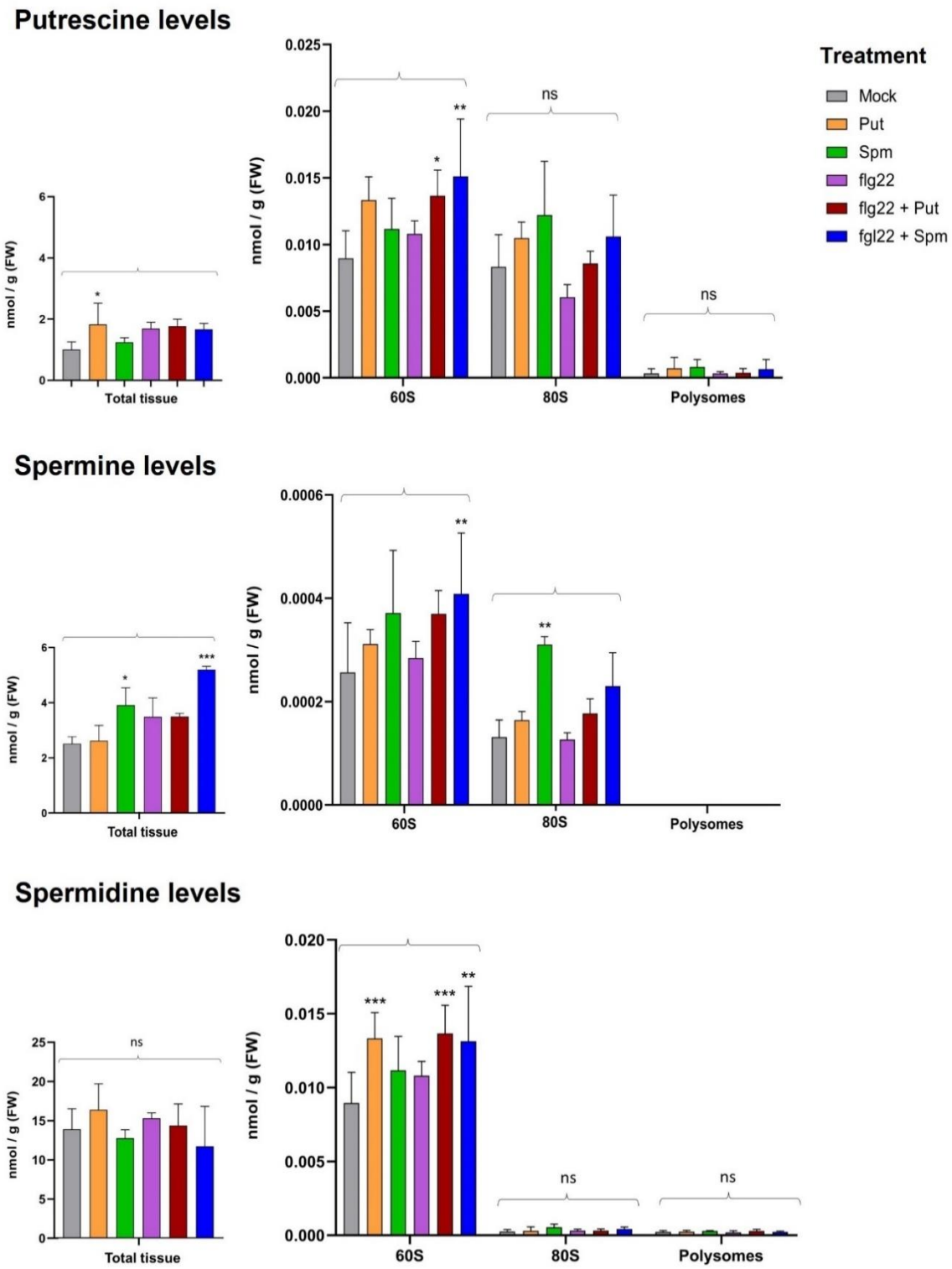

Figure 13. Putrescine (shown above), spermine (shown in the middle) and spermidine (shown below) levels of total tissue, 60S, 80S and polysome complexes from *A. thaliana* leaves collected from plants grown on soil for 5 weeks at 22ºC under 12 h light / 12 h dark cycles. Leaves were infiltrated with mock (H_2O), 100 µM Put, 100 µM Spm, 1 µM flg22, 1 µM flg22 + 100 µM Put, 1 µM flg22 + 100 µM Spm and samples collected at 24 h for polyamine analysis. The data are presented as mean ± SD, with $N = 3$ replicates. Statistical analysis was performed using a two-way ANOVA test against the mock conditions, denoted as follows: ⋆ $P \leq 0.05$, ⋆⋆$P \leq 0.01$, ⋆⋆⋆$P \leq 0.001$, ns = non-significant.

Collectively, these findings demonstrated that Put is the most prevalent polyamine in the ribosome complexes. Interestingly, the association of polyamines with the different ribosome complexes does not appear to be directly related to the detected abundance of these ribosome complexes or the enriched RPs.

1.1.5. Proteomic analysis in polyamine deficient mutants

The data suggested the involvement of polyamines, particularly Put, in plant ribosome biogenesis. To further investigate this possibility, an untargeted proteomic analysis in *A. thaliana* plants deficient in Put (*adc1-1*) and Spm (*spms*) was performed.

Of the 1612 proteins quantified across the three genotypes, 30 proteins displayed fold differences of 1.2 or higher in abundance between *adc1-1* and the wild-type (**Table 9**). Consistent with the previous findings that indicated a correlation between Put and translation, proteins that exhibited significantly higher abundance in *adc1-1* compared to the wild type were found to be enriched in ribonucleoprotein binding complexes (**Figure 14**). In contrast, no such enrichment in ribonucleoproteins was observed in the protein abundances of *spms* mutant when compared to the wild type.

Overall, the proteomics data suggested the involvement of Put but not Spm in plant ribosome biogenesis.

Table 9. List of differentially accumulating proteins (≥ 1.2-fold) between *adc1-1* and the wild type. The list includes the gene identifier (TAIR), the protein identifier, protein description, fold change and *P* value for *adc1-1* and *spms* mutants compared to the wild type. The heat map color scale ranges from fold change 7.85 (red) to 0.67 (blue).

Gene ID	Protein ID	Protein name	Fold change *adc1-1* vs wt	*P* value *adc1-1* vs wt	Fold change *spms* vs wt	*P* value *spms* vs wt
At5g37600	Q56WN1	Glutamine synthetase cytosolic isozyme 1-1	7.85	0.00	0.67	NaN
At4g24930	Q9SW33	Thylakoid lumenal 17.9 kDa protein, chloroplastic	2.33	0.02	0.76	0.66
At5g47210	Q9LVT8	RGG repeats nuclear RNA binding protein C	2.32	0.02	1.45	0.27
At2g24060	O82234	Translation initiation factor IF3-2, chloroplastic	2.27	0.04	1.77	0.19
At1g55210	Q9C891	Dirigent protein 20	2.07	0.02	1.38	0.47
At1g53210	Q8L636	Sodium/calcium exchanger	1.97	0.00	0.96	0.88
At2g33120	P47192	Vesicle-associated membrane protein 722	1.90	0.02	1.03	0.93
At5g66720	Q9LVQ8	Probable protein phosphatase 2C 80	1.86	0.04	1.45	0.35
At1g17745	O04130	D-3-phosphoglycerate dehydrogenase 2, chloroplastic	1.70	0.00	2.21	0.00
At5g03350	Q9LZF5	Lectin-like protein	1.58	0.02	1.18	0.03
At4g29810	Q9S7U9	Mitogen-activated protein kinase kinase 2	1.44	0.00	1.18	0.15
At4g27440	P21218	Protochlorophyllide reductase B, chloroplastic	1.43	0.01	1.22	0.00
At1g23290	Q9LR33	60S ribosomal protein L27a-2	1.41	0.03	0.96	0.82
At3g49010	P41127	60S ribosomal protein L13-1	1.39	0.02	0.97	0.81
At5g28050	Q94BU8	Guanosine deaminase	1.33	0.00	1.12	0.67
At4g38630	P55034	26S proteasome non-ATPase regulatory subunit 4 homolog	1.33	0.01	1.29	0.08
At5g14060	O23653	Aspartokinase 2, chloroplastic	1.32	0.03	1.30	0.03
At2g26540	O48721	Uroporphyrinogen-III synthase, chloroplastic	1.30	0.02	1.27	0.02
At2g45770	O80842	Cell division protein FtsY homolog, chloroplastic	1.27	0.00	1.07	0.49
At5g36160	Q9LVY1	Tyrosine aminotransferase	1.27	0.01	1.35	0.01
At4g19170	O49675	Probable carotenoid cleavage dioxygenase 4, chloroplastic	1.25	0.02	1.11	0.16
At1g17890	Q9LMU0	Putative GDP-L-fucose synthase 2	1.25	0.01	1.37	0.08
At2g21660	Q03250	Glycine-rich RNA-binding protein 7	1.25	0.01	1.31	0.00
At4g14716	Q8GXE2	Acireductone dioxygenase 2	1.23	0.02	1.14	0.07
At3g48170	Q9STS1	Aminoaldehyde dehydrogenase ALDH10A9, peroxisomal	1.23	0.02	1.29	0.00
At2g21280	Q9SJU9	Epimerase family protein SDR39U1 homolog, chloroplastic	1.23	0.05	1.19	0.10
At3g47650	Q9SN73	Protein BUNDLE SHEATH DEFECTIVE 2, chloroplastic	1.23	0.02	1.24	0.04
At3g25770	Q9LS02	Allene oxide cyclase 2, chloroplastic	1.23	0.02	1.19	0.00
At1g49760	Q9FXA2	Polyadenylate-binding protein 8	1.21	0.01	1.04	0.28
At1g59870	Q9XIE2	ABC transporter G family member 36	1.20	0.05	1.13	0.01

A **Differentially accumulating proteins *adc1-1* / wt (≥ 1.2-fold)**

Gene Ontology (GO)		Description	Genes	FDR adjusted *P* value
GO:0043021	F	ribonucleoprotein complex binding	3	0.027
GO:0003729	F	mRNA binding	9	0.046
GO:0016053	P	organic acid biosynthetic process	7	0.004
GO:1901605	P	alpha-amino acid metabolic process	5	0.032
GO:0009536	C	plastid	19	4.96×10^{-8}

B **Differentially accumulating proteins *spms* / wt (≥ 1.2-fold)**

Gene Ontology (GO)		Description	Genes	FDR adjusted *P* value
GO:0003727	F	single-stranded RNA binding	4	0.0035
GO:0004072	F	aspartate kinase activity	2	0.0116
GO:0015995	P	chlorophyll biosynthetic process	5	0.0001
GO:0009628	P	response to abiotic stimulus	15	0.0131
GO:0009536	C	plastid	32	1.62×10^{-14}
GO:0005829	C	cytosol	25	2.27×10^{-8}

Figure 14. Summary of the GO terms associated with the differentially accumulating (≥ 1.2-fold) proteins in *adc1-1* (**A**) and *spms* (**B**) mutants compared to the wild type. GO terms, intersection genes and FDR adjusted *P* value were obtained from g:Profiler web server. (F = molecular function, P = biological process, C = cellular component).

1. Involvement of Polyamines in Ribosome Biogenesis in *A. thaliana*

1.2. DISCUSSION

In this work, we report that polyamines increase the abundance of polysome complexes (**Figure 9**) in *A. thaliana* plants. An increase in polysome abundance is generally associated with increased translational activity, but it can also be attributed to translational stalling (Darnell et al., 2011; Faye et al., 2014; Graber et al., 2013) A recent investigation revealed an increase in ribosome collisions was associated to an increase in polysome abundance and a decrease in 80S abundance, thereby affecting the P/M (Gurzeler et al., 2023). However, our analysis of P/M ratio does not show any significant difference between the polyamine/flg22 treatments (Put, Spm, flg22, (flg22 + Put), (flg22 + Spm)) and the mock treatment (**Figure 10**), suggesting that the observed increase in polysome abundance is the result of a global enhancement in translational activity rather than translational stalling. This finding is consistent with previous studies (Dörner et al., 2022; Hunter et al., 1977; Landau et al., 2010; Mandal et al., 2013; Takeda, 1969) which suggested that polyamines are required for the translation processes at the initiation and elongation steps.

Recent studies conducted in mitochondria, prokaryotes and mammalian cells (Faundes et al., 2021; Han et al., 2022; Sun et al., 2020; Zhou et al., 2022) have proposed a role for Spd in ribosome biogenesis as it serves as a substrate for the hypusination of the translation initiation factor eIF5A. This factor is required to promote peptide-bond formation indicating its involvement in translation elongation of "problematic" codons and supporting the idea polyamines contribute to increase translational activity (Gutierrez et al., 2013).

In agreement with these studies, a "polyamine modulon" has been described in bacteria and mammalian cells that comprises a group of genes whose protein synthesis is generally stimulated by polyamines. Several mechanisms have been identified that explain how polyamines stimulate the synthesis of proteins within the polyamine modulon. These mechanisms include enhancing the translation of inefficient codon UUG or GUG, promoting ribosomal frameshifting or inducing structural changes in the mRNA when Shine-Dalgarno (SD) sequence is distant from the initiation codon AUG (Igarashi & Kashiwagi, 2018). Interestingly, polyamines can repress the translation of specific mRNAs, particularly those encoding proteins involved in the polyamine pathway, such as ODC, antizyme (OAZ), antizyme inhibitor 1 (AZIN1), S-adenosylmethionine decarboxylase (AdoMetDC), and spermine synthase and SSAT1. This suggests that the specific suppression of translation serves as a regulatory mechanism to maintain polyamine homeostasis (Ivanov et al., 2018; Perez-Leal et al., 2012). In the context of plants,

polyamines regulate the translation of *SAMDC* mRNA, providing further evidence for the involvement of polyamines in translation regulation (Hanfrey et al., 2005).

Our study demonstrates that treatments with Put, Spm, (flg22 + Put) and (flg22 + Spm) significantly increase the abundance of polysomes compared to the mock treatment. However, although flg22 treatment also led to increases in polysome abundance, the difference was not statistically significant (**Figure 9; Figure S2**). These findings are in line with a recent study (C. Zhang et al., 2023), which highlighted the transcriptional impact of Put and (flg22 + Put) treatments on ribosome biogenesis in *A. thaliana plants*. Interestingly, in this study flg22 treatment also induced a similar effect. Another recent study investigating the effects of cold exposure on the ribosomal proteome evidenced that altered transcript levels and RP abundances were mainly responsive at 7 days (Martinez-seidel et al., 2021). A longer duration of the treatments may be necessary to observe the transcriptional effect of flg22 on ribosome biogenesis reflected in the translational machinery. Furthermore, regarding Spm and (flg22 + Spm) treatments, it appears that their impact on translation does not rely on transcriptional effects, as no significant changes in ribosome biogenesis were observed with these treatments in the transcriptional analysis conducted by (C. Zhang et al., 2023).

Based on these findings, we propose that polyamines, specifically Spd, play a direct role in translational activity, potentially acting as co-substrates for eIF5A hypusination (Gutierrez et al., 2013) Additionally, they can indirectly support the translation process through various mechanisms discussed earlier (Igarashi & Kashiwagi, 2018; C. Zhang et al., 2023), including the observed increase in polysome abundance described in our study. However, the specific details of these mechanisms remain poorly understood. To gain a deeper understanding of the role of polyamines in translational activity, ribosome profiling (Ribo-seq) might be necessary (Ingolia et al., 2019).

The results of our riboproteomic analysis in polysome fractions reveal that, with the exception of Spm, the treatments (Put, flg22, (flg22 + Put) and (flg22 + Spm) lead to an enrichment of certain RPs compared to the mock treatment (**Table 8**). This observation suggests that Spm may be less effective in promoting the enrichment of RPs compared to the other polyamines and treatments. Notably, among the RPs analyzed, eL13 was the only one that displayed a significant decrease compared to the mock treatment under Spm, flg22, (flg22 + Put), and (flg22 + Spm) treatments. This decrease suggests that eL13 may be a particularly important target of these treatments. However, further research is needed

to determine the specific role of eL13 in this context. A recent study (Z. Shi et al., 2017) revealed that the diversity of RP composition in ribosomes influences their selectivity in translating different subsets of transcripts, including those involved in metabolism processes, cell cycle regulation, and development. Additionally, the loss of specific ribosomal proteins is linked to the translation of stress-specific mRNAs that are needed to respond appropiratly to oxidative stress in yeast (Ferretti et al., 2017). These findings support the notion that polyamine-induce RP substoichiometry can play a role in promoting the translation of specific proteins. It is also consistent with the concept of a "polyamine modulon" mentioned earlier (Igarashi & Kashiwagi, 2018), further supporting the idea of the existence of such a polyamine modulon in plants. Taken together, these findings provide support for our hypothesis that polyamines participate in translational activity through various mechanisms.

The observed pattern indicates that in (flg22 + Spm) treatment, all the increased RPs are from the 40S SSU, whereas in Put and (flg22 + Put) treatments, the majority of increased RPs also belongs to 40S SSU. In contrast, the effect of flg22 treatment is more heterogenous, with increased RPs evenly distributed between the 40S SSU and 60S SLU. This suggest that flg22 treatment behaves differently compared to the other treatments. These findings align with the fact that increased RPs can be induced by either multiple treatments or individual treatments, with the flg22 treatment having a stronger individual effect (**Figure 11).** Furthermore, the affected RPs in Put and (flg22 + Spm) treatments are significantly confined to one (Put) or two specific regions (flg22 + Spm) of the 40S SSU (**Figure 12**). This observation suggests that these treatments have stronger impact on translational activity. However, in the case of (flg22 + Put) treatment, the affected RPs are not significantly confined to a specific region of the ribosome, suggesting that its impact may not be as pronounced as Put treatment alone.

Our analysis of polyamine levels (**Figure 13**) indicates the presence of Put and Spd in the polysome complexes, with Put being significantly more abundant than Spd. These findings are consistent with an earlier report (Cohen & Lichtenstein, 1960) that identified Spd and Put as the major polyamines in *E. coli* ribosome complexes. Interestingly, we did not observe significant differences in the levels of Put and Spd among the treatments (Put, Spm, flg22, (flg22 + Put), and (flg22 + Spm)) compared to the mock treatment. This suggests that the association of polyamines with the different ribosome complexes is not directly linked to the detected abundance of these ribosome complexes or the enrichment of RPs.

Our study also reveals the presence of Put, Spd and Spm in the 60S SLU and in the 80S monosomes. While most high-resolution structures of eukaryotic ribosomes have not explicitly mapped polyamines, our findings align with recent studies (Noeske et al., 2015; Watson et al., 2020) that observed polyamines in the high-resolution electron density of *E. coli* ribosomal structures. Specifically, (Noeske et al., 2015) mapped one Spd near the subunit interface in bridge B3 of the large subunit, and one Put near the base of helix H69 in the 23S rRNA in a 2.4 °A structure of *E. coli* 70S ribosome. (Watson et al., 2020) identified 17 polyamine moieties, including a cluster of Spd in the 50S subunit, in a 2.0 ° A structure of *E. coli*. Additionally, cross-linking experiments using a photoreactive analogue of Spm detected Spm in both the 30S and 50S subunits of mature *E. coli* ribosomes (Amarantos et al., 2002; Xaplanteri et al., 2005). However, it remains unclear whether the mapped polyamine sites are stably or transiently bound, or whether the occupancy of polyamine binding sites varies in a stochastic manner (Dever & Ivanov, 2018). Moreover, these polyamine positions were determined in structures obtained from ribosomes likely purified with polyamine-containing buffers, so it is yet to be determined whether these positions can be confirmed in structures obtained from ribosomes that encountered polyamines solely within living cells (Dörner et al., 2022).

Our findings provide strong evidence that polyamines bind to ribosomes in plants, suggesting their direct involvement as structural components in translational activity. Notably, we observe significantly higher levels of Put compared to Spm in both the 60S SLU and the 80S monosomes, while Spm is not detected in polysomes. Specifically, the abundance of Put is approximately 20-fold higher than Spm in the 60S SLU, 20-fold higher in the 80S monosomes, and 2-fold higher in polysomes (**Figure 13**). When compared to Spd, the levels of Put are similar in 60S SSLU, 20-fold higher in the 80S monosomes and 2-fold higher in polysomes. These results, combined with the higher abundance of Spm and Spd compared to Put in the bulk tissue, indicate that Put is the predominant polyamine present in ribosome complexes in *A. thaliana*.

One possible explanation for this observation is that Spm may be required in smaller amounts than Put to facilitate translation, which aligns with previous *in vitro* studies conducted in *E. coli,* where spermine was found to be the most effective polyamine in promoting cell growth (Xaplanteri et al., 2005). However, based on the results obtained in this study, it is also plausible to consider that Put is the predominant polyamine, as it appears to have stronger impact on the translational machinery compared to the other

polyamines. Furthermore, although certain treatments led to a significant increase in polyamine levels in the 60S SLU or 80S monosomes, the overall distribution pattern of polyamines remained similar across all treatments compared to the mock, indicating that polyamines do not bind to ribosome complexes in a stochastic manner. However, given the limited understanding of polyamine binding sites on ribosomes, it is important to interpret these results with caution.

Collectively our findings strongly suggest that the (flg22 + Spm) treatment has an important impact in translational activity. Specifically, it increases the abundance of RPs confined to two specific regions of the 40S (**Figure 12**), accompanied by a significant increase in the abundance of 80S monosomes and polysomes (**Figure 9**; **Figure S2**) as well as elevated levels of polyamines (Put, Spd, and Spm) in 60S SLU (**Figure 13**). Similarly, the Put and (flg22 + Put) treatment are also implicated in influencing translation. In conjunction with the transcriptional effects on ribosome biogenesis (C. Zhang et al., 2023), our results reveal an increase in polysome abundance (**Figure 9**; **Figure S2**), and the enrichment of several RPs (**Table 8**). However, unlike the Put treatment alone, the RPs affected by the combination treatment are not significantly confined to a specific region of the ribosome (**Figure 12**), suggesting that the impact of the (flg22 + Put) treatment may not be as pronounced as Put treatment alone. Furthermore, our proteomic analysis in the *adc1-1* mutant further supports the involvement of Put in translation (**Figure 14**).

In contrast to our findings regarding Put, our results indicate that Spm treatment is the less effective in influencing translational activity. While Spm treatment leads to an increase in polysome abundance (**Figure 9**), it does not significantly enrich polysome RPs compared to the other treatments (**Table 8**). Moreover, our proteomic data from *spms* mutants did not show a correlation between Spm and ribosome biogenesis (**Figure 14**), supporting the notion that role of Spm in translational machinery is less determinant than the role of Put. This contrasts with previous studies that have highlighted the importance of Spm in protein synthesis, particularly in mammalian systems (Peng et al., 2021; H. X. Shi et al., 2022), and one study found that Spm stimulated translation initiation in mammalian mitochondria (Christian et al., 2010). It is worth noting that these studies were conducted in mammalian cells and mitochondria, whereas our study focuses on plants. Furthermore, our observation of significantly higher levels of Spm in the 80S monosomes with Spm treatment compared to the mock (**Figure 13**) raises intriguing possibilities. It would be interesting to analyze the RPs associated with the 80S monosomes under Spm treatment to explore any potential

relationships or effects that may contribute to our understanding of the role of Spm in translational activity.

In summary, this study demonstrates an involvement of Put in the ribosome machinery of plants and suggests that Spm is not as crucial for ribosome biogenesis, as it occurs in animal cells.

2. Identification of Potential Genes Associated with Spermine Resistance in *A. thaliana*

2.1. RESULTS

2.1.1. Identification of mutations associated with spermine tolerance in *A. thaliana*

2.1.1.1. Identification of spermine insensitive (*smpi*) mutants through EMS mutagenesis in *A. thaliana*

To determine potential polyamine receptors, transporters, or TFs associated with polyamine signaling, an EMS population of 3,000 Col-0 wild type *A. thaliana* plants was generated. Col-0 background was used because its genome is sequenced and used as reference, which facilitates mapping through next generation sequencing.

Specifically, a total of 2,784 M1 mutants were obtained, which carried heterozygous mutations. The progeny of these mutants was collected to obtain M2 seeds, where homozygous mutations were segregating. To assess the degree of saturation in the EMS population, an independent calibration by screening visible traits such as albinism was conducted (Y. Kim et al., 2006). The degree of saturation was determined by counting the number of mutants exhibiting albino phenotypes (31 albino mutants) (**Figure 15A**). To calculate the probability of finding at least one mutation in any given gene in the M1 population, a formula derived from a study (Jander et al., 2003) was employed. The formula used was $P = 1 - (1 - F)^N$, where P represented the probability of finding a mutation, F was the mutation frequency per base pair, and N was the number of lines. Based on the mutation frequency of albinos (0.0111), which was calculated by diving the number of identified mutants (31) by the number of plants in the M1 population (2,784), we calculated an almost 100% probability of discovering at least one mutation in any given gene (**Figure 15B; Figure 15C**).

A

B

	Number of plants	Frecuency (*F*)	Probability (*P*)
Albins	31	0.011135057471264	0.999999999999997
M1 population (*N*)	2,784		

C

$$P = 1 - (1 - F)^N = 1 - (1 - 0.011135057471264)^{2784}$$

Figure 15. Establishment of the saturation degree of M1 population by the number of mutants exhibiting albino phenotypes. (**A**) Albino sectors in a M1 mutant. (**B**) Frequency and probability calculation of albino plants in the M1 population. (**C**) Formula employed to calculate the probability of discovering a mutation in any given gene in the M1 population.

The observed probability indicated that the genome of the M1 population reached a sufficient level of saturation, enabling it to be utilized for screening *spmi* mutants.

A previous study conducted in our lab evidenced that exogenously supplied Spm inhibits growth of *A. thaliana* seedlings *in vitro*. We argued that this could be a viable method for identifying potential *Spm insensitive* (*spmi*) mutants associated with Spm perception, transport or signaling.

To determine the optimal Spm concentration in our screen, various concentrations of Spm were tested (100 µM, 200 µM, 300 µM, 400 µM, 500 µM and 0 µM as control). The results showed that Spm inhibits seedling growth at all tested concentrations (100 µM, 200 µM, 300 µM, 400 µM, 500 µM) compared to the control (0 µM) (**Figure 16**). However, at 100 µM and 200 µM Spm, some seedlings escaped from selection after few weeks of growth. Therefore, 300 µM was established as the most reliable concentration to identify *spmi* mutants in the M2 generation.

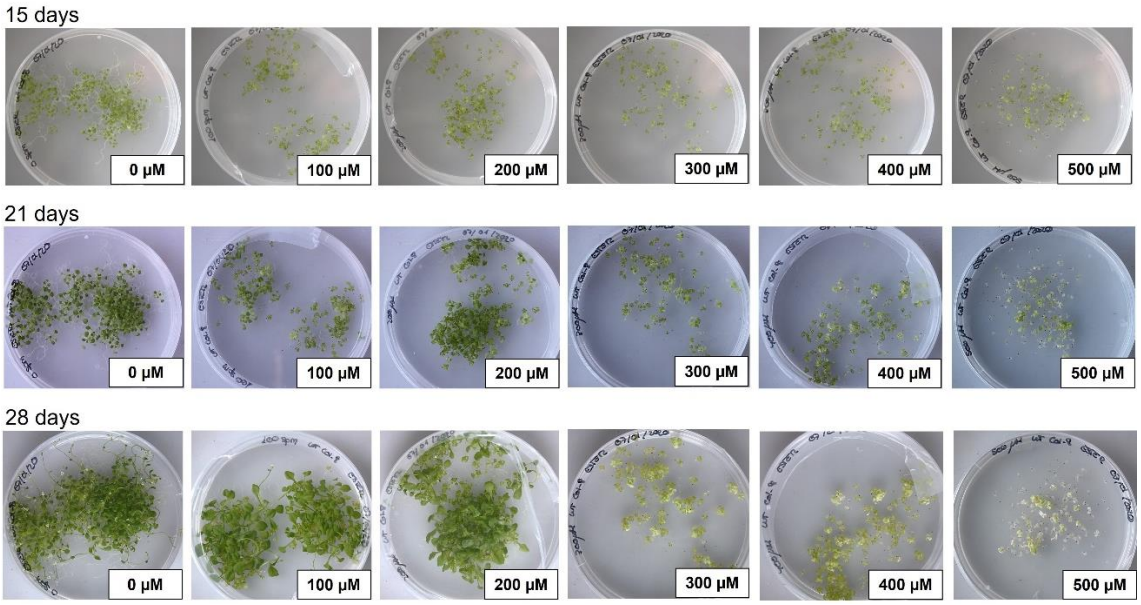

Figure 16. Comparison of growth *in vitro* of Col-0 wild type *A. thaliana* seedlings under different concentrations of Spm (0 µM, 100 µM, 200 µM, 300 µM, 400 µM, and 500 µM). The seedings were cultivated on 1 ½ MS supplemented with 1% sucrose and 1% plant agar. The seedlings were incubated in 16 h light / 8 h dark cycles at 20-22 °C and pictures were taken after 15 days (above), 21 days (in the middle) and 28 days (below).

A total of 107 *spmi* mutants from the M2 generation were identified as resistant to Spm. To further narrow down the number of candidates, the Spm concentration was increased to 400 µM. Interestingly, Spm showed a greater inhibitory effect on seedling growth when sucrose was absent from the culture media (**Figure 17**). Therefore, to further reduce the

number of candidates, in addition to increasing the Spm concentration, sucrose was removed from the media.

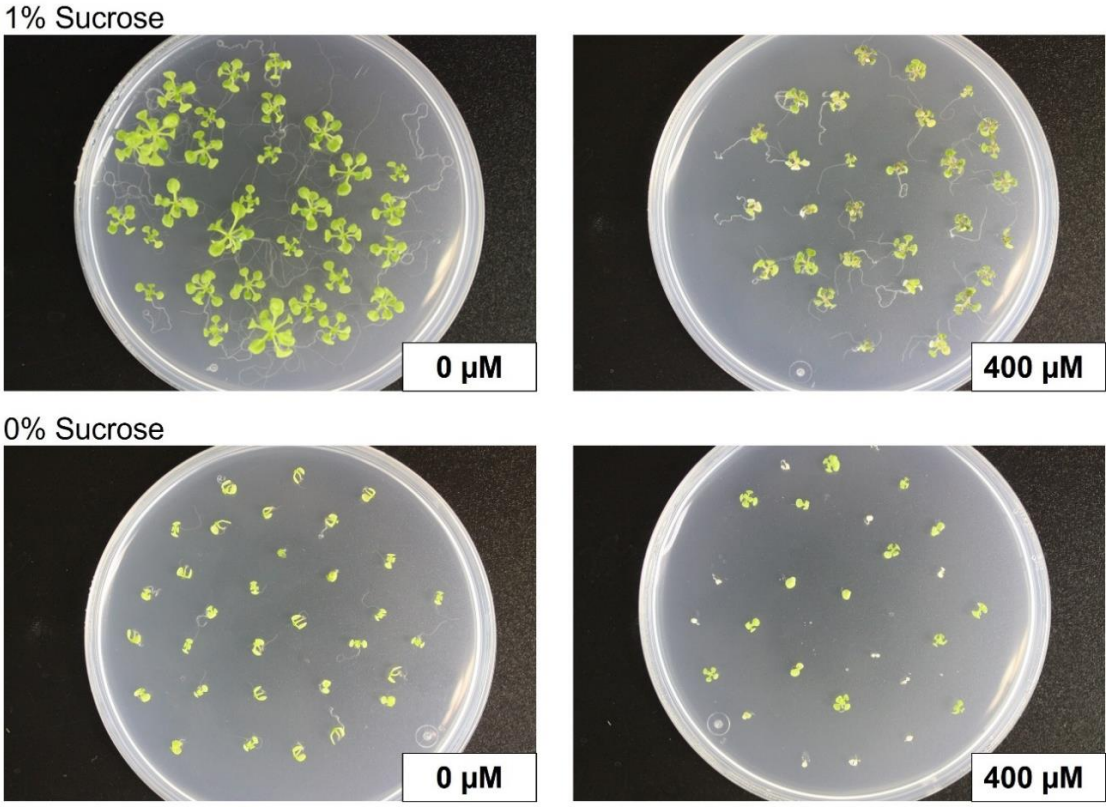

Figure 17. Comparison of growth *in vitro* of Col-0 wild type *A. thaliana* seedlings under supplementation of 400 µM Spm (right) vs 0 µM (left), and with 1% sucrose (above) vs 0% (below). The seedlings were cultivated on 1 ½ MS with 1% plant agar. The seedlings were incubated in 16 h light / 8 h dark cycles at 20-22 °C and pictures were taken after 15 days.

The seeds from these 107 mutants were collected, and the screening process with the implementations was repeated in the M3 generation. After 3 weeks, 19 mutants displaying the highest resistance were identified (**Figure 18**). These mutants were designated as *spmi-1*, to *spmi-19*.

2.1.1.2. Selection of candidate gene mutations underlying spermine insensitivity

Our hypothesis regarding gene mapping was based on the assumption that a subset of the identified mutants would exhibit mutations in the same causative genes. This assumption stemmed from the low probability of observing mutations on the same genes purely by chance. By analyzing the number of mutants sharing mutations in these specific genes, we aimed to increase the likelihood of identifying the genuine mutations responsible for the observed phenotypes. In the M4 generation, DNA from 10 *spmi* mutants (*spmi-1*, *spmi-2*, *spmi-4*, *spmi-5*, *spmi-6*, *spmi-7*, *spmi-8*, *spmi-12*, *spmi-16*, *spmi-19*) was extracted and

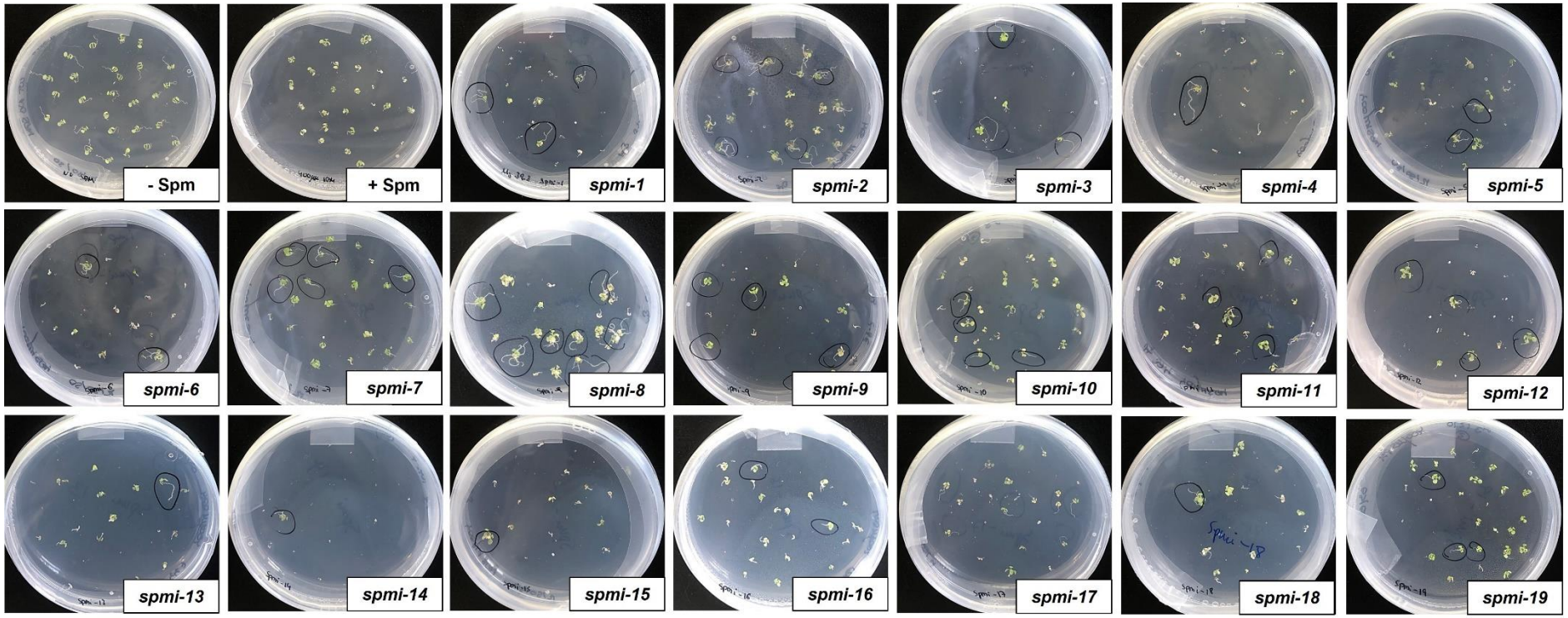

Figure 18. Identification of 19 *spmi* (*1-19*) mutants in the M3 generation obtained through EMS mutagenesis in *A. thaliana* plants. The seedlings were grown *in vitro* on ½ MS medium supplemented with 1% plant agar in the presence of 400 μM Spm. The seedlings were then incubated in 16 h light / 8 h dark cycles at 20-22 °C for three weeks. - Spm corresponds to wild type seedlings in absence of Spm and + Spm corresponds to wild type seedlings in presence of 400 μM Spm.

sequenced. The sequencing was performed using the Illumina technique, and the resulting sequences were mapped to the *A. thaliana* Col-0 reference genome using CLC Genomics Workbench 21 version 21.0.5 (Qiagen). Mutations were filtered to identify non-synonymous substitutions or alternative splicing events. The reliability of these mutations was assessed based on parameters such as coverage, count, sequence quality, and the presence of mutations in the same genes in other mutants (**Table S1**).

Applying these criteria, a total of 21 genes were identified as potential candidates responsible for Spm resistance. These genes exhibited mutations in at least three of the sequenced *spmi* mutants (**Table 10**).

Table 10. List of identified genes through EMS mutagenesis as potential candidates responsible for Spm resistance.

Nº mutants	Candidate gene	Description
4	At1g03060	Encodes a WD/BEACH domain protein involved in cell morphogenesis and ribonucleoprotein particle formation.
3	At1g32750	This gene is predicted to encode a histone acetyltransferase.
3	At1g45130	beta-galactosidase 5
3	At1g52150	Member of the class III HD-ZIP protein family.
4	At2g28860	Member of CYP710A
3	At2g38290	Encodes a high-affinity ammonium transporter, which is expressed in shoot and root.
3	At3g11910	Ubiquitin-specific protease, which together with UBP12 deubiquitinates DA1 reducing their peptidase activity.
5	At3g43148	Myosin heavy chain-like protein.
3	At3g45040	Encodes a putative dolichol kinase that is localized to the endoplasmic reticulum and involved in pollen tube reception.
3	At3g50380	Vacuolar protein sorting-associated protein, putative (DUF1162).
4	At4g00020	Ortholog of breast cancer susceptibility protein 2. Essential at meiosis.
4	At4g00450	Encodes the Arabidopsis homolog of the transcriptional regulator MED12.
3	At4g09660	Zinc finger MYM-type-like protein.
3	at4g16340	Encodes SPIKE1 (SPK1), the lone DOCK family guanine nucleotide exchange factor (GEF) in Arabidopsis.
3	At4g27430	Positive regulator of light-regulated genes. Novel nuclear protein which requires light for its high-level expression.
5	At4g32700	Encodes a DNA polymerase required for microhomology mediated repair of DNA double strand breaks.
3	At4g35870	Early-responsive to dehydration stress protein (ERD4).
3	At5g01050	Putative laccase.
3	At5g28090	Hypothetical protein.
4	At5g50170	C2 calcium/lipid-binding and GRAM domain containing protein.
4	At5g51200	Originally identified as EDS4, enhanced disease sensitive phenotype and subsequently identified as NUCLEOPORIN205.

To conduct a more in-depth investigation of the genes, we assumed the mutations corresponded to loss of function alleles. Subsequently, loss-of-function mutants from the 21 genes identified as potential candidates were studied for their Spm tolerance. The loss-of-function mutants were subjected to screening *in vitro* on ½ MS medium supplemented

with 1% plant agar and 400 μM Spm for three weeks, in 16 h light / 8 h dark cycles at 20-22 °C. This screening aimed to confirm whether these genes were responsible for the Spm resistance observed in the *spmi* mutants.

After the screening, three mutants showing the most pronounced resistance to Spm were selected. These mutants corresponded to *ammonium transporter 2*, (*amt2*, *At2g38290*), the *putative laccase 9*, (*lac9*, *At5g01050*) and a hypothetical protein (*At5g28090*) with of unknown function (**Table 10**).

2.1.1.3. Characterization of candidate genes identified for spermine resistance

To characterize the identified candidate genes as responsible for Spm resistance, assays were performed to measure the length of the main root (**Figure 19**) and quantify H_2O_2 levels in the presence of Spm (**Figure 20**). The measurement of roots was chosen for analysis due to the visible characteristic of root shortening phenotype in the presence of Spm, which was used to select the mutants. Additionally, quantification of H_2O_2 levels was selected due to the known association of polyamines with ROS production.

For the analysis, the mutants (*amt2*, *lac9*, *at5g28090*) and the wild type were grown on ½ MS medium supplemented with 0 μM (mock), 300 μM or 400 μM Spm for two weeks and grown under 16 h light / 8 h dark cycles at 20-22 °C. Notably, the root length of *amt2* and *at5g28090* mutants in the absence of Spm was already longer than the wild type in the absence of Spm. To account for this difference, the root length values in the 300 μM and 400 μM Spm treatments were normalized against the values in the absence of Spm.

The results showed that at 300 μM Spm, only the root shorting in the *amt2* mutant was significantly less than in the wild type (**Figure 19**). However, at 400 μM Spm, all the mutants (*amt2*, *lac9, and at5g28090*) exhibited significantly less root shorting than the wild type. Interestingly, while the root of the wild type was significantly shorter at 400 μM Spm compared to the 300 μM Spm concentration, *lac9,* and *at5g28090* mutants did not show differences between the two treatments.

In summary, the growth assay confirmed that the primary root length of the mutants *amt2*, *lac9, and at5g28090* was less affected by Spm treatment compared to the wild type, indicating increased resistance to Spm.

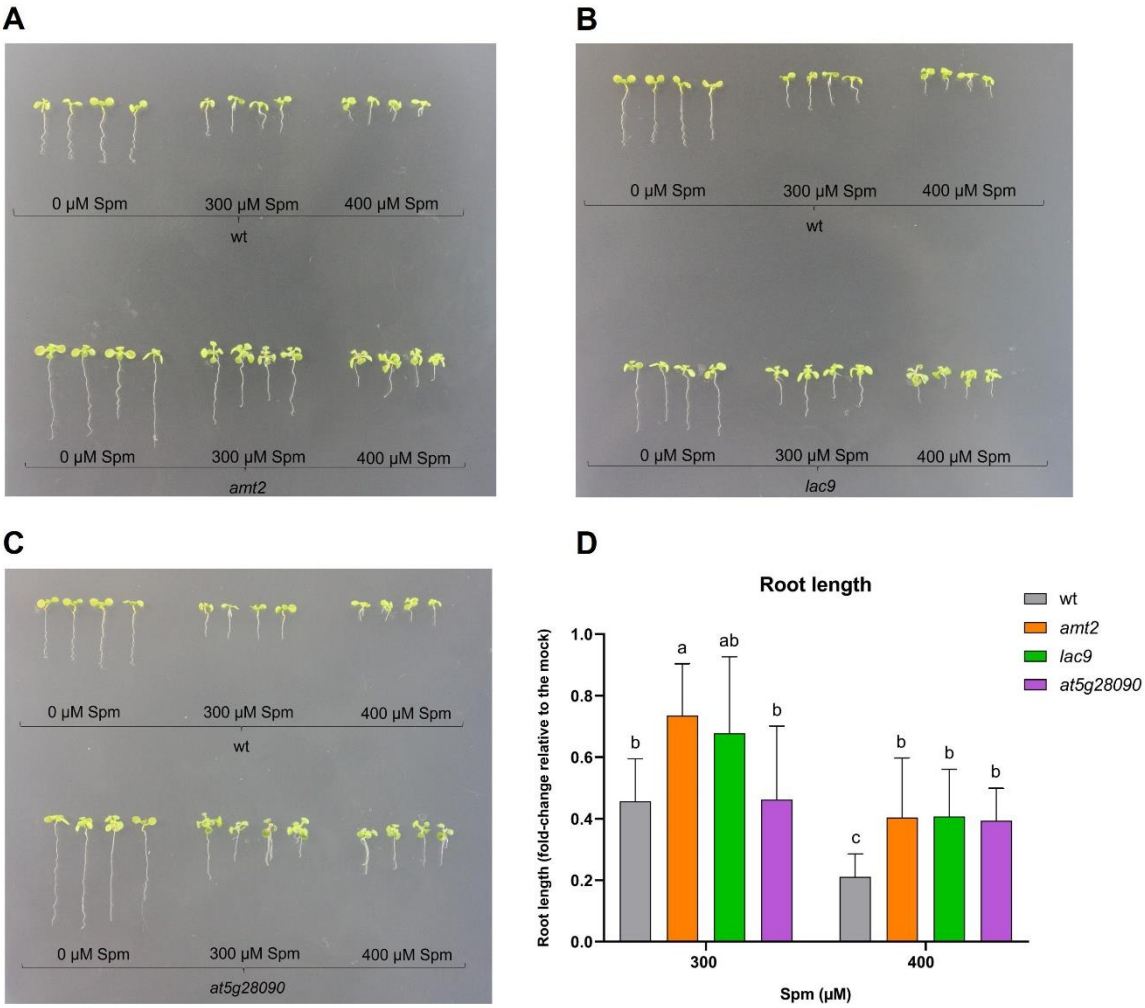

Figure 19. Root growth assay in the *amt2* (**A**), *lac9* (**B**), and *at5g28090* (**C**) mutans compared to the wild type. The seedlings were grown *in vitro* on ½ MS medium supplemented with 1% plant agar and in presence of 0 µM (mock), 300 µM or 400 µM Spm for two weeks under 16 h light / 8 h dark cycles at 20-22 °C. (**D**) Statistical analysis of main root length. The data are presented as mean ± SD, with $N = 10$ replicates. A two-way ANOVA test was conducted, and different letters indicate significant differences $P \leq 0.05$.

The results of H_2O_2 quantification revealed that amount of H_2O_2 in wild type seedlings was significantly higher in the presence of 400 µM Spm compared to both 300 µM Spm treatment and the absence of Spm (**Figure 20**). In contrast, the mutants *amt2, lac9, at5g28090* did not show significant differences in H_2O_2 levels between the treatments. Among the genotypes, *amt2* and *at5g28090* showed significantly lower H_2O_2 in response to 400 µM Spm treatment compared to the wild type.

In summary, the H_2O_2 quantification indicated that 400 µM Spm induced increases in H_2O that were compromised in *amt2*, *lac9,* and *at5g28090* mutants.

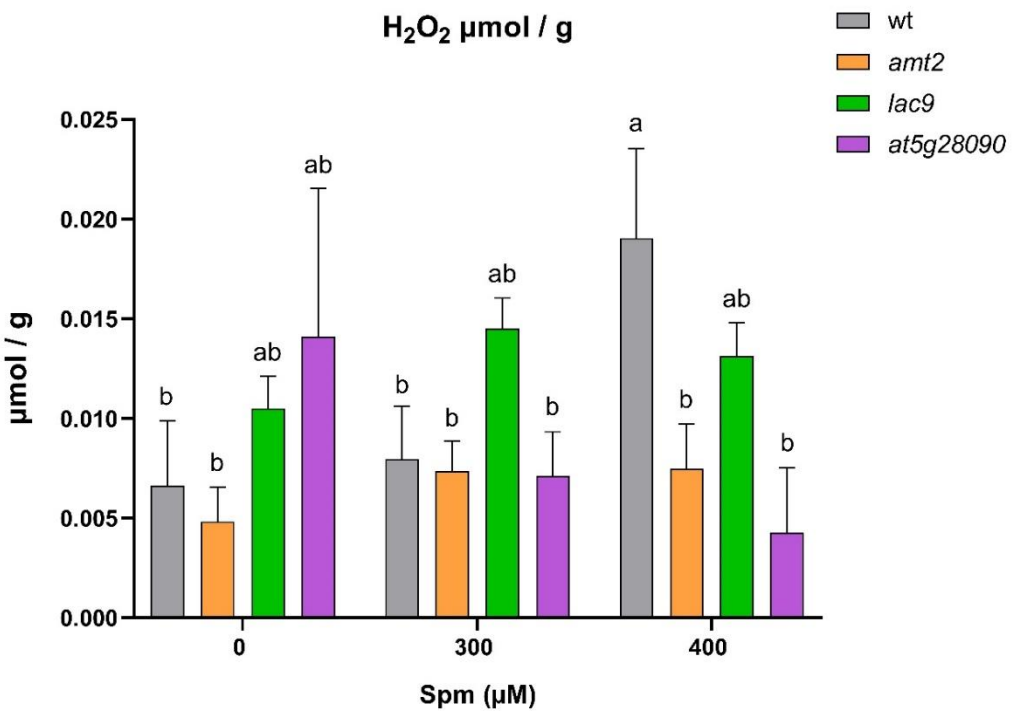

Figure 20. H_2O_2 quantification in the *amt2*, *lac9,* and *at5g28090* mutans compared to the wild type. The seedlings were grown *in vitro* on ½ MS medium supplemented with 1% plant agar and in presence of 0 µM, 300 µM or 400 µM Spm for two weeks under 16 h light / 8 h dark cycles at 20-22 °C. The data are presented as mean ± SD, with $N = 3$ replicates. Statistical analysis was performed using a two-way ANOVA test, and different letters indicate significant differences $P \leq 0.05$.

To provide a more comprehensive analysis about the biological function of the candidate genes and their potential involvement in Spm uptake and/or signaling, gene ontology (GO) studies of co-regulated genes were conducted (**Figure 21**). Interestingly, the gene ontology analysis of *AMT2* co-expressed genes indicated an enrichment in transporter activity, particularly in the ammonium transport, as well as in the response to external stimuli. Considering that Spm carries several amino groups, we speculate that AMT2 might be involved in Spm transport. On the other hand, co-expressed genes with *LAC9* were associated with cell wall organization. This finding is consistent with a previous study suggesting that Spm contributed to cell wall integrity (Aloisi et al., 2017) and that exogenously supplied Put and Spm trigger the expression of genes related to cell wall modifications. No significant information based on GO enrichment analysis was found for *At5g28090*.

A **Co-expressed genes with *AMT2***

Gene Ontology (GO)		Description	Genes	FDR adjusted *P* value
GO:0005215	F	transporter activity	17	8.90×10^{-9}
GO:0005516	F	calmodulin binding	6	0.0012
GO:0043168	F	anion binding	17	0.0074
GO:0097367	F	carbohydrate derivative binding	15	0.0217
GO:0032559	F	adenyl ribonucleotide binding	14	0.0217
GO:0055085	P	transmembrane transport	16	9.18×10^{-7}
GO:0043207	P	response to external biotic stimulus	15	3.60 x 10-5
GO:0008219	P	cell death	5	0.0345
GO:1902074	P	response to salt	7	0.0428
GO:0005886	C	plasma membrane	30	2.41×10^{-14}

B **Co-expressed genes with *LAC9***

Gene Ontology (GO)		Description	Genes	FDR adjusted *P* value
GO:0016762	F	xyloglucan:xyloglucosyl transferase activity	4	2.93×10^{-5}
GO:0030247	F	polysaccharide binding	4	0.0021
GO:0045330	F	aspartyl esterase activity	3	0.0220
GO:0052716	F	hydroquinone:oxygen oxidoreductase activity	2	0.0427
GO:0071555	P	cell wall organization	12	9.77×10^{-9}
GO:0010053	P	root epidermal cell differentiation	7	1.11×10^{-6}
GO:0005976	P	polysaccharide metabolic process	8	0.0003
GO:0005576	C	extracellular region	14	0.0007

Figure 21. Summary of the GO terms associated with the co-expressed genes with *AMT2* (**A**) and *LAC9* (**B**) GO terms, intersection genes and FDR adjusted *P* value were obtained from g:Profiler web server. (F = molecular function, P = biological process, C = cellular component). Co-expressed genes were obtained from ATTED-II web server.

2.1.1.4. Identification of candidate genes responsible for spermine resistance by reverse genetics.

Besides EMS mutagenesis, we performed a Spm tolerance screen using a set of homozygous loss-of-function mutants obtained from the Nottingham Arabidopsis Stock Center. This approach has the advantage that it does not require mapping, but in contrast, it does not cover all the genes in the Arabidopsis genome (25,500).

A total of 240 homozygous mutants were tested for their Spm tolerance. Among the mutants, 214 were selected that mapped to genes which expression is differentially regulated in response to Spm (C. Zhang et al., 2023). The remaining 26 mutants were chosen randomly and used as "controls". Seedlings for each of the mutants were grown *in vitro* on ½ MS medium supplemented with 400 μM Spm. The seedlings were then grown under 16 h light / 8 h dark cycles at 20-22 °C for three weeks and checked for Spm tolerance.

The results revealed that most of the screened mutants did not exhibit resistance to 400 µM Spm (**Table S3**). However, two mutants showed some resistance (**Table 11**). These mutants corresponded to *cuaor2*, a copper-amine oxidase mutant that is involved in polyamine catabolism, and *ein3*, which is involved in the ethylene signaling.

Table 11. *A.thaliana* mutants resistant to Spm.

Mutant name	Gene ID	Function
cuaor2	At3g43670	Polyamine catabolism
ein3	At3g20770	Ethylene signaling pathway

Characterization of *cuaor2* mutant.

The characterization of *cuaor2* mutant involved conducting similar analyses to those performed in the EMS population. These assays included measuring the main root length (**Figure 22**) quantifying H_2O_2 levels (**Figure 23**) and GO analyses of co-regulated genes (**Figure 24**).

The results indicated that at both concentrations of Spm (300 µM and 400 µM), the *cuaor2* mutant exhibited significantly longer root length compared to the wild type (**Figure 22**). Furthermore, in both wild-type and *cuaor2*, the root length was significantly shorter at 400 µM Spm compared to the 300 µM Spm concentration.

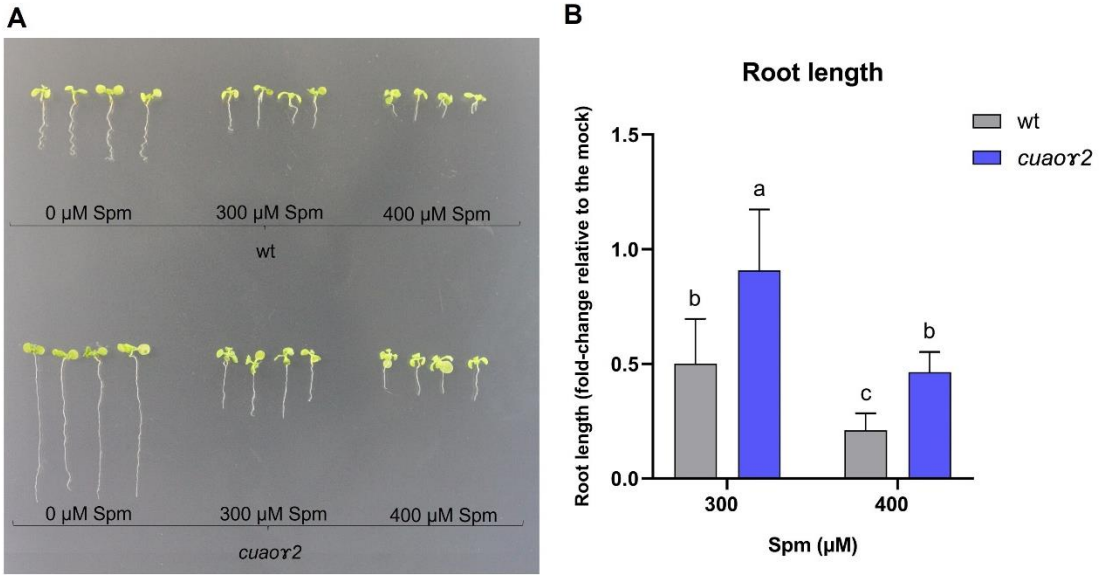

Figure 22. Root growth assay in the *cuaor2* mutant (**A**) compared to the wild type. The seedlings were grown *in vitro* on ½ MS medium supplemented with 1% plant agar and in presence of 0 µM, 300 µM or 400 µM Spm for two weeks under 16 h light / 8 h dark cycles at 20-22 °C. (**B**) Statistical analysis of main root length. The data are presented as mean ± SD, with $N = 10$ replicates. A two-way ANOVA test was conducted, and different letters indicate significant differences $P \leq 0.05$.

The results of H_2O_2 quantification revealed that the amount of H_2O_2 in wild type seedlings was significantly higher in the presence of 400 μM Spm compared to the 300 μM Spm treatment or mock (0 μM Spm) (**Figure 23**). In contrast, the *cuaor2* mutant did not exhibit significant differences in H_2O_2 levels among the treatments. Notably, the *cuaor2* mutant displayed significantly lower H_2O_2 levels compared to the wild type under the 400 μM Spm treatment, while no differences were observed at 300 μM Spm or in the absence of Spm. These findings align with the previous results of H_2O_2 quantification in the *amt2*, *lac9*, and *at5g28090* mutants, suggesting that Spm resistance is associated with reduced H_2O_2 production in the presence of high doses of Spm.

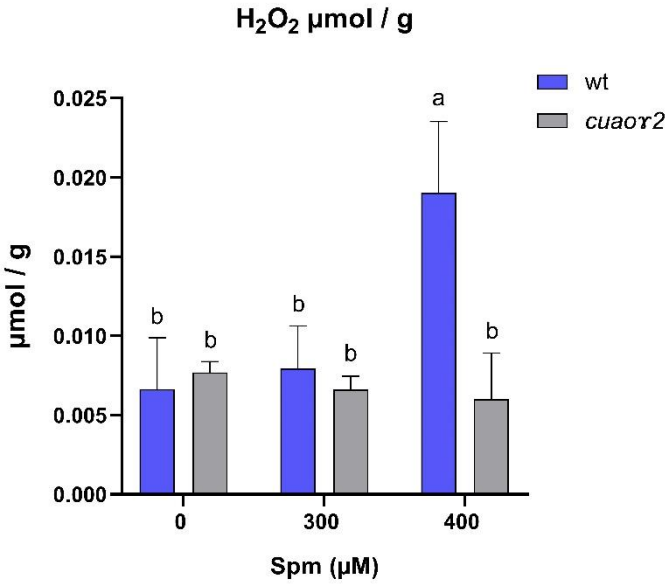

Figure 23. H_2O_2 quantification in *cuaor2* mutant and wild type. The seedlings were grown *in vitro* on ½ MS medium supplemented with 1% plant agar and in presence of 0 μM, 300 μM or 400 μM Spm for two weeks under 16 h light / 8 h dark cycles at 20-22 °C. The data are presented as mean ± SD, with $N = 3$ replicates. Statistical analysis was performed using a two-way ANOVA test, and different letters indicate significant differences $P \leq 0.05$.

GO analysis (**Figure 24**) revealed that the co-expressed genes with *CuAOr2* were associated with oxidoreductase activity and putrescine responses, aligning with the role of CuAOr2 as an enzyme involved in polyamine catabolism. Interestingly, the GO analysis also indicated the involvement of these genes in Fe homeostasis, suggesting a potential relationship between Spm and Fe.

Co-expressed genes with *CuAOζ2*

Gene Ontology (GO)		Description	Genes	FDR adjusted *P* value
GO:0016491	F	oxidoreductase activity	16	6.46×10^{-6}
GO:0008199	F	ferric iron binding	3	0.0003
GO:0019904	F	protein domain specific binding	5	0.0003
GO:0000302	P	response to reactive oxygen species	9	1.39×10^{-8}
GO:0015979	P	photosynthesis	7	0.0006
GO:0006879	P	intracellular iron ion homeostasis	4	0.0007
GO:0000041	P	transition metal ion transport	5	0.0012
GO:1904585	P	response to putrescine	2	0.0122
GO:0009507	C	chloroplast	27	2.27×10^{-11}
GO:0009505	C	plant-type cell wall	6	0.0368

Figure 24. Summary of the GO terms associated with the co-expressed genes with *CuAOζ2*. GO terms, intersection genes and FDR adjusted *P* value were obtained from g:Profiler web server. (F = molecular function, P = biological process, C = cellular component). Co-expressed genes were obtained from ATTED-II web server.

Characterization of ethylene signaling mutants

In order to characterize the response of the *ein3* mutant to Spm, a root growth assay was performed (**Figure 25**). To obtain a more comprehensive understanding of the relationship between Spm and ethylene, the assay included additional ethylene signaling mutants: *ctr1* (Kieber et al., 1993), *ein1* and *ein2* (Guzman & Ecker 1990), *ein6* (Roman et al., 1995), and the *ein3eil1* double mutant (Chao & Rothenberg, 1997).

For the assay, the mutants (*ctr1, ein1, ein2, ein3, ein3eil1* and *ein6)* along with the wild type were grown *in vitro* on ½ MS medium supplemented with 0 μM or 400 μM Spm for two weeks under 16 h light / 8 h dark cycles at 20-22 ºC (**Figure 25A**).

At 400 μM Spm, the main root of the ethylene insensitive mutants *ein1, ein2, ein3* and *ein3eil1*, was significantly longer than the wild type. No differences in root length were found in the *ein6* mutant compared to the wild type (**Figure 25B**). Notably, the *crt1* mutant, which exhibits a constitutive activation of the ethylene pathway, displayed a significantly shorter root length compared to the wild type. These findings suggested a relationship between the Spm and the ethylene signaling and indicated that *ein6* was not involved in this interaction.

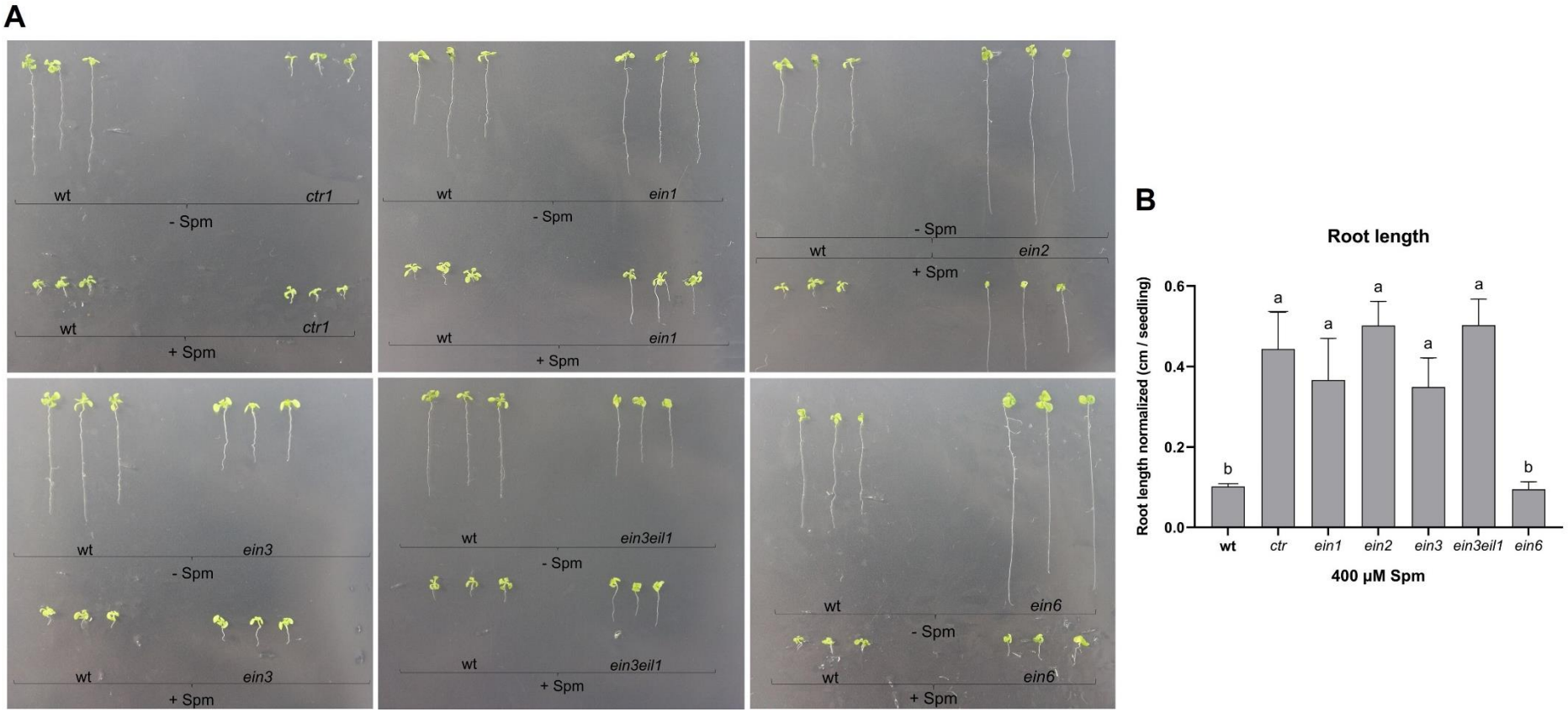

Figure 25. Root growth assay in the ethylene mutants (*ctr1, ein1, ein2, ein3, ein3eil1, ein6*) compared to the wild type (**A**). The seedlings were grown *in vitro* on ½ MS medium supplemented with 1% plant agar and in presence of 0 µM or 400 µM Spm for two weeks under 16 h light / 8 h dark cycles at 20-22 °C. (**B**) Statistical analysis of main root length. The data are presented as mean ± SD, with $N = 10$ replicates. One-way ANOVA test was conducted, and different letters indicate significant differences $P \leq 0.05$.

Based on the results obtained from the root growth assay and the already short root phenotype of the *ctr1* mutant, we formulated the hypothesis that exogenous Spm may induce ethylene production leading to root growth inhibition. To investigate this hypothesis, a dark growth assay using wild type seedlings was conducted, in which Spm was utilized as a potential compound triggering ethylene biosynthesis, and likely the triple response (**Figure 26**). Additionally, the *ctr1* mutant was used as a positive control for the triple response, and the *ein3eil1* served as a negative control. The seedlings were grown *in vitro* on ½ MS medium supplemented with Spm (100 μM, 300 μM and 400 μM) as well as a control group without Spm. To explore the potential relationship between ethylene and another polyamine, an additional treatment with 100 μM Spd was included. Subsequently, the seedlings were incubated for two weeks in dark at 20-22ºC.

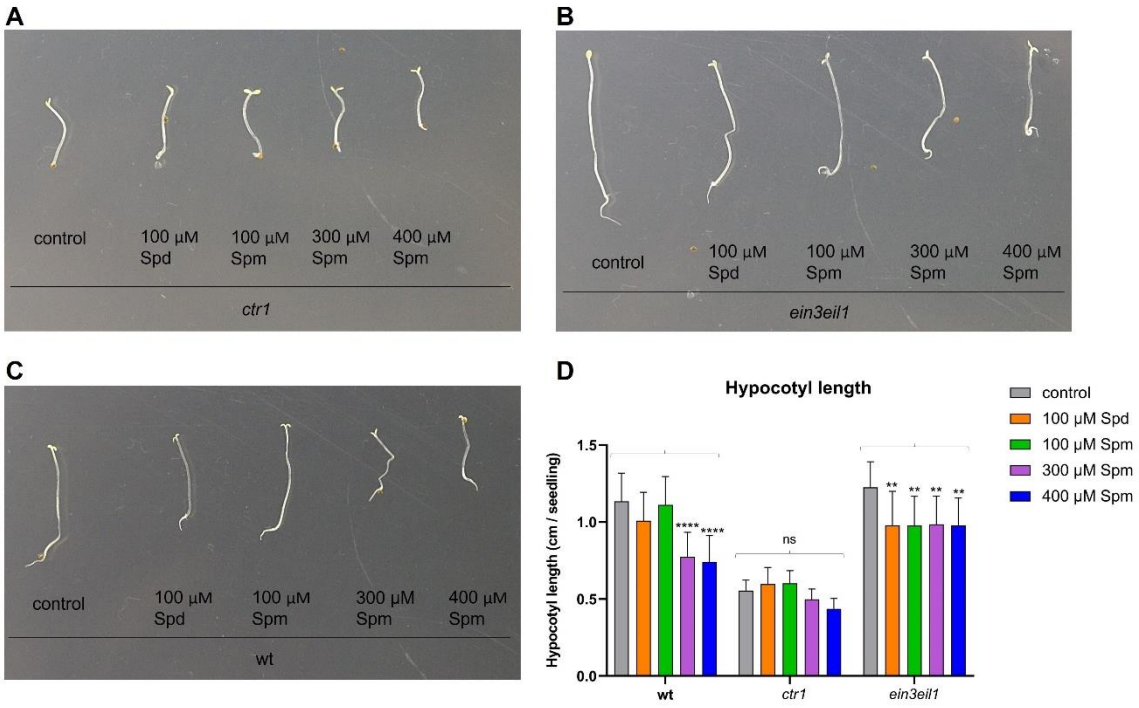

Figure 26. Ethylene dark growth assay in *ctr1* (**A**), *ein3eil1*(**B**) and wild type (**C**). The seedlings were grown *in vitro* on ½ MS medium supplemented with 1% plant agar and in presence of the different treatments (control, 100 μM Spd, 100 μM Spm, 300 μM Spm, 400 μM Spm) for two weeks in dark at 20-22 °C. Control conditions referred to the absence of any treatment. (**D**) Statistical analysis of hypocotyl length. The data are presented as mean ± SD, with $N = 10$ replicates. Two-way ANOVA test was conducted to compare the data against the control conditions, denoted as follows: $\star P \leq 0.05$, $\star\star P \leq 0.01$, $\star\star\star P \leq 0.001$, $\star\star\star\star P \leq 0.0001$, ns = non-significant.

The *ctr1* mutant already showed shorter hypocotyl consistent with the constitutive activation of the triple response. However, increasing concentrations of Spm (100 μM Spd, 100 μM Spm, 300 μM Spm, 400 μM Spm) did not lead to shorter hypocotyl length (**Figure**

26A). In contrast, the *ein3eil1* mutant exhibited a significant reduction in hypocotyl length at increasing concentrations of Spm. Interestingly, the wild type showed no differences in hypocotyl length in the treatments with 100 µM Spd and 100 µM Spm compared to the control, whereas they were evident in *ein3eil1*. Overall, the reduction in hypocotyl length triggered by Spm is not dependent on EIN3/EIL1, which suggests that this is an ET-independent response. Additionally, it appeared that the treatments (100 µM Spd, 100 µM Spm, 300 µM Spm, 400 µM Spm) led to a more frequent opening of the cotyledons, especially in the *ctr1* and *ein3eil1* mutants. However, further analyses are necessary to fully understand this particular effect, which might be associated with skotomorphogenic responses.

To further investigate the effect of exogenous Spm on ethylene production, an ethylene synthesis inhibition assay was conducted using the AVG inhibitor, which inhibits the ACC synthase enzyme (Kieber et al., 1993)(**Figure 27**). Wild type seedlings were grown *in vitro* on ½ MS growth medium, supplemented with different treatments: 400 µM Spm, 10 µM AVG, its combinations (AVG + Spm) or mock. The seedlings were then incubated under 16 h light / 8 h dark cycles at 20-22 °C and root phenotyping performed at 15 days post-germination.

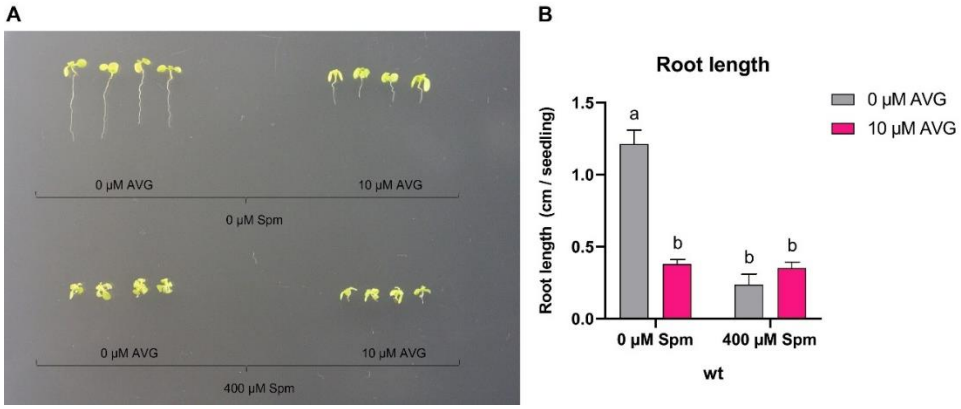

Figure 27. Ethylene inhibition assay using AVG inhibitor in wild type plants in presence of Spm (**A**). The seedlings are grown *in vitro* on ½ MS medium supplemented with 1% plant agar and in presence of the different treatment combinations: 0 µM Spm + 0 µM AVG (mock); 0 µM Spm + 10 µM AVG; 400 µM Spm + 0 µM AVG; 400 µM Spm + 10 µM AVG. The seedlings are incubated for two weeks in 16 h light / 8 h dark cycles at 20-22 °C. (**B**) Statistical analysis of main root length. The data are presented as mean ± SD, with $N = 10$ replicates. Two-way ANOVA test was conducted, and different letters indicate significant differences $P \leq 0.05$.

The AVG inhibitor alone caused root shortening, even in the absence of Spm. However, no differences in root length were found in the absence or presence of AVG in plants treated with Spm. We concluded that the root shortening phenotype triggered by Spm is

not rescued by inhibition of ethylene biosynthesis. The effect of Spm on ethylene might be related to biosynthesis inhibition or to signaling.

2.1.2. Interaction between Fe deficiency and spermine treatment in *A. thaliana*

2.1.2.1. Activation of Fe deficiency signaling pathway after exogenous spermine treatment

A

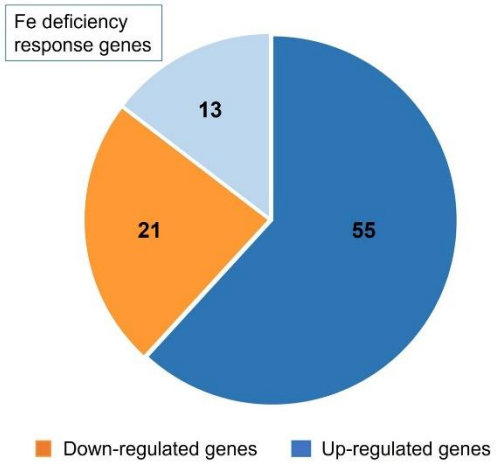

B

Differentially up-regulated genes 400 µM Spm / no Spm (≥ 2-fold)

Gene Ontology (GO)		Description	Genes	FDR adjusted *P* value
GO:0010106	P	cellular response to iron ion starvation	4	9.57×10^{-7}
GO:0034758	P	positive regulation of iron ion transport	3	1.16×10^{-5}
GO:1990641	P	response to iron ion starvation	3	0.0041

Differentially down-regulated genes 400 µM Spm / no Spm (≤ -2-fold)

Gene Ontology (GO)		Description	Genes	FDR adjusted *P* value
GO:0004601	F	peroxidase activity	3	0.0126
GO:0072593	P	reactive oxygen species metabolic process	4	0.0077
GO:0042744	P	hydrogen peroxide catabolic process	3	0.0306

Figure 28. (**A**) Differentially expressed genes in wild type seedlings treated with 400 µM Spm compared to untreated wild type seedlings. The seedlings were grown *in vitro* on ½ MS medium supplemented with 1% plant agar, with or without 400 µM Spm, for three weeks at 22°C under 12 h light / 12 h dark cycles. (**B**) Summary of the GO terms associated with the upregulated (≥ 2-fold) and downregulated (≤ -2-fold) genes. GO terms, intersection genes and FDR adjusted *P* values were obtained from g:Profiler web server. (F = molecular function, P = biological process).

During the screening process to identify mutants resistant to exogenous Spm, a small percentage of wild type seedlings consistently displayed resistance. Although their growth was affected, they were able to survive. To investigate the underlying differences between Spm resistant and sensitive seedlings, an RNA sequencing (RNA-seq) experiment was

conducted. It involved comparing wild type seedlings grown *in vitro* on ½ MS medium for three weeks in 16 h light / 8 h dark cycles at 20-22 °C with wild type seedlings that managed to survive under the same conditions but with the addition of 400 μM Spm.

Out of all the *A. thaliana* genes analyzed, 68 genes were found to be upregulated (fold change > 2, *P* value < 0.05) in seedlings treated with 400 μM Spm compared to untreated seedlings (**Figure 28A; Table S4**). These deregulated genes were enriched in Fe starvation responses (**Figure 28B**), with 13 out of the 68 genes identified as involved in Fe deficiency signaling pathway (**Table 12**). This finding suggested that the treatment of Spm induced the activation of the Fe deficiency signaling pathway. On the other hand, 21 genes were downregulated (fold change < -2, *P* value < 0.05) in seedlings treated with 400 μM Spm compared to untreated seedlings (**Figure 28A; Table S4**). These downregulated genes were enriched in H_2O_2 catabolic processes (**Figure 28B**). This finding aligned with previous results, which indicated that wild type seedlings treated with 400 μM Spm exhibited increased levels of H_2O_2 levels.

Table 12. Differentially expressed genes (≥ 2-fold) involved in Fe deficiency signaling pathway in seedlings treated with 400 μM Spm compared to untreated seedlings.

Name	Gene ID	Fold change	FDR *P* value	Function
BHLH100	At2g41240	50.62	6.54×10^{-29}	Fe deficiency response
AT1G13608	At1g13608	49.76	0.04	Fe deficiency response
BHLH38	At3g56970	29.64	7.67×10^{-28}	Fe deficiency response
IMA1	At1g47400	20.65	2.33×10^{-7}	Fe deficiency response
IMA3	At2g30766	15.58	1.25×10^{-5}	Fe deficiency response
IMA6	At1g07373	14.14	0.04	Fe deficiency response
IMA2	At1g47395	13.50	8.19×10^{-13}	Fe deficiency response
BHLH39	At3g56980	6.54	2.65×10^{-13}	Fe deficiency response
BHLH101	At5g04150	5.37	1.96×10^{-9}	Fe deficiency response
CYP82C4	At4g31940	5.00	0.03	Fe deficiency response
FRO2	At1g01580	3.41	3.22×10^{-5}	Fe deficiency response
IRT1	At4g19690	2.56	0.01	Fe deficiency response
BTS	At3g18290	2.09	2.52×10^{-5}	Fe deficiency response

To further investigate the effect of Spm in activating the Fe deficiency signaling pathway, the expression of selected differentially upregulated genes identified in the RNA-seq analysis (*BHLH100*, *BHLH38*, *IMA2*, *IMA3*, *BHLHH39* and *CYP82C4*) was determined by qRT-PCR in wild type seedlings treated with 400 μM Spm compared to untreated wild type seedlings. The seedlings were incubated under the same conditions as the RNA-seq experiments.

The qRT-PCR results demonstrated that all the tested genes (*BHLH100*, *BHLH38*, *IMA2*, *IMA3*, *BHLHH39* and *CYP82C4*) exhibited significantly higher expression levels in seedlings treated with 400 μM Spm compared to untreated seedlings (**Figure 29**). These findings aligned with the RNA-seq analysis, suggesting that Spm induced the activation of Fe deficiency signaling pathway.

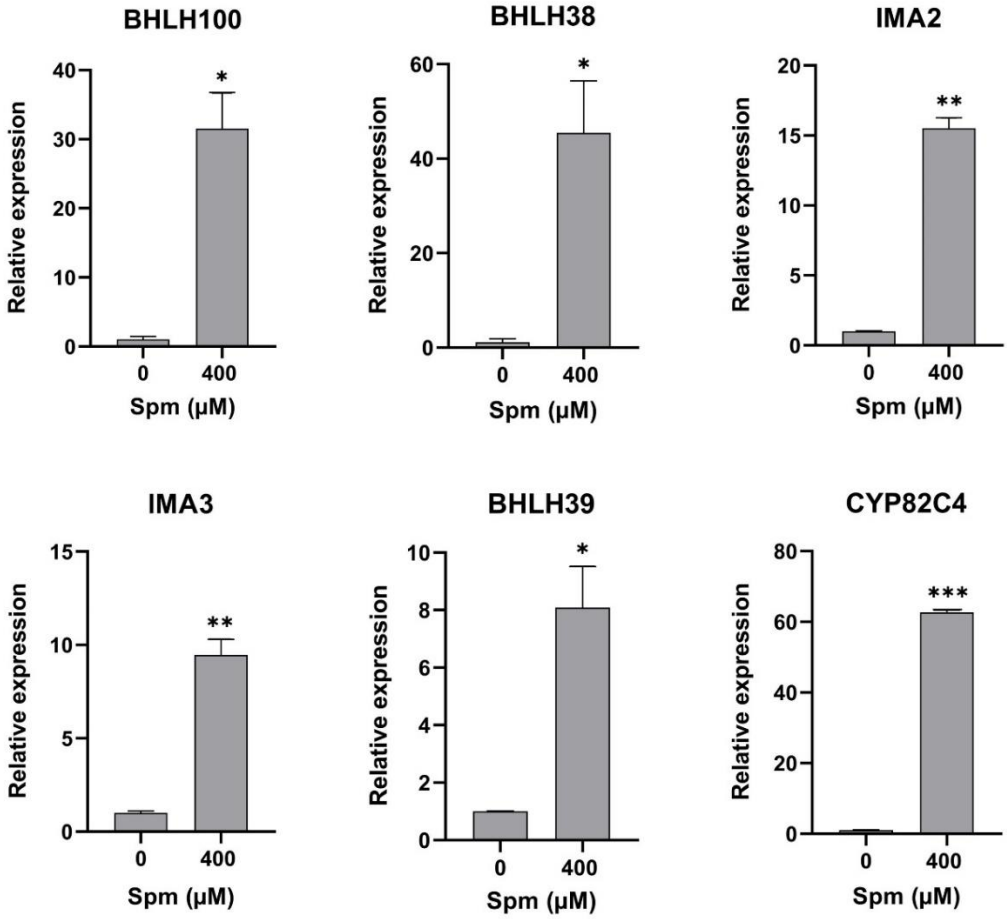

Figure 29. qRT–PCR gene expression analyses of the Fe deficiency signaling pathway genes, including *BHLH100*, *BHLH38*, *IMA2*, *IMA3*, *BHLH39*, and *CYP92C4* in wild type seedlings treated with 400 μM Spm compared to untreated wild type seedlings. The seedlings were grown *in vitro* on ½ MS medium supplemented with 1% plant agar, with or without 400 μM Spm, for three weeks at 22°C under 16 h light / 8 h dark cycles. The data are presented as mean ± SD, with $N = 3$ replicates. T-test was conducted to compare the data against untreated seedlings, denoted as follows: * $P \leq 0.05$, ** $P \leq 0.01$, *** $P \leq 0.001$.

2.1.2.2. Fe supplementation ameliorates the inhibitory effect of spermine on growth

To investigate whether Fe counteracted the effect of Spm, root length and seedling biomass assays were conducted in wild type seedlings. The seedlings were grown in *vitro* on ½ MS medium supplemented with 1% plant agar, with or without 400 μM Spm, under

different Fe concentrations (50 µM, 100 µM, 150 µM, 250 µM) for three weeks in 16 h light / 8 h dark cycles at 20-22 °C. The control Fe concentration was set at 50 µM, which corresponds to basal concentration (**Figure 30A**).

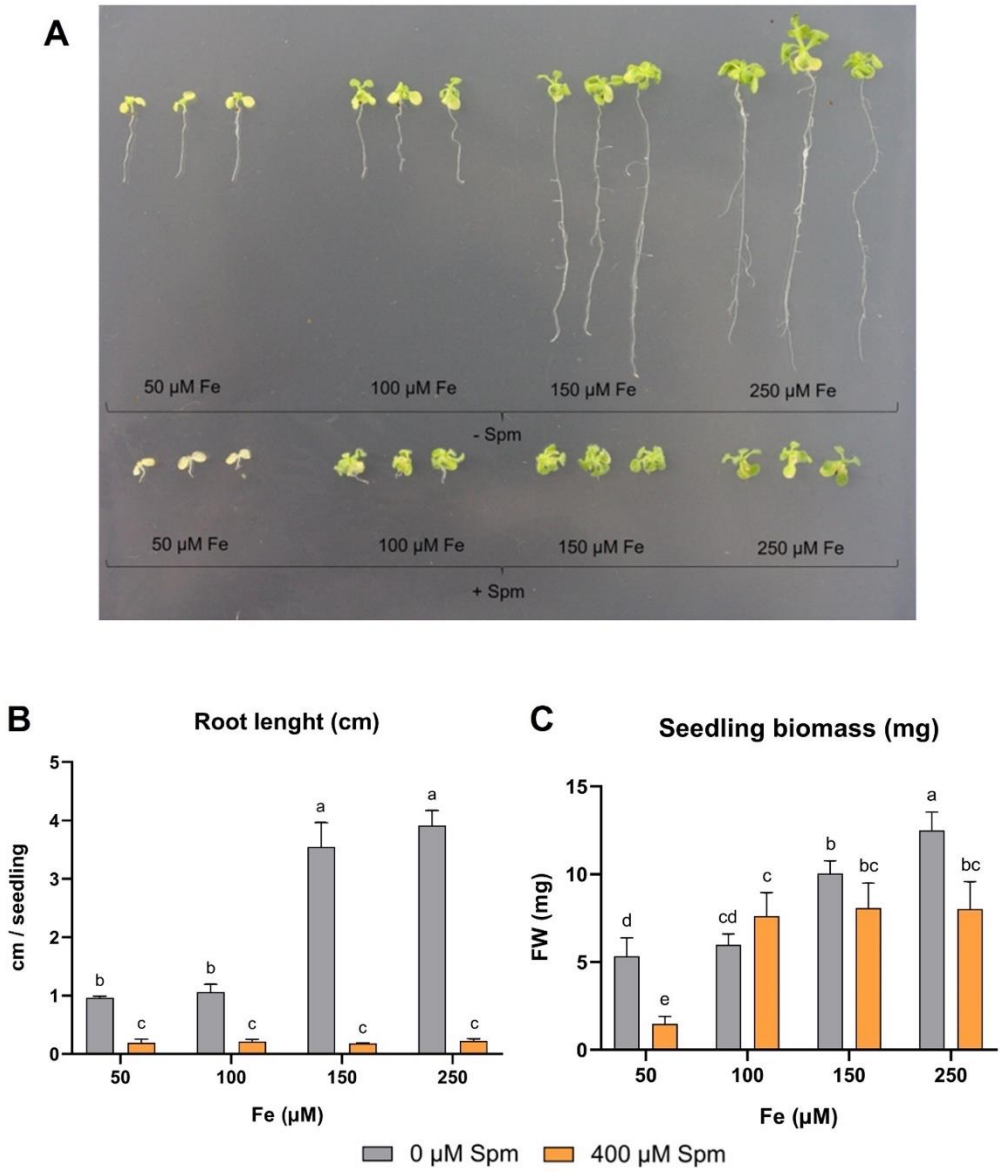

Figure 30. (**A**) Root length and seedling biomass assay in wild type seedlings grown *in vitro* on ½ MS medium supplemented with 1% plant agar, with or without 400 µM Spm, under different Fe concentrations (50 µM, 100 µM, 150 µM, 250 µM). The seedlings were incubated for three weeks in 16 h light / 8 h dark cycles at 20-22 °C. (**B**) Statistical analysis of main root length, mean ± SD, $N = 10$ replicates, two-way ANOVA test. (**C**) Statistical analysis of seedling biomass. Each replicate comprises 3 seedlings, mean ± SD, $N = 5$ replicates, two-way ANOVA test. Different letters indicate significant differences $P \leq 0.05$.

The results showed that in absence of Spm, the root length was significantly longer at 150 µM and at 250 µM Fe compared to 50 µM and 100 µM Fe (**Figure 30B**). However, in the presence of 400 µM Spm, no significant differences in root length were observed at any

Fe concentration (50 μM, 100 μM, 150 μM, 250 μM). Furthermore, irrespective of the Fe concentration, the root length was significantly shorter at 400 μM Spm compared to the absence of Spm. These findings indicated that the effect of exogenous Spm on the main root shortening of wild type seedlings was independent of the Fe concentration.

The results of seedling biomass assay revealed that in the absence of Spm, the biomass of the seedlings was significantly higher at 250 μM Fe compared to the rest of Fe concentrations (50 μM, 100 μM and 150 μM). Additionally, the biomass at 150 μM Fe was greater compared to 50 μM and 100 μM Fe (**Figure 30C**). Interestingly, in the presence of Spm (400 μM), the biomass of the seedlings was significantly higher at 100 μM, 150 μM, and 250 μM Fe concentrations compared to 50 μM Fe. Furthermore, at 50 μM and at 250 μM Fe the seedling biomass was lower in the presence of Spm (400 μM) compared to the absence whereas at 100 μM and at 150 μM there were no difference between the presence and absence of Spm. This finding suggested that supplementation with Fe, specifically 100 μM and 150 μM Fe, reduced the effect of Spm in shoot growth inhibition.

In summary these results indicated that, increasing the Fe concentration resulted in a rescue of seedling biomass in the presence of Spm, while the root shortening phenotype was not rescued.

2.1.2.3. Detection of coumarins after spermine treatment

Coumarins are synthesized and exudated through the roots in response to iron deficiency. We investigated whether Spm treatment, in addition to activating the Fe deficiency, induced the production of fluorescence phenolic compounds such as coumarins. *f6´h1-1* (*feruloyl CoA 6´-hydroxylase 1*) mutant was used as a negative control since it lacks the ability to synthesize coumarins.

Wild type, *spms* and *f6´h1-1* seedlings were grown *in vitro* on ½ MS growth medium supplemented with 1% sucrose. They were vertically incubated in a growth chamber under 16 h light / 8 h dark cycles at 20-22 °C. After eight days, the seedlings were transferred to new plates containing ½ MS growth medium without sucrose, supplemented with different treatments: basal Fe (50 μM) without Spm supplementation (+Fe -Spm, mock treatment), Fe deficiency (-Fe -Spm), 400 μM Spm (+Fe +Spm), or a combination of Fe deficiency and 400 μM Spm (-Fe +Spm). The addition and subsequent removal of sucrose in the media were performed to ensure sufficient plant growth for coumarin production and to assess the specific effect of Spm, respectively.

After four days, the presence of coumarins exudated by the roots was detected under UV light at 365 nm, conditions at which coumarins exhibit a characteristic fluorescence.

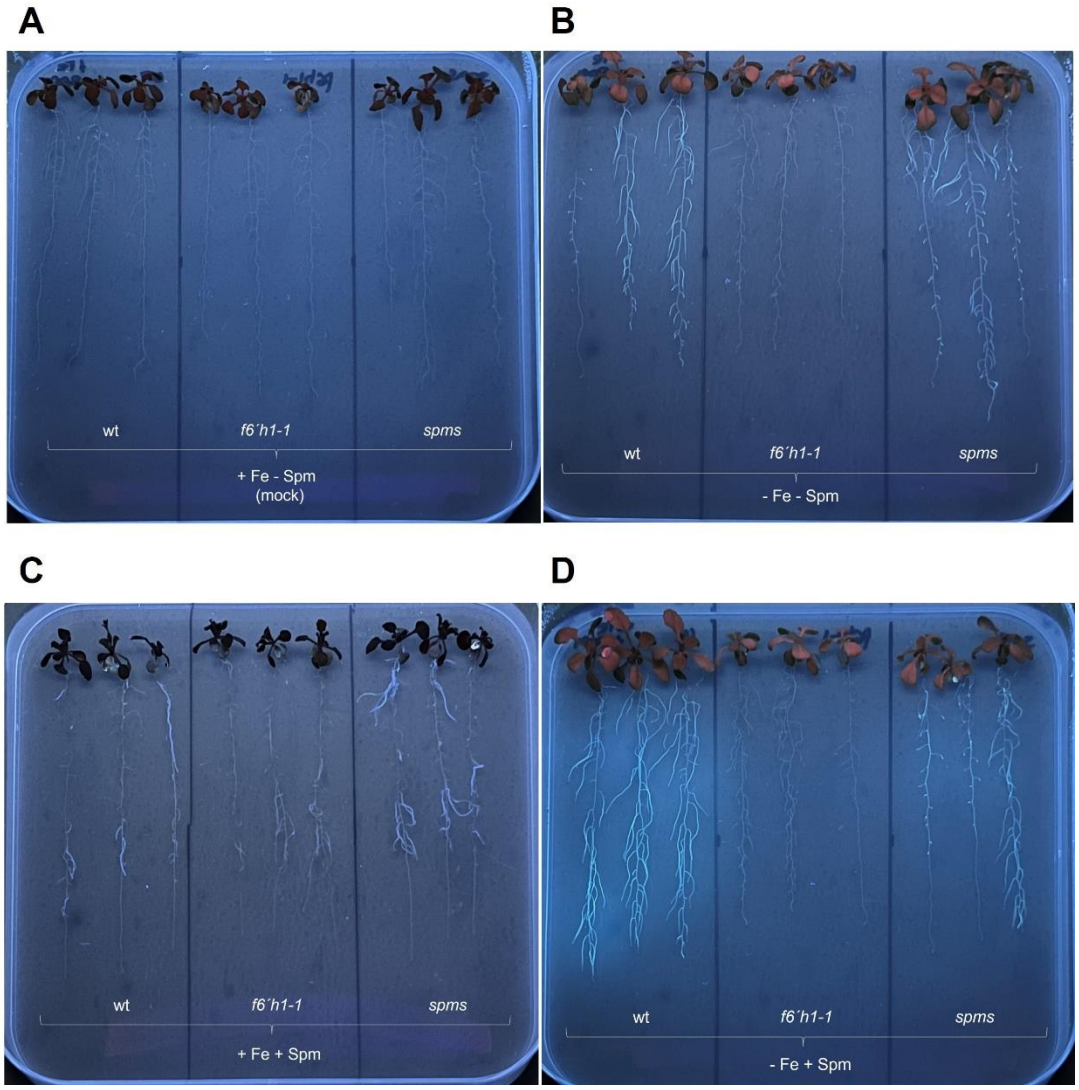

Figure 31. Coumarins detection under UV light (365 nm) in wild type, *f6´h1-1* and *spms* seedlings (*N*=12 replicates) under different treatments: (**A**) basal Fe (50 µM) without Spm supplementation (+Fe -Spm, mock treatment), (**B**) Fe deficiency (-Fe -Spm), (**C**) 400 µM Spm (+Fe +Spm), (**D**) Fe deficiency and 400 µM Spm (-Fe +Spm). The seedlings were grown *in vitro* on ½ MS growth medium supplemented with 1% sucrose and 1% plant. They were vertically incubated under 16 h light / 8 h dark cycles at 20-22 °C. After eight days, the seedlings were transferred to new plates containing ½ MS growth medium and 1% plant agar, supplemented with the different treatments. Four days later, the presence of coumarins was detected.

The results showed that under normal conditions (mock treatment), no coumarins were detected in any of the genotypes (wild type, *f6´h1-1* and *spms*) (**Figure 31A**). In contrast, fluorescence compounds were detected in the roots of wild type and *spms* seedlings under Fe deficiency treatment (**Figure 31B**), 400 µM Spm treatment (**Figure 31C**) and the combination of both treatments (Fe deficiency and 400 µM Spm) (**Figure 31D**). However,

f6´h1-1 seedlings did not exhibit fluorescence compounds under Fe deficiency treatment (**Figure 31B**) and the combination of both treatments (**Figure 31D**). They showed only minimal fluorescence under 400 µM Spm treatment (**Figure 31C**). These findings indicate that the detected fluorescence compounds were primarily coumarins, with some presence of other phenolic compounds.

Among the treatments, it was observed that at 400 µM Spm treatment (**Figure 31C**), the fluorescence was particularly concentrated at the secondary roots, whereas in the other treatments (Fe deficiency, and the combination of Fe deficiency and 400 µM Spm) the fluorescence was more evenly distributed along primary and secondary roots (**Figure 31B**; **Figure 31D**). Additionally, in wild type seedlings, the combination of Fe deficiency and 400 µM Spm treatment showed a higher fluorescence intensity compared to the individual Fe deficiency and 400 µM Spm treatments. However, no visible differences in fluorescence were observed in *spms* seedlings.

This finding suggested that exogenous Spm induced the production of coumarins, although in a different pattern compared to Fe deficiency conditions, and likely dependent on *F6´H1.*

To further investigate the effect of Spm in coumarin production, the expression of *F6´H1* gene was determined by qRT-PCR in the wild type and *spms* genotypes under the different treatments: mock (+Fe -Spm), Fe deficiency (-Fe -Spm), 400 µM Spm (-Fe +Spm), and the combination of Fe deficiency and 400 µM Spm (-Fe + Spm). Furthermore, since the fluorescence was specifically detected in the roots, the expression of the gene was focused on this tissue.

The results revealed that the expression of *F6´H1* in wild type and *spms* roots was significantly higher under the different treatments (-Fe -Spm, +Fe +Spm, and -Fe +Spm) compared to the mock treatment (+Fe -Spm) (**Figure 32**). Furthermore, in wild type roots, *F6´H1* showed significantly higher expression under the 400 µM Spm (+Fe +Spm) and the combination of Fe deficiency and 400 µM Spm (-Fe +Spm) treatments compared to *spms* roots, likely due to the deficiency in endogenous Spm of the *spms* mutant.

Collectively, the results indicated that Spm induced the production of coumarins in the roots, showing some variations between wild type and *spms*.

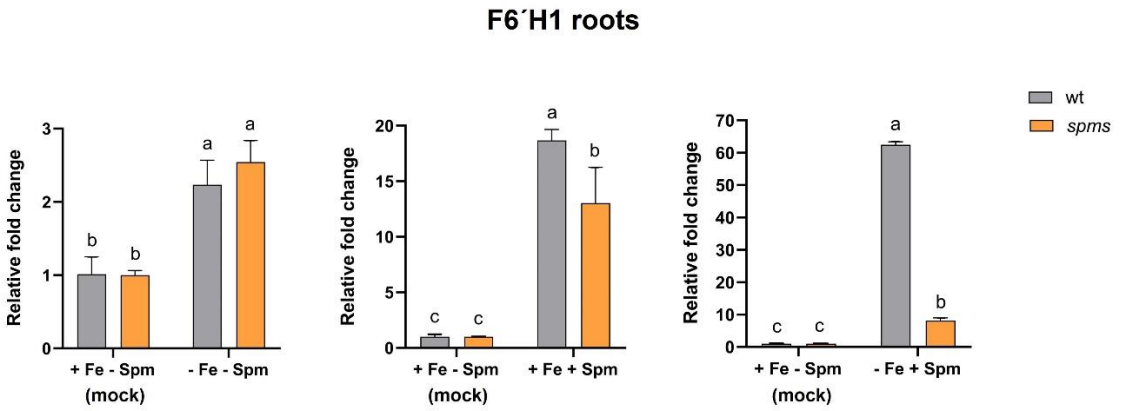

Figure 32. qRT–PCR gene expression analyses of the coumarin synthesis gene *F6´H1* in roots of wild type and *spms* seedlings under different treatments: mock (+Fe -Spm), Fe deficiency (-Fe Spm), 400 μM Spm (+Fe +Spm), or a combination of Fe deficiency and 400 μM Spm (-Fe +Spm). The seedlings were grown *in vitro* on ½ MS growth medium supplemented with 1% sucrose and 1% plant agar and vertically incubated under 16 h light / 8 h dark cycles at 20-22 ºC. After eight days, the seedlings were transferred to new plates containing ½ MS growth medium and 1% plant agar, supplemented with different treatments. The seedlings were then incubated four more days. The data are presented as mean ± SD, with $N = 3$ replicates. Statistical analysis was performed using a two-way ANOVA test, and different letters indicate significant differences $P \leq 0.05$.

2.1.2.4. Comparative gene expression analysis of wild type and *spms* seedlings under Fe deficiency conditions

Previous results in the coumarins detection revealed certain different behavior in wild type and *spms* mutants. To further investigate these differences, the expression of *BHLH100*, *BHLH38*, *IMA2*, *IMA3*, *BHLHH39* and *CYP82C4* genes, involved in Fe deficiency signaling pathway, was determined by qRT–PCR in both genotypes (wild type and *spms*) under Fe deficiency conditions. The seedlings were grown *in vitro* on ½ MS growth medium and incubated under 16 h light / 8 h dark cycles at 20-22 ºC. After eight days, the seedlings were transferred to new plates under Fe basal conditions (50 μM) and Fe deficiency conditions (0 μM). The seedlings were then incubated eight more days.

The results showed that the expression *BHLH100*, *BHLH38*, *IMA2*, *IMA3* and *BHLH39* genes was significantly higher in wild type and *spms* under Fe deficiency conditions compared to normal conditions (**Figure 33**). Furthermore, in the case of *BHLH100*, *BHLH38*, and *IMA2* genes, their increase in expression under Fe deficiency was significantly higher in *spms* than the wild type, indicating that Spm deficiency also plays a role in Fe deficiency signaling. Interestingly, the expression of *CYP82C4* was not significantly different between Fe conditions in any of the genotypes. However, in wild

type the expression of *CYP82C4* gene was significantly higher than in *spms,* indicating that Spm may be important for the basal expression of these gene.

In summary these results suggested that endogenous Spm was also involved in Fe deficiency signaling pathway.

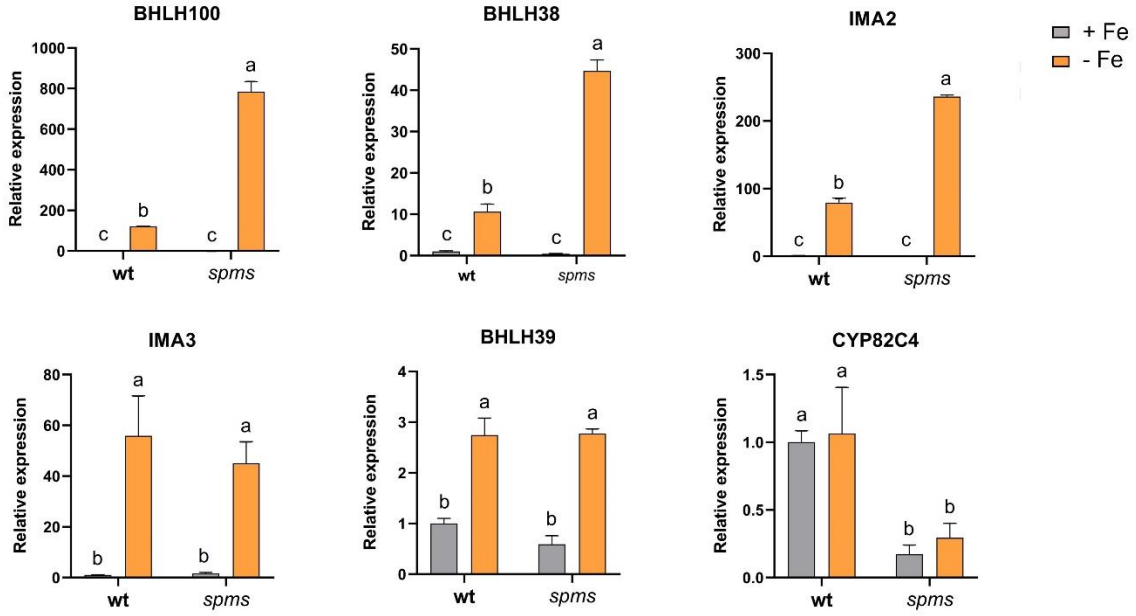

Figure 33. qRT–PCR gene expression analyses of Fe deficiency signaling pathway genes *BHLH100*, *BHLH38*, *IMA2*, *IMA3*, *BHLH39*, and *CYP92C4* in wild type and *spms* seedlings. The seedlings were grown *in vitro* on ½ MS growth medium and 1% plant agar and incubated under 16 h light / 8 h dark cycles at 20-22 °C. After eight days, the seedlings were transferred to new plates under Fe basal conditions (50 μM, +Fe) and Fe deficiency conditions (0 μM, -Fe). The seedlings were then incubated eight more days. The data are presented as mean ± SD, with N = 3 replicates. Statistical analysis was performed using a two-way ANOVA test, and different letters indicate significant differences $P \leq 0.05$.

2. Identification of Potential Genes Associated with Spermine Resistance in *A. thaliana*

2.2. DISCUSSION

In this work, we report the identification of candidate genes which mutations underlie Spm tolerance in Arabidopsis. *AMT2*, *LAC9* and *At5g28090* were identified through forward genetics, whereas *Cua0r2* and ethylene signaling pathway *CTR1, EIN1, EIN2, EIN3, EIN3EIL,* were identified through reverse genetics approaches.

We show that exogenous Spm inhibits root elongation (**Figure 16; Figure 17**), consistent with previous findings (Liu, et al., 2014b; Takahashi et al., 2019). The observation that loss-of-function mutations at *amt2*, *lac9*, *at5g28090, cua0r2*, *ein1*, *ein2*, *ein3*, *ein3eil1* partly rescue the root-growth inhibitory effect of Spm (**Figure 19; Figure 22; Figure 25)**, suggests the involvement of amine transporters, polyamine oxidases and ethylene signaling components in Spm responses.

Previous studies in plants, revealed that exogenous Spm induces the production of H_2O_2 (Liu, et al., 2014b; van Rensburg et al., 2021), which is also consistent with our findings (**Figure 20**; **Figure 21**). However, such increase is attenuated or absent in *amt2*, *lac9*, *at5g28090,* and c*ua0r2* mutants (**Figure 20**; **Figure 23**), supporting the idea that they may be involved in Spm tolerance through the inhibition of ROS production or limiting the availability of Spm.

Gene ontology analyses of *AMT2* co-expressed genes were consistent with the predicted function of AMT2 as ammonium transporter (**Figure 21**). *AMT2* is phylogenetically distant to other AMT family members in Arabidopsis, suggesting it may play a distinct role among AMT transporters (Sohlenkamp et al., 2002). AMT2 significantly contributes to root-to-shoot translocation of ammonium, notably under elevated ammonium supply conditions (Giehl et al., 2017). Given these observations and the fact that Spm is a polyamine carrying several amino groups, it seems tempting to speculate that AMT2 is involved in Spm transport, an aspect that has not been furtherly investigated.

Co-expressed genes with *LAC9* are associated with cell wall organization (**Figure 21**). *A. thaliana* contains 17 lacasses, which belong to the family of multicopper oxidoreductases (Turlapati et al., 2011). Some lacasses (*LAC4*, *LAC5*, *LAC7*, *LAC10* and *LAC12*) have non-redundant activities in lignin polymerization within specific cell types and cell wall layers (Blaschek et al., 2023). However, the specific role of *LAC9* remains poorly understood. A study based on microarray databases suggests a potential role, along with *LAC8* and *LAC1*, in wound responses (Turlapati et al., 2011). Several studies report that cell wall-bound polyamines, including Spm, contribute to cell wall integrity (Aloisi et al., 2017; Berta et al., 1997; Hura et al., 2015) and exogenous application of Spm triggers

transcriptional reprogramming of genes involved in cell wall modification (C. Zhang et al., 2023). Considering these findings, we hypothesize that Spm may trigger changes in cell wall lignification underlying some of the root-growth inhibitory effects, and that *LAC9* mutation would rescue such cell wall alterations.

Regarding the *CuAOγ2* gene candidate identified through reverse genetics, GO analyses (**Figure 19**) revealed that *CuAOγ2* co-expressed genes were associated with oxidoreductase activity and putrescine responses, aligning with the function of CuAOγ2 in polyamine catabolism. CuAOγ2 is an apoplastic enzyme localized in hydathodes of new emerging leaves, cotyledons, and specifically in columella cells (Fraudentali et al., 2020). The expression of *CuAOγ2* is upregulated by Put (500 μM) after 1 h and 3 h of treatment (Fraudentali et al., 2020). Conversely, a recent study performed in our lab (C. Zhang et al., 2023) shows that *CuAOγ2* is downregulated in leaves after 24h of treatment with lower concentrations of Put (100 μM) and Spm (100 μM). These findings suggest the significance of this enzyme in maintaining polyamine homeostasis through polyamine oxidation and ROS production. The high ROS derived from Spm supplementation was suppressed in the *cuaoγ2* mutant and might underlie the suppression of Spm responses in roots, provided that Spm is also substrate of the enzyme.

Interestingly, GO analyses of *CuAOγ2* co-expressed genes suggested its involvement in Fe homeostasis (**Figure 24**). This is consistent with our gene expression analyses, which showed increased expression of several genes associated with Fe deficiency in seedlings treated with Spm (**Figure 28**; **Table 12**; **Table S4**). These results suggested a potential relationship between Spm and Fe deficiency response.

qRT-PCR gene expression analyses confirmed the upregulation in the expression of genes involved in Fe deficiency signaling (*BHLH100*, *BHLH38*, *IMA2*, *IMA3*, *BHLHH39* and *CYP82C4*) in seedlings treated with 400 μM Spm (**Figure 29**), supporting a cross-modulation between Spm supplementation and Fe deficiency.

In *A. thaliana*, exogenous Put alleviates the symptoms of Fe deficiency (Zhu et al., 2016). However, studies conducted in bacteria indicate that high doses of Spm induce the expression of genes involved in Fe acquisition and regulation (Yao & Lu, 2014), and excessive amounts of Spd reduce Fe availability (Kumar et al., 2022). These findings provide additional support to the idea that exogenous Spm triggers Fe deficiency responses.

Our results show that increasing Fe in the presence of Spm does not rescue the root shortening phenotype, but it leads to an increase in shoot biomass (**Figure 30**). These results suggest the occurrence of different mechanisms for Spm toxicity in roots and shoots, and those involving iron responses only operate in photosynthetic tissues.

Several investigations indicate that coumarins are secreted under Fe-limited conditions (Clemens & Weber, 2016; Lan et al., 2011; Yang et al., 2010). In line with this, we detected the presence of coumarins or other polyphenolic derivatives exudated by the roots of wild type and *spms* seedlings treated with 400 μM Spm (**Figure 31**). Additionally, and consistent with this finding, higher *F6'H1* expression was observed in the roots of wild type and *spms* seedlings treated with 400 μM Spm (**Figure 32**).

Furthermore, a study indicates that, apart from β-Glucosidase BGLU42 enzyme, other enzymes may contribute to coumarin secretion, suggesting BLG21, BLG22 and BLG23 as potential candidates (Ahn et al., 2010). Consistent with this, our transcriptional analysis shows that *BGL21* and *BGL22* genes are upregulated in wild type seedlings treated with 400 μM Spm (**Table S4**), supporting the idea that Spm induce the synthesis of coumarins.

The expression of certain genes *(BHLH100*, *BHLH38*, *IMA2*) involved in Fe deficiency signaling pathway is higher in *spms* seedlings compared to wild type under Fe deficiency conditions (**Figure 33**). This suggests a potential role of endogenous Spm in the Fe deficiency signaling pathway. It has been previously described that Spm can form a ternary complex with Fe in the presence of membrane lipids (Mozdzan et al., 2006; Tadolini, 1988). This complex formation reduces Fe^{2+} oxidation and ROS production. Based on these results, we hypothesize that in the case of the *spms* mutant, Fe may be less bioavailable due to the potential disruption of these complexes.

Taken together, these findings suggest that in both scenarios - supplementing the media with Spm or having a Spm deficit (*spms* mutant) - the most severe iron deficiency symptoms are observed. This indicates that the interaction of Spm with Fe essentially "traps" iron in a compartment, preventing its deficiency or inducing it in the case of the media supplementation.

Furthermore, the recent discovery of the role of *IMA/FEP* genes in positively regulating plant responses to iron deficiency (Grillet et al., 2018) and their possible implication in the regulation of long-distance Fe signaling under Fe deficiency or Fe heterogenous conditions (Tabata et al., 2022), together with the fact that our transcriptional analysis shows increased

expression of *IMA/FEP* genes (*IMA1*, *IMA2*, *IMA3*, *IMA6*) in wild type seedlings treated with Spm, open a new avenue to better understand Fe signaling pathway.

Regarding the ethylene signaling, we observed a reduced impact on root shortening in the mutant seedlings (*ein1*, *ein2*, *ein3*, *ein3eil1*) in the presence of 400 μM Spm (**Figure 25**). This finding, and the short root phenotype typical of the triple response and the *ctr1* mutant, led us to hypothesize that Spm induced the synthesis of ethylene. However, our results from the dark growth assay showed that exogenous Spm does not induce the characteristic phenotype of ethylene triple response (**Figure 26**). The use of the ethylene inhibitor AVG in wild type seedlings revealed that the inhibitor alone also caused root shortening, producing a similar phenotype to Spm (**Figure 27**). Therefore, ethylene pathway activation and inhibition results in the same root shortening phenotype. In such regard, Spm may lead to an imbalance in ethylene biosynthesis or signaling. Previous investigations showed that Spm inhibits ethylene biosynthesis leading to an antagonistic effect on senescence (S. Pandey et al., 2000), fruit ripening (Kushand & Dumbroff, 1991; Mo et al., 2020; R. Pandey et al., 2015; Torrigiani et al., 2012) and the response to different stresses (Lechowska et al., 2022; Zapata et al., 2003). A recent study in Arabidopsis suggests that Spd reduces the levels of the EIN3 by suppressing the degradation of EBF1/2 protein (Liebsch et al., 2022). Based on this finding, another hypothesis arises, suggesting that Spm may act in a similar way as Spd, reducing the levels of EIN3 and/or acting on other signaling components of the ethylene pathway, which could explain why ethylene signaling mutants show certain root-resistance to Spm.

To gain a better understanding about the connection between Spm and ethylene, further investigations are required. Testing the levels of ethylene or the EIN3 protein in wild type seedlings treated with 400 μM Spm would provide more information to validate the previous hypotheses, as well as performing global expression analyses in these backgrounds under Spm supplementation conditions.

Conclusions

1. Polyamines increase the abundance of polysome complexes in *A. thaliana*, resulting of a global enhancement in translational activity.
2. The presence of polyamines in different ribosome complexes does not seem to have a direct correlation with either the detected abundance of these complexes or the enrichment of RPs within them.
3. Put is important in the ribosome machinery of plants whereas Spm is not as crucial.
4. Through an EMS-based mutagenesis screen, *AMT2*, *LAC9* and *At5g28090* have been identified as candidate genes responsible for Spm tolerance in roots. Such tolerance associates with reduced ROS production under Spm treatments.
5. In addition, *CuAOχ2* and mutations in ethylene pathway genes, *EIN1*, *EIN2*, *EIN3*, and *EIN3EIL1,* have been identified as candidates underlying Spm tolerance in roots through reverse genetics approaches. *CuAOχ2* mutation might be related to reduced ROS production. The lack of rescue using ethylene inhibitors and lack of reconstitution of the triple response by Spm feeding suggests an effect of Spm on ethylene signaling.
6. Exogenous Spm triggers Fe deficiency responses, and Fe supplementation only reconstitutes the growth of photosynthetic tissues. Additionally, exogenous Spm induces coumarin production, a known response to Fe deficiency.
7. In the *spms* mutant, most severe Fe deficiency symptoms are observed compared to the wild type. This observation leads us to conclude that alterations in Spm homeostasis can influence Fe availability.
8. Overall, polyamines show multifaceted effects on the modulation of translation and intricate coordination with ethylene signaling and iron deficiency sensing.
   Importantly, not all polyamines behave similarly but we find specific roles for Put and Spm in every analyzed process. Hence, polyamines are key metabolites that affect fundamental cell processes and modulate hormonal and nutritional cues in plants.

Bibliography

Agurla, S., Gayatri, G., & Raghavendra, A. S. (2018). Polyamines increase nitric oxide and reactive oxygen species in guard cells of *Arabidopsis thaliana* during stomatal closure. *Protoplasma*, *255*(1), 153–162. https://doi.org/10.1007/s00709-017-1139-3

Ahn, Y. O., Shimizu, B. I., Sakata, K., Gantulga, D., Zhou, Z., Bevan, D. R., & Esen, A. (2010). Scopolin-hydrolyzing β-glucosidases in roots of Arabidopsis. *Plant and Cell Physiology*, *51*(1), 132–143. https://doi.org/10.1093/pcp/pcp174

Alcázar, R., Marco, F., Cuevas, J. C., Patron, M., Ferrando, A., Carrasco, P., Tiburcio, A. F., & Altabella, T. (2006). Involvement of polyamines in plant response to abiotic stress. *Biotechnology Letters, 28*(23), 1867–1876. https://doi.org/10.1007/s10529-006-9179-3

Alcázar, R., Planas, J., Saxena, T., Zarza, X., Bortolotti, C., Cuevas, J., Bitrián, M., Tiburcio, A. F., & Altabella, T. (2010). Putrescine accumulation confers drought tolerance in transgenic *Arabidopsis* plants over-expressing the homologous *Arginine decarboxylase 2* gene. *Plant Physiology and Biochemistry*, *48*(7), 547–552. https://doi.org/10.1016/j.plaphy.2010.02.002

Alcázar, R., & Tiburcio, A. F. (2014). Plant polyamines in stress and development: An emerging area of research in plant sciences. *Frontiers in Plant Science*, *5*, 319. https://doi.org/10.3389/fpls.2014.00319

Aloisi, I., Cai, G., Faleri, C., Navazio, L., Serafini-Fracassini, D., & Del Duca, S. (2017). Spermine regulates pollen tube growth by modulating Ca^{2+}-dependent actin organization and cell wall structure. *Frontiers in Plant Science*, *8*, 1701. https://doi.org/10.3389/fpls.2017.01701

Alonso, J. M., Stepanova, A. N., Solano, R., Wisman, E., Ferrari, S., Ausubel, F. M., & Ecker, J. R. (2003). Five components of the ethylene-response pathway identified in a screen for weak ethylene-insensitive mutants in Arabidopsis. *Proceedings of the National Academy of Sciences of the Unites States of America*, *100*(5), 2992–2997. https://doi.org/10.1073/pnas.0438070100

Amarantos, I., Zarkadis, I. K., & Kalpaxis, D. L. (2002). The identification of spermine binding sites in 16S rRNA allows interpretation of the spermine effect on ribosomal 30S subunit functions. *Nucleic Acids Research*, *30*(13), 2832–2843. https://doi.org/10.1093/nar/gkf404.

Apelbaum, A., & Goldlust, A. (1985). Control by ethylene of arginine decarboxylase activity in pea seedlings and its implication for hormonal regulation of plant growth. *Plant physiology*, *79*(3), 635–640. https://doi.org/10.1104/pp.79.3.635

Atkins, J. F., Lewis, J. B., Anderson, C. W., & Gesteland, R. F. (1975). Enhanced differential synthesis of proteins in a mammalian cell free system by addition of polyamines. *Journal of Biological Chemistry*, *250*(14), 5688–5695. https://doi.org/10.1016/s0021-9258(19)41234-9

Bakshi, A., Shemansky, J. M., Chang, C., & Binder, B. M. (2015). History of research on the plant hormone ethylene. *Journal of Plant Growth Regulation*, *34*(4), 809–827. https://doi.org/10.1007/s00344-015-9522-9

Ban, N., Beckmann, R., Cate, J. H. D., Dinman, J. D., Dragon, F., Ellis, S. R., Lafontaine, D. L. J., Lindahl, L., Liljas, A., Lipton, J. M., McAlear, M. A., Moore, P. B., Noller, H. F., Ortega, J., Panse, V. G., Ramakrishnan, V., Spahn, C. M. T., Steitz, T. A., Tchorzewski, M., Tollervey, D., … Yusupov, M. (2014). A new system for naming ribosomal proteins. *Current Opinion in Structural Biology*, *24*, 165–169. https://doi.org/10.1016/j.sbi.2014.01.002

Barakat, A., Szick-Miranda, K., Chang, I. F., Guyot, R., Blanc, G., Cooke, R., Delseny, M., & Bailey-Serres, J. (2001). The organization of cytoplasmic ribosomal protein genes in

the Arabidopsis genome. *Plant Physiology*, *127*(2), 398–415. https://doi.org/10.1104/pp.010265

Barrington, C. L., Koch, A. L., Galindo, G., Larkin-Gero, E., Morrison, E. J., Tisa, S., Stasevich, T. J., & Rissland, O. S. (2022). Synonymous codon usage regulates translation initiation. *BioRxiv 2022.05.13.491887*. https://doi.org/10.1101/2022.05.13.491887

Benavente, L. M., & Alonso, J. M. (2006). Molecular mechanisms of ethylene signaling in Arabidopsis. *Molecular BioSystems*, *2*(3–4), 165–173. https://doi.org/10.1039/b513874d

Benkő, P., Jee, S., Kaszler, N., Fehér, A., & Gémes, K. (2020). Polyamines treatment during pollen germination and pollen tube elongation in tobacco modulate reactive oxygen species and nitric oxide homeostasis. *Journal of Plant Physiology*, *244*, 153085. https://doi.org/10.1016/j.jplph.2019.153085

Berta, G., Altamura, M. M., Fusconi, A., Cerruti, F., Capitani, F., & Bagni, N. (1997). The plant cell wall is altered by inhibition of polyamine biosynthesis. *New Phytologist*, *137*(4), 569–577. https://doi.org/10.1046/j.1469-8137.1997.00868.x

Blaschek, L., Murozuka, E., Serk, H., Ménard, D., & Pesquet, E. (2023). Different combinations of laccase paralogs nonredundantly control the amount and composition of lignin in specific cell types and cell wall layers in Arabidopsis. *Plant Cell*, *35*(2), 889–909. https://doi.org/10.1093/plcell/koac344

Bleecker A. B. (1999). Ethylene perception and signaling: an evolutionary perspective. *Trends in Plant Science*, *4*(7), 269–274. https://doi.org/10.1016/s1360-1385(99)01427-2

Browning, K. S., & Bailey-Serres, J. (2015). Mechanism of Cytoplasmic mRNA Translation. *The Arabidopsis Book*, *13*, e0176. https://doi.org/10.1199/tab.0176

Carbon, S., Douglass, E., Dunn, N., Good, B., Harris, N. L., Lewis, S. E., Mungall, C. J., Basu, S., Chisholm, R. L., Dodson, R. J., Hartline, E., Fey, P., Thomas, P. D., Albou, L. P., Ebert, D., Kesling, M. J., Mi, H., Muruganujan, A., Huang, X., … Westerfield, M. (2019). The Gene Ontology Resource: 20 years and still GOing strong. *Nucleic Acids Research*, *47*(D1), D330–D338. https://doi.org/10.1093/nar/gky1055

Chang, I. F., Szick-Miranda, K., Pan, S., & Bailey-Serres, J. (2005). Proteomic characterization of evolutionarily conserved and variable proteins of Arabidopsis cytosolic ribosomes. *Plant Physiology*, *137*(3), 848–862. https://doi.org/10.1104/pp.104.053637

Chao, Q., & Rothenberg, M. (1997). Activation of the ethylene gas response pathway in Arabidopsis by the nuclear protein ETHYLENE-INSENSITIVE3 and related proteins. *Cell*, *89*(7), 1133–1144. https://doi.org/10.1016/s0092-8674(00)80300-1

Chattopadhyay, M. K., Tabor, C. W., & Tabor, H. (2003). Spermidine but not spermine is essential for hypusine biosynthesis and growth in *Saccharomyces cerevisiae*: Spermine is converted to spermidine in vivo by the *FMS1*-amine oxidase. *Proceedings of the National Academy of Sciences of the Unites States of America*, *100*(24), 13869–13874. www.pnas.orgcgidoi10.1073pnas.1835918100

Chen, W. W., Yang, J. L., Qin, C., Jin, C. W., Mo, J. H., Ye, T., & Zheng, S. J. (2010). Nitric oxide acts downstream of auxin to trigger root ferric-chelate reductase activity in response to iron deficiency in Arabidopsis. *Plant Physiology*, *154*(2), 810–819. https://doi.org/10.1104/pp.110.161109

Chen, Y. F., Randlett, M. D., Findell, J. L., & Schaller, G. E. (2002). Localization of the ethylene receptor ETR1 to the endoplasmic reticulum of *Arabidopsis*. *The Journal of Biological Chemistry*, *277*(22), 19861–19866. https://doi.org/10.1074/jbc.M201286200

Cheng, C. Y., Krishnakumar, V., Chan, A. P., Thibaud-Nissen, F., Schobel, S., & Town, C. D. (2017). Araport11: a complete reannotation of the *Arabidopsis thaliana* reference genome. *Plant Journal*, *89*(4), 789–804. https://doi.org/10.1111/tpj.13415

Christian, B. E., Haque, M. E., & Spremulli, L. L. (2010). The effect of spermine on the initiation of mitochondrial protein synthesis. *Biochemical and Biophysical Research Communications*, *391*(1), 942–946. https://doi.org/10.1016/j.bbrc.2009.11.169

Clemens, S., & Weber, M. (2016). The essential role of coumarin secretion for Fe acquisition from alkaline soil. *Plant Signaling and Behavior*, *11*(2), e1114197. https://doi.org/10.1080/15592324.2015.1114197

Cohen, S. S., & Lichtenstein, J. (1960). Polyamiues and Ribosome Structure. The *Journal of Biological Chemistry*, *235*(7), 2112–2116.

Colangelo, E. P., & Guerinot, M. L. (2004). The essential basic helix-loop-helix protein FIT1 is required for the iron deficiency response. *The Plant Cell*, *16*(12), 3400–3412. https://doi.org/10.1105/tpc.104.024315

Cona, A., Rea, G., Angelini, R., Federico, R., & Tavladoraki, P. (2006). Functions of amine oxidases in plant development and defence. *Trends in Plant Science*, *11*(2), 80–88. https://doi.org/10.1016/j.tplants.2005.12.009

Cowley, T., & Walters, D. R. (2002). Polyamine metabolism in an incompatible interaction between barley and the powdery mildew fungus, *Blumeria graminis* f. sp. *hordei*. *Journal of Phytopathology*, *150*(11–12), 581–586. https://doi.org/10.1046/j.1439-0434.2002.00816.x

Cuevas, J. C., Sánchez, D. H., Marina, M., & Ruiz, O. A. (2004). Do polyamines modulate the *Lotus glaber* NADPH oxidation activity induced by the herbicide methyl viologen? *Functional Plant Biology*, *31*(9), 921–928. https://doi.org/10.1071/FP04007

Curie, C., & Briat, J. F. (2003). Iron Transport and Signaling in Plants. *Annual Review of Plant Biology*, *54*, 183–206. https://doi.org/10.1146/annurev.arplant.54.031902.135018

Darnell, J. C., Van Driesche, S. J., Zhang, C., Ying, K., Hung, S., Mele, A., Fraser, C. E., Stone, E. F., Chen, C., Fak, J. J., Chi, S. W., Licatalosi, D. D., Richter, J. D., & Darnell, R. B. (2011). FMRP stalls ribosomal translocation on mRNAs linked to synaptic function and autism. *Cell*, *46*(2), 247–261. https://doi.org/10.1016/j.cell.2011.06.013

Demiralay, M., Sağlam, A., Yetişsin, F., & Kadioğlu, A. (2022). Investigation of the roles of hydrogen peroxide and NADPH oxidase in the regulation of polyamine metabolism in maize plants under drought stress conditions. *Journal of Agricultural Sciences*, *28*(4), 613–625. https://doi.org/10.15832/ankutbd.861008

Desikan, R., Last, K., Harrett-Williams, R., Tagliavia, C., Harter, K., Hooley, R., Hancock, J. T., & Neill, S. J. (2006). Ethylene-induced stomatal closure in Arabidopsis occurs via AtrbohF-mediated hydrogen peroxide synthesis. *Plant Journal*, *47*(6), 907–916. https://doi.org/10.1111/j.1365-313X.2006.02842.x

Dever, T. E., & Ivanov, I. P. (2018). Roles of polyamines in translation. *The Journal of Biological Chemistry*, 293(*48*), 18719–18729. https://doi.org/10.1074/jbc.TM118.003338

Do, T. H. T., Choi, H., Palmgren, M., Martinoia, E., Hwang, J. U., & Lee, Y. (2019). *Arabidopsis* ABCG28 is required for the apical accumulation of reactive oxygen species in growing pollen tubes. *Proceedings of the National Academy of Sciences of the United States of America*, *116*(25), 12540–12549. https://doi.org/10.1073/pnas.1902010116

Dörner, K., Badertscher, L., Horváth, B., Hollandi, R. D. S., Molnár, C., Fuhrer, T., Meier, R., Sárazová, M., Van Den Heuvel, J., Zamboni, N., Horvath, P., & Kutay, U. (2022).

Genome-wide RNAi screen identifies novel players in human 60S subunit biogenesis including key enzymes of polyamine metabolism. *Nucleic Acids Research*, *50*(5), 2872–2888. https://doi.org/10.1093/nar/gkac072

Doyle, J., & Hortorium, B. (1991). DNA Protocols for Plants. *Molecular Techniques in Taxonomy, 57*, 283–293. https://doi.org/10.1007/978-3-642-83962-7_18

Faundes, V., Jennings, M. D., Crilly, S., Legraie, S., Withers, S. E., Cuvertino, S., Davies, S. J., Douglas, A. G. L., Fry, A. E., Harrison, V., Amiel, J., Lehalle, D., Newman, W. G., Newkirk, P., Ranells, J., Splitt, M., Cross, L. A., Saunders, C. J., Sullivan, B. R., … Banka, S. (2021). Impaired eIF5A function causes a Mendelian disorder that is partially rescued in model systems by spermidine. *Nature Communications*, *12*(1). https://doi.org/10.1038/s41467-021-21053-2

Faye, M. D., Graber, T. E., & Holcik, M. (2014). Assessment of selective mRNA translation in mammalian cells by polysome profiling. *Journal of Visualized Experiments*, (92), e52295. https://doi.org/10.3791/52295

Ferretti, M. B., Ghalei, H., Ward, E. A., Potts, E. L., & Karbstein, K. (2017). Rps26 directs mRNA-specific translation by recognition of Kozak sequence elements. *Nature Structural and Molecular Biology*, *24*(9), 700–707. https://doi.org/10.1038/nsmb.3442

Firmino, A. A. P., Gorka, M., Graf, A., Skirycz, A., Martinez-Seidel, F., Zander, K., Kopka, J., & Beine-Golovchuk, O. (2020). Separation and paired proteome profiling of plant chloroplast and cytoplasmic ribosomes. *Plants (Basel, Switzerland)*, *9*(7), 1–29. https://doi.org/10.3390/plants9070892

Fraudentali, I., Ghuge, S. A., Carucci, A., Tavladoraki, P., Angelini, R., Rodrigues-Pousada, R. A., & Cona, A. (2020). Developmental, hormone- and stress-modulated expression profiles of four members of the Arabidopsis copper-amine oxidase gene family. *Plant Physiology and Biochemistry*, *147*, 141–160. https://doi.org/10.1016/j.plaphy.2019.11.037

Freitas, V. S., Miranda, R. de S., Costa, J. H., Oliveira, D. F. de, Paula, S. de O., Miguel, E. de C., Freire, R. S., Prisco, J. T., & Gomes-Filho, E. (2018). Ethylene triggers salt tolerance in maize genotypes by modulating polyamine catabolism enzymes associated with H_2O_2 production. *Environmental and Experimental Botany*, *145*, 75–86. https://doi.org/10.1016/j.envexpbot.2017.10.022

Gao, H., Wu, X., Yang, X., Sun, M., Liang, J., Xiao, Y., & Peng, F. (2022). Silicon inhibits gummosis by promoting polyamine synthesis and repressing ethylene biosynthesis in peach. *Frontiers in Plant Science*, *13*, 986688. https://doi.org/10.3389/fpls.2022.986688

Gebauer, F., & Hentze, M. W. (2004). Molecular mechanisms of translational control. *Nature Reviews. Molecular Cell Biology*, *5*(10), 827–835. https://doi.org/10.1038/nrm1488

Gerlin, L., Baroukh, C., & Genin, S. (2021). Polyamines: double agents in disease and plant immunity. *Trends in Plant Science*, *26*(10), 1061–1071. https://doi.org/10.1016/j.tplants.2021.05.007

Giehl, R. F. H., Laginha, A. M., Duan, F., Rentsch, D., Yuan, L., & von Wirén, N. (2017). A Critical Role of AMT2;1 in Root-To-Shoot Translocation of Ammonium in *Arabidopsis*. *Molecular Plant*, *10*(11), 1449–1460. https://doi.org/10.1016/j.molp.2017.10.001

Graber, T. E., Hébert-Seropian, S., Khoutorsky, A., David, A., Yewdell, J. W., Lacaille, J. C., & Sossin, W. S. (2013). Reactivation of stalled polyribosomes in synaptic plasticity. *Proceedings of the National Academy of Sciences of the United States of America*, *110*(40), 16205–16210. https://doi.org/10.1073/pnas.1307747110

Graziano, M., & Lamattina, L. (2007). Nitric oxide accumulation is required for molecular and physiological responses to iron deficiency in tomato roots. The *Plant Journal*, *52*(5), 949–960. https://doi.org/10.1111/j.1365-313X.2007.03283.x

Grillet, L., Lan, P., Li, W., Mokkapati, G., & Schmidt, W. (2018). IRON MAN is a ubiquitous family of peptides that control iron transport in plants. *Nature Plants*, *4*(11), 953–963. https://doi.org/10.1038/s41477-018-0266-y

Gurzeler, L.A., Link, M., Ibig, Y., Schmidt, I., Galuba, O., Schoenbett, J., Gasser-Didierlaurant, C., Parker, C. N., Mao, X., Bitsch, F., Schirle, M., Couttet, P., Sigoillot, F., Ziegelmüller, J., Uldry, A.-C., Schmiedeberg, N., Mühlemann, O., & Reinhardt, J. (2023). Drug-induced eRF1 degradation promotes readthrough and reveals a new branch of ribosome quality control. *BioRxiv 2023.01.31.526456.* https://doi.org/10.1101/2023.01.31.526456

Gutierrez, E., Shin, B. S., Woolstenhulme, C. J., Kim, J. R., Saini, P., Buskirk, A. R., & Dever, T. E. (2013). eif5A promotes translation of polyproline motifs. *Molecular Cell*, *51*(1), 35–45. https://doi.org/10.1016/j.molcel.2013.04.021

Guzman, P., & Ecker, J. R. (1990). Exploiting the triple response of *Arabidopsis* to identify ethylene-related mutants. *The Plant Cell*, *2*(6), 513–523. https://academic.oup.com/plcell/article/2/6/513/5983205

Han, X., Shangguan, J., Wang, Z., Li, Y., Fan, J., Ren, A., & Zhao, M. (2022). Spermidine regulates mitochondrial function by enhancing eIF5A hypusination and contributes to reactive oxygen species production and ganoderic acid biosynthesis in *Ganoderma lucidum*. *Applied and Environmental Microbiology*, *88*(6), e0203721. https://journals.asm.org/journal/aem

Hanfrey, C., Elliott, K. A., Franceschetti, M., Mayer, M. J., Illingworth, C., & Michael, A. J. (2005). A dual upstream open reading frame-based autoregulatory circuit controlling polyamine-responsive translation. *The Journal of Biological Chemistry*, *280*(47), 39229–39237. https://doi.org/10.1074/jbc.M509340200

Hanfrey, C., Sommer, S., Mayer, M. J., Burtin, D., & Michael, A. J. (2001). *Arabidopsis* polyamine biosynthesis: absence of ornithine decarboxylase and the mechanism of arginine decarboxylase activity. *The Plant Journal*, *27*(6), 551–560. https://doi.org/10.1046/j.1365-313X.2001.01100.x

Huang, Z., Zhang, Z., Zhang, X., Zhang, H., Huang, D., & Huang, R. (2004). Tomato TERF1 modulates ethylene response and enhances osmotic stress tolerance by activating expression of downstream genes. *FEBS Letters*, *573*(1–3), 110–116. https://doi.org/10.1016/j.febslet.2004.07.064

Hunter, A. R., Farrel, P. J., Jackson, R. J., & Hunt, T. (1977). The role of polyamines in cell-free protein synthesis in the wheat-germ system. *European Journal of Biochemistry*, *75*(1), 149–157. https://doi.org/10.1111/j.1432-1033.1977.tb11512.x

Hura, T., Dziurka, M., Hura, K., Ostrowska, A., & Dziurka, K. (2015). Free and cell wall-bound polyamines under long-term water stress applied at different growth stages of ×*Triticosecale Wittm*. *PLoS one*, *10*(8), e0135002. https://doi.org/10.1371/journal.pone.0135002

Igarashi, K., & Kashiwagi, K. (2018). Effects of polyamines on protein synthesis and growth of *Escherichia coli*. *The Journal of Biological Chemistry*, *93*(48), 18702–18709. https://doi.org/10.1074/jbc.TM118.003465

Ingolia, N. T., Hussmann, J. A., & Weissman, J. S. (2019). Ribosome profiling: global views of translation. *Cold Spring Harbor Perspectives in Biology*, *11*(5), a032698. https://doi.org/10.1101/cshperspect.a032698

Ioannidis, N. E., Zschiesche, W., Barth, O., Kotakis, C., Navakoudis, E., Humbeck, K., & Kotzabasis, K. (2014). The genetic reprogramming of polyamine homeostasis during the functional assembly, maturation, and senescence-specific decline of the photosynthetic apparatus in *Hordeum vulgare*. *Journal of Plant Growth Regulation*, *33*, 77–90. https://doi.org/10.1007/s00344-013-9387-8

Ivanov, I. P., Shin, B. S., Loughran, G., Tzani, I., Young-Baird, S. K., Cao, C., Atkins, J. F., & Dever, T. E. (2018). Polyamine control of translation elongation regulates start site selection on antizyme inhibitor mRNA via ribosome queuing. *Molecular Cell*, *70*(2), 254-264.e6. https://doi.org/10.1016/j.molcel.2018.03.015

Jander, G., Baerson, S. R., Hudak, J. A., Gonzalez, K. A., Gruys, K. J., & Last, R. L. (2003). Ethylmethanesulfonate saturation mutagenesis in Arabidopsis to determine frequency of herbicide resistance. *Plant Physiology*, *131*(1), 139–146. https://doi.org/10.1104/pp.102.010397

Janowitz, T., Kneifel, H., & Piotrowski, M. (2003). Identification and characterization of plant agmatine iminohydrolase, the last missing link in polyamine biosynthesis of plants. *FEBS Letters*, *544*(1–3), 258–261. https://doi.org/10.1016/S0014-5793(03)00515-5

Janse van Rensburg, H. C., Limami, A. M., & Van den Ende, W. (2021). Spermine and spermidine priming against *Botrytis cinerea* modulates ROS dynamics and metabolism in Arabidopsis. *Biomolecules*, *11*(2), 223. https://doi.org/10.3390/biom11020223

Ju, C., & Chang, C. (2015). Mechanistic insights in ethylene perception and signal transduction. *Plant Physiology*, *169*(1), 85–95. https://doi.org/10.1104/pp.15.00845

Kieber, J. J., Rothenberg, M., Roman, G., Feldmann, K. A., & Ecker, J. R. (1993). *CTR1*, a negative regulator of the ethylene pathway in Arabidopsis, encodes a member of the Raf family of protein kinases. *Cell*, 72, 427–441. https://doi.org/10.1016/0092-8674(93)90119-b

Kim, Y. J., Lee, H. M., Wang, Y., Wu, J., Kim, S. G., Kang, K. Y., Park, K. H., Kim, Y. C., Choi, I. S., Agrawal, G. K., Rakwal, R., & Kim, S. T. (2013). Depletion of abundant plant RuBisCO protein using the protamine sulfate precipitation method. *Proteomics*, *13*(14), 2176–2179. https://doi.org/10.1002/pmic.201200555

Kim, Y., Schumaker, K. S., & Zhu, J.-K. (2006). EMS Mutagenesis of *Arabidopsis*. *Methods in Molecular Biology (Clifton, N.J.)*, 323, 101–103. https://doi.org/https://doi-org.sire.ub.edu/10.1385/1-59745-003-0:101

Kobayashi, T. (2019). Understanding the complexity of iron sensing and signaling cascades in plants. *Plant and Cell Physiology*, *60*(7), 1440–1446. https://doi.org/10.1093/pcp/pcz038

Krämer, U. (2015). Planting molecular functions in an ecological context with *Arabidopsis thaliana*. *eLife*, 4, e06100. https://doi.org/10.7554/eLife.06100.001

Kumar, V., Mishra, R. K., Ghose, D., Kalita, A., Dhiman, P., Prakash, A., Thakur, N., Mitra, G., Chaudhari, V. D., Arora, A., & Dutta, D. (2022). Free spermidine evokes superoxide radicals that manifest toxicity. *eLife*, *11*, e77704. https://doi.org/10.7554/eLife.77704

Kushand, M. M., & Dumbroff, E. B. (1991). Metabolic and physiological relationships between the polyamine and ethylene biosynthetic pathways. *Biochemistry and Physiology of polyamines in plants*, 77–90.

Lan, P., Li, W., Wen, T. N., Shiau, J. Y., Wu, Y. C., Lin, W., & Schmidt, W. (2011). iTRAQ protein profile analysis of Arabidopsis roots reveals new aspects critical for iron homeostasis. *Plant Physiology*, *155*(2), 821–834. https://doi.org/10.1104/pp.110.169508

Landau, G., Bercovich, Z., Park, M. H., & Kahana, C. (2010). The role of polyamines in supporting growth of mammalian cells is mediated through their requirement for translation initiation and elongation. *The Journal of Biological Chemistry*, *285*(17), 12474–12481. https://doi.org/10.1074/jbc.M110.106419

Lechowska, K., Wojtyla, L., Quinet, M., Kubala, S., Lutts, S., & Garnczarska, M. (2022). Endogenous polyamines and ethylene biosynthesis in relation to germination of osmoprimed *Brassica napus* seeds under salt stress. *International Journal of Molecular Sciences*, *23*(1), 349. https://doi.org/10.3390/ijms23010349

Lei, G. J., Zhu, X. F., Wang, Z. W., Dong, F., Dong, N. Y., & Zheng, S. J. (2014). Abscisic acid alleviates iron deficiency by promoting root iron reutilization and transport from root to shoot in *Arabidopsis*. *Plant, Cell and Environment*, *37*(4), 852–863. https://doi.org/10.1111/pce.12203

Li, C. Z., Jiao, J., & Wang, G. X. (2004). The important roles of reactive oxygen species in the relationship between ethylene and polyamines in leaves of spring wheat seedlings under root osmotic stress. *Plant Science*, *166*(2), 303–315. https://doi.org/10.1016/j.plantsci.2003.09.019

Li, N., Parsons, B. L., Liu, D., & Mattoo, A. K. (1992). Accumulation of wound-inducible ACC synthase transcript in tomato fruit is inhibited by salicylic acid and polyamines. *Plant Molecular Biology*, *18*(3), 477–487. https://doi.org/10.1007/BF00040664

Li, Y., Lu, C. K., Li, C. Y., Lei, R. H., Pu, M. N., Zhao, J. H., Peng, F., Ping, H. Q., Wang, D., & Liang, G. (2021). IRON MAN interacts with BRUTUS to maintain iron homeostasis in *Arabidopsis*. *Proceedings of the National Academy of Sciences of the United States of America*, *118*(39), e2109063118. https://doi.org/10.1073/pnas.2109063118

Liebsch, D., Juvany, M., Li, Z., Wang, H. L., Ziolkowska, A., Chrobok, D., Boussardon, C., Wen, X., Law, S. R., Janečková, H., Brouwer, B., Lindén, P., Delhomme, N., Stenlund, H., Moritz, T., Gardeström, P., Guo, H., & Keech, O. (2022). Metabolic control of arginine and ornithine levels paces the progression of leaf senescence. *Plant Physiology*, *189*(4), 1943–1960. https://doi.org/10.1093/plphys/kiac244

Liu, T., Dobashi, H., Kim, D. W., Sagor, G. H. M., Niitsu, M., Berberich, T., & Kusano, T. (2014b). *Arabidopsis* mutant plants with diverse defects in polyamine metabolism show unequal sensitivity to exogenous cadaverine probably based on their spermine content. *Physiology and Molecular Biology of Plants*, *20*(2), 151–159. https://doi.org/10.1007/s12298-014-0227-5

Liu, T., Kim, D. W., Niitsu, M., Maeda, S., Watanabe, M., Kamio, Y., Berberich, T., & Kusano, T. (2014a). Polyamine oxidase 7 is a terminal catabolism-type enzyme in *Oryza sativa* and is specifically expressed in anthers. *Plant and Cell Physiology*, *55*(6), 1110–1122. https://doi.org/10.1093/pcp/pcu047

López-Millán, A. F., Grusak, M. A., Abadía, A., & Abadía, J. (2013). Iron deficiency in plants: An insight from proteomic approaches. *Frontiers in Plant Science 4,* 254. https://doi.org/10.3389/fpls.2013.00254

Mandal, S., Mandal, A., Johansson, H. E., Orjalo, A. V., & Park, M. H. (2013). Depletion of cellular polyamines, spermidine and spermine, causes a total arrest in translation and growth in mammalian cells. *Proceedings of the National Academy of Sciences of the United States of America*, *110*(6), 2169–2174. https://doi.org/10.1073/pnas.1219002110

Marce, M., Brown, D. S., Capell, T., Figueras, X., & Tiburcio, A. F. (1995). Rapid high-performance liquid chromatographic method for the quantitation of polyamines as their dansyl derivatives: application to plant and animal tissues. *Journal of Chromatography. B,*

Biomedical Applications, *666*(2), 329–335. https://doi.org/10.1016/0378-4347(94)00586-t

Marina, M., Maiale, S. J., Rossi, F. R., Romero, M. F., Rivas, E. I., Gárriz, A., Ruiz, O. A., & Pieckenstain, F. L. (2008). Apoplastic polyamine oxidation plays different roles in local responses of tobacco to infection by the necrotrophic fungus *Sclerotinia sclerotiorum* and the biotrophic bacterium *Pseudomonas viridiflava*. *Plant Physiology*, *147*(4), 2164–2178. https://doi.org/10.1104/pp.108.122614

Martinez-seidel, F., Beine-golovchuk, O., Hsieh, Y. C., El Eshraky, K., Gorka, M., Cheong, B. E., Jimenez-posada, E. V., Walther, D., Skirycz, A., Roessner, U., Kopka, J., & Firmino, A. A. P. (2021). Spatially enriched paralog rearrangements argue functionally diverse ribosomes arise during cold acclimation in Arabidopsis. *International Journal of Molecular Sciences*, *22*(11), 6160. https://doi.org/10.3390/ijms22116160

Martinez-Seidel, F., Beine-Golovchuk, O., Hsieh, Y. C., & Kopka, J. (2020). Systematic review of plant ribosome heterogeneity and specialization. *Frontiers in Plant Science*, *11*, 948. https://doi.org/10.3389/fpls.2020.00948

Martinez-Seidel, F., Hsieh, Y. C., Walther, D., Kopka, J., & Pereira Firmino, A. A. (2021). COSNet*i*: ComplexOme-Structural Network Interpreter used to study spatial enrichment in metazoan ribosomes. *BMC Bioinformatics*, *22*, 605. https://doi.org/10.1186/s12859-021-04510-z

Martinez-Seidel, F., Suwanchaikasem, P., Gentry-Torfer, D., Rajarathinam, Y., Ebert, A., Erban, A., Augusto, A., Firmino, P., Nie, S., Leeming, M. G., Williamson, N. A., Kopka, J., & Boughton, B. A. (2022). Remodelled ribosomes synthesise a specific proteome in proliferating plant tissue during cold. *BioRxiv 2022.11.28.518201.* https://doi.org/10.1101/2022.11.28.518201

Mehta, R. A., Cassol, T., Li, N., Ali, N., Handa, A. K., & Mattoo, A. K. (2002). Engineered polyamine accumulation in tomato enhances phytonutrient content, juice quality, and vine life. *Nature Biotechnology*, *20*(6), 613–618. https://doi.org/10.1038/nbt0602-613

Mellidou, I., Karamanoli, K., Beris, D., Haralampidis, K., Constantinidou, H. I. A., & Roubelakis-Angelakis, K. A. (2017). Underexpression of apoplastic polyamine oxidase improves thermotolerance in *Nicotiana tabacum*. *Journal of Plant Physiology*, *218*, 171–174. https://doi.org/10.1016/j.jplph.2017.08.006

Merchante, C., & Stepanova, A. N. (2017). The triple response assay and its use to characterize ethylene mutants in Arabidopsis. *Methods in Molecular Biology* (*Clifton, N.J.*), *1573*, 163–209. https://doi.org/10.1007/978-1-4939-6854-1_13

Merchante, C., Stepanova, A. N., & Alonso, J. M. (2017). Translation regulation in plants: an interesting past, an exciting present and a promising future. *The Plant Journal*, *90*(4), 628–653. https://doi.org/10.1111/tpj.13520

Mo, A., Xu, T., Bai, Q., Shen, Y., Gao, F., & Guo, J. (2020). FaPAO5 regulates Spm/Spd levels as a signaling during strawberry fruit ripening. *Plant Direct*, *4*(5), e00217. https://doi.org/10.1002/pld3.217

Moschou, P. N., Delis, I. D., Paschalidis, K. A., & Roubelakis-Angelakis, K. A. (2008b). Transgenic tobacco plants overexpressing polyamine oxidase are not able to cope with oxidative burst generated by abiotic factors. *Physiologia Plantarum*, *133*(2), 140–156. https://doi.org/10.1111/j.1399-3054.2008.01049.x

Moschou, P. N., Paschalidis, K. A., Delis, I. D., Andriopoulou, A. H., Lagiotis, G. D., Yakoumakis, D. I., & Roubelakis-Angelakis, K. A. (2008c). Spermidine exodus and oxidation in the apoplast induced by abiotic stress is responsible for H_2O_2 signatures that

direct tolerance responses in tobacco. *The Plant Cell*, *20*(6), 1708–1724. https://doi.org/10.1105/tpc.108.059733

Moschou, P. N., Paschalidis, K. A., & Roubelakis-Angelakis, K. A. (2008a). Plant polyamine catabolism: the state of the art. *Plant Signaling and Behavior*, *3*(12), 1061–1066. https://doi.org/10.4161/psb.3.12.7172

Moschou, P. N., Sarris, P. F., Skandalis, N., Andriopoulou, A. H., Paschalidis, K. A., Panopoulos, N. J., & Roubelakis-Angelakis, K. A. (2009). Engineered polyamine catabolism preinduces tolerance of tobacco to bacteria and oomycetes. *Plant Physiology*, *149*(4), 1970–1981. https://doi.org/10.1104/pp.108.134932

Mozdzan, M., Szemraj, J., Rysz, J., Stolarek, R. A., & Nowak, D. (2006). Anti-oxidant activity of spermine and spermidine re-evaluated with oxidizing systems involving iron and copper ions. *The International Journal of Biochemistry and Cell Biology*, *38*(1), 69–81. https://doi.org/10.1016/j.biocel.2005.07.004

Narula, A., Ellis, J., Taliaferro, J. M., & Rissland, O. S. (2019). Coding regions affect mRNA stability in human cells. *RNA* (*New York, N.Y.*), *25*(12), 1751–1764. https://doi.org/10.1261/rna.073239.119

Nishimura, K., Murozumi, K., Shirahata, A., Park, M. H., Kashiwagi, K., & Igarashi, K. (2005). Independent roles of eIF5A and polyamines in cell proliferation. *The Biochemical journal*, *385*(Pt 3), 779–785. https://doi.org/10.1042/BJ20041477

Noeske, J., Wasserman, M. R., Terry, D. S., Altman, R. B., Blanchard, S. C., & Cate, J. H. D. (2015). High-resolution structure of the *Escherichia coli* ribosome. *Nature Structural and Molecular Biology*, *22*(4), 336–341. https://doi.org/10.1038/nsmb.2994

Ogasawara, T., Ito, K., & Igarashi, K. (1989). Effect of polyamines on globin synthesis in a rabbit reticulocyte polyamine-free protein synthetic system. *Journal of Biochemistry*, *105*(2), 164–167. https://doi.org/10.1093/oxfordjournals.jbchem.a122633

Okada, S., Lei, G. J., Yamaji, N., Huang, S., Ma, J. F., Mochida, K., & Hirayama, T. (2022). FE UPTAKE-INDUCING PEPTIDE1 maintains Fe translocation by controlling Fe deficiency response genes in the vascular tissue of *Arabidopsis*. *Plant, Cell & Environment*, *45*(11), 3322–3337. https://doi.org/10.1111/pce.14424

Pandey, R., Gupta, A., Chowdhary, A., Pal, R. K., & Rajam, M. V. (2015). Over-expression of mouse ornithine decarboxylase gene under the control of fruit-specific promoter enhances fruit quality in tomato. *Plant Molecular Biology*, *87*(3), 249–260. https://doi.org/10.1007/s11103-014-0273-y

Pandey, S., Ranade, S. A., Nagar, P. K., & Kumar, N. (2000). Role of polyamines and ethylene as modulators of plant senescence. *Journal of Biosciences*, *25*(3), 291–299. https://doi.org/10.1007/BF02703938

Park, M. H., & Wolff, E. C. (2018). Hypusine, a polyamine-derived amino acid critical for eukaryotic translation. *The Journal of Biological Chemistry*, *293*(48), 18710–18718. https://doi.org/10.1074/jbc.TM118.003341

Peng, Q., Wong, C. Y. P., Cheuk, I. W. Y., Teoh, J. Y. C., Chiu, P. K. F., & Ng, C. F. (2021). The emerging clinical role of spermine in prostate cancer. *International Journal of Molecular Sciences*, *22*(9), 4382. https://doi.org/10.3390/ijms22094382

Pérez-Leal, O., Barrero, C. A., Clarkson, A. B., Casero, R. A., & Merali, S. (2012). Polyamine-regulated translation of spermidine/spermine-N1-acetyltransferase. *Molecular and Cellular Biology*, *32*(8), 1453–1467. https://doi.org/10.1128/mcb.06444-11

Planas-Portell, J., Gallart, M., Tiburcio, A. F., & Altabella, T. (2013). Copper-containing amine oxidases contribute to terminal polyamine oxidation in peroxisomes and apoplast

of *Arabidopsis thaliana*. *BMC Plant Biology*, *13*, 109. https://doi.org/10.1186/1471-2229-13-109

Pospísek, M., & Valásek, L. (2013). Polysome profile analysis - yeast. M*ethods in Enzymology*, *530*, 173–181. https://doi.org/10.1016/B978-0-12-420037-1.00009-9

Rakitin, V. Y., Prudnikova, O. N., Rakitina, T. Y., Karyagin, V. V., Vlasov, P. V., Novikova, G. V., & Moshkov, I. E. (2009). Interaction between ethylene and ABA in the regulation of polyamine level in *Arabidopsis thaliana* during UV-B stress. *Russian Journal of Plant Physiology*, *56*(2), 147–153. https://doi.org/10.1134/S1021443709020010

Robinson, N. J., Procter, C. M., Connolly, E. L., & Guerinot, M. L. (1999). A ferric-chelate reductase for iron uptake from soils. *Nature*, *397*(6721), 694–697. https://doi.org/10.1038/17800

Roman, G., Lubarsky, B., Kieber, J. J., Rothenberg, M., & Ecker, J. R. (1995). Genetic analysis of ethylene signal transduction in *Arabidopsis thaliana*: five novel mutant loci integrated into a stress response pathway. *Genetics*, *139*(3), 1393–1409. https://doi.org/10.1093/genetics/139.3.1393

Römheld, V., & Marschner, H. (1983). Mechanism of iron uptake by peanut plants: I. Fe reduction, chelate splitting, and release of phenolics. *Plant Physiology*, *71*(4), 949–954. https://doi.org/10.1104/pp.71.4.949

Römheld, V., & Marschner, H. (1986). Evidence for a specific uptake system for iron phytosiderophores in roots of grasses. *Plant Physiology*, *80*(1), 175–180. https://doi.org/10.1104/pp.80.1.175

Sagor, G. H. M., Zhang, S., Kojima, S., Simm, S., Berberich, T., & Kusano, T. (2016). Reducing cytoplasmic polyamine oxidase activity in *Arabidopsis* increases salt and drought tolerance by reducing reactive oxygen species production and increasing defense gene expression. *Frontiers in Plant Science*, *7*,214. https://doi.org/10.3389/fpls.2016.00214

Santi, S., & Schmidt, W. (2009). Dissecting iron deficiency-induced proton extrusion in Arabidopsis roots. *The New Phytologist*, *183*(4), 1072–1084. https://doi.org/10.1111/j.1469-8137.2009.02908.x

Santos, C., & Ballestat, J. P. G. (1995). The highly conserved protein P0 carboxyl end is essential for ribosome activity only in the absence of proteins P1 and P2. *The Journal of Biological Chemistry*, *270*(35), 20608–20614. https://doi.org/10.1074/jbc.270.35.20608

Scholz, P., Anstatt, J., Krawczyk, H. E., & Ischebeck, T. (2020). Signalling pinpointed to the tip: the complex regulatory network that allows pollen tube growth. *Plants (Basel, Switzerland)*, *9*(9), 1098. https://doi.org/10.3390/plants9091098

Schuller, A. P., Wu, C. C. C., Dever, T. E., Buskirk, A. R., & Green, R. (2017). eIF5A functions globally in translation elongation and termination. *Molecular Cell*, *66*(2), 194-205.e5. https://doi.org/10.1016/j.molcel.2017.03.003

Seo, S. Y., Kim, Y. J., & Park, K. Y. (2019). Increasing polyamine contents enhances the stress tolerance *via* reinforcement of antioxidative properties. *Frontiers in Plant Science*, *10*, 1331. https://doi.org/10.3389/fpls.2019.01331

Sequera-Mutiozabal, M. I., Erban, A., Kopka, J., Atanasov, K. E., Bastida, J., Fotopoulos, V., Alcázar, R., & Tiburcio, A. F. (2016). Global metabolic profiling of *Arabidopsis Polyamine Oxidase 4* (*AtPAO4*) loss-of-function mutants exhibiting delayed dark-induced senescence. *Frontiers in Plant Science*, *7*, 173. https://doi.org/10.3389/fpls.2016.00173

Shen, W., Nada, K., & Tachibana, S. (2000). Involvement of polyamines in the chilling tolerance of cucumber cultivars. *Plant physiology*, *124*(1), 431–439. https://doi.org/10.1104/pp.124.1.431

Shi, H. X., Liang, C., Yao, C. Y., Gao, Z. X., Qin, J., Cao, J. L., Zhang, M. Z., Li, Y. Y., Wang, M. Q., Sun, H., Xie, S. Q., & Fang, D. (2022). Elevation of spermine remodels immunosuppressive microenvironment through driving the modification of PD-L1 in hepatocellular carcinoma. *Cell Communication and Signaling*, *20*(1), 175. https://doi.org/10.1186/s12964-022-00981-6

Shi, Z., Fujii, K., Kovary, K. M., Genuth, N. R., Röst, H. L., Teruel, M. N., & Barna, M. (2017). Heterogeneous ribosomes preferentially translate distinct subpools of mRNAs genome-wide. *Molecular Cell*, *67*(1), 71-83.e7. https://doi.org/10.1016/j.molcel.2017.05.021

Singh, A., Mehta, S., Yadav, S., Nagar, G., Ghosh, R., Roy, A., Chakraborty, A., & Singh, I. K. (2022). How to cope with the challenges of environmental stresses in the era of global climate change: an update on ROS stave off in plants. *International Journal of Molecular Sciences*, 23(4), 1995. https://doi.org/10.3390/ijms23041995

Sobieszczuk-Nowicka, E., Kubala, S., Zmienko, A., Małecka, A., & Legocka, J. (2016). From accumulation to degradation: reprogramming polyamine metabolism facilitates dark-induced senescence in barley leaf cells. *Frontiers in Plant Science*, *6*, 1198. https://doi.org/10.3389/fpls.2015.01198

Sohlenkamp, C., Wood, C. C., Roeb, G. W., & Udvardi, M. K. (2002). Characterization of Arabidopsis AtAMT2, a high-affinity ammonium transporter of the plasma membrane. *Plant Physiology*, *130*(4), 1788–1796. https://doi.org/10.1104/pp.008599

Somerville, C., & Koornneef, M. (2002). A fortunate choice: the history of *Arabidopsis* as a model plant. *Nature Reviews. Genetics*. *3*(11), 883–889. https://doi.org/10.1038/nrg927

Sun, W., Zhang, X., Chen, D., & Murchie, A. I. H. (2020). Interactions between the 5' UTR mRNA of the *spe2* gene and spermidine regulate translation in *S. pombe*. *RNA (New York, N.Y.)*, *26*(2), 137–149. https://doi.org/10.1261/rna.072975.119

Tabata, R. (2023). Regulation of the iron-deficiency response by IMA/FEP peptide. *Frontiers in Plant Science*, *14*, 1107405. https://doi.org/10.3389/fpls.2023.1107405

Tabata, R., Kamiya, T., Imoto, S., Tamura, H., Ikuta, K., Tabata, M., Hirayama, T., Tsukagoshi, H., Tanoi, K., Suzuki, T., Hachiya, T., & Sakakibara, H. (2022). Systemic regulation of iron acquisition by *Arabidopsis* in environments with heterogeneous iron distributions. *Plant and Cell Physiology*, *63*(6), 842–854. https://doi.org/10.1093/pcp/pcac049

Tadolini, B. (1988). Polyamine inhibition of lipoperoxidation. The influence of polyamines on iron oxidation in the presence of compounds mimicking phospholipid polar heads. *The Biochemical journal*, *249*(1), 33–36. https://doi.org/10.1042/bj2490033

Takahashi, Y., Uemura, T., & Teshima, Y. (2019). Polyamine oxidase 2 is involved in regulating excess spermidine contents during seed germination and early seedling development in *Arabidopsis thaliana*. *Biochemical and Biophysical Research Communications*, *516*(4), 1248–1251. https://doi.org/10.1016/j.bbrc.2019.07.022

Takeda, Y. (1969). Polyamines and protein synthesis. I. The effect of polyamines on cell free polyphenylalanine synthesis in *Escherichia coli*. *Journal of biochemistry*, *66*(3), 345–349. https://doi.org/10.1093/oxfordjournals.jbchem.a129152

Tatsuki, M., & Mori, H. (2001). Phosphorylation of tomato 1-aminocyclopropane-1-carboxylic acid synthase, LE-ACS2, at the C-terminal region. *The Journal of Biological Chemistry*, *276*(30), 28051–28057. https://doi.org/10.1074/jbc.M101543200

Tavladoraki, P., Cona, A., & Angelini, R. (2016). Copper-containing amine oxidases and FAD-dependent polyamine oxidases are key players in plant tissue differentiation and organ development. *Frontiers in Plant Science*, *7*, 824. https://doi.org/10.3389/fpls.2016.00824

Tisi, A., Angelini, R., & Cona, A. (2011). Does polyamine catabolism influence root development and xylem differentiation under stress conditions? *Plant Signaling & Behaviour*, *6*(11), 1844–1847. https://doi.org/10.4161/psb.6.11.17640

Tisi, A., Federico, R., Moreno, S., Lucretti, S., Moschou, P. N., Roubelakis-Angelakis, K. A., Angelini, R., & Cona, A. (2011). Perturbation of polyamine catabolism can strongly affect root development and xylem differentiation. *Plant Physiology*, *157*(1), 200–215. https://doi.org/10.1104/pp.111.173153

Torrigiani, P., Bressanin, D., Beatriz Ruiz, K., Tadiello, A., Trainotti, L., Bonghi, C., Ziosi, V., & Costa, G. (2012). Spermidine application to young developing peach fruits leads to a slowing down of ripening by impairing ripening-related ethylene and auxin metabolism and signaling. *Physiologia Plantarum*, *146*(1), 86–98. https://doi.org/10.1111/j.1399-3054.2012.01612.x

Tripathy, B. C., & Oelmüller, R. (2012). Reactive oxygen species generation and signaling in plants. *Plant Signaling and Behavior*, *7*(12), 1621–1633. https://doi.org/10.4161/psb.22455

Turlapati, P. V., Kim, K. W., Davin, L. B., & Lewis, N. G. (2011). The laccase multigene family in *Arabidopsis thaliana*: towards addressing the mystery of their gene function(s). *Planta*, *233*(3), 439–470. https://doi.org/10.1007/s00425-010-1298-3

Uchiumi, T., & Kominami, R. (1992). Direct evidence for interaction of the conserved GTPase domain within 28 S RNA with mammalian ribosomal acidic phosphoproteins and L12. *The Journal of Biological Chemistry*, *267*(27), 19179–19185.

Vert, G., Grotz, N., Dédaldéchamp, F., Gaymard, F., Guerinot, M. L., Briat, J. F., & Curie, C. (2002). IRT1, an Arabidopsis transporter essential for iron uptake from the soil and for plant growth. *The Plant Cell*, *14*(6), 1223–1233. https://doi.org/10.1105/tpc.001388

Wang, W., & Liu, J. H. (2016). *CsPAO4* of *Citrus sinensis* functions in polyamine terminal catabolism and inhibits plant growth under salt stress. *Scientific Reports*, *6*, 31384. https://doi.org/10.1038/srep31384

Wang, Y., Ye, X., Yang, K., Shi, Z., Wang, N., Yang, L., & Chen, J. (2019). Characterization, expression, and functional analysis of polyamine oxidases and their role in selenium-induced hydrogen peroxide production in *Brassica rapa*. *Journal of the Science of Food and Agriculture*, *99*(8), 4082–4093. https://doi.org/10.1002/jsfa.9638

Watson, Z. L., Ward, F. R., Méheust, R., Ad, O., Schepartz, A., Banfield, J. F., & Cate, J. H. D. (2020). Structure of the bacterial ribosome at 2 Å resolution. *eLife*, *9*, e60482. https://doi.org/10.7554/eLife.60482

Wu, J., Shang, Z., Wu, J., Jiang, X., Moschou, P. N., Sun, W., Roubelakis-Angelakis, K. A., & Zhang, S. (2010). Spermidine oxidase-derived H_2O_2 regulates pollen plasma membrane hyperpolarization-activated Ca^{2+}-permeable channels and pollen tube growth. *Plant Journal*, *63*(6), 1042–1053. https://doi.org/10.1111/j.1365-313X.2010.04301.x

Xaplanteri, M. A., Petropoulos, A. D., Dinos, G. P., & Kalpaxis, D. L. (2005). Localization of spermine binding sites in 23S rRNA by photoaffinity labeling: parsing the spermine

contribution to ribosomal 50S subunit functions. *Nucleic Acids Research*, *33*(9), 2792–2805. https://doi.org/10.1093/nar/gki557

Xu, J., Kang, Z., Zhu, K., Zhao, D., Yuan, Y., Yang, S., Zhen, W., & Hu, X. (2021). *RBOH1*-dependent H_2O_2 mediates spermine-induced antioxidant enzyme system to enhance tomato seedling tolerance to salinity–alkalinity stress. *Plant Physiology and Biochemistry*, *164*, 237–246. https://doi.org/10.1016/j.plaphy.2021.04.017

Yang, T. J. W., Lin, W. D., & Schmidt, W. (2010). Transcriptional profiling of the Arabidopsis iron deficiency response reveals conserved transition metal homeostasis networks. *Plant Physiology*, *152*(4), 2130–2141. https://doi.org/10.1104/pp.109.152728

Yao, X., & Lu, C. D. (2014). Characterization of *Staphylococcus aureus* responses to spermine stress. *Current Microbiology*, *69*(3), 394–403. https://doi.org/10.1007/s00284-014-0603-y

Yoda, H., Yamaguchi, Y., & Sano, H. (2003). Induction of hypersensitive cell death by hydrogen peroxide produced through polyamine degradation in tobacco plants. *Plant Physiology*, *132*(4), 1973–1981. https://doi.org/10.1104/pp.103.024737

Yu, Y., Zhou, W., Zhou, K., Liu, W., Liang, X., Chen, Y., Sun, D., & Lin, X. (2018). Polyamines modulate aluminum-induced oxidative stress differently by inducing or reducing H_2O_2 production in wheat. *Chemosphere*, *212*, 645–653. https://doi.org/10.1016/j.chemosphere.2018.08.133

Zapata, P. J., Serrano, M., Pretel, M. T., Amorós, A., & Botella, M. Á. (2003). Changes in ethylene evolution and polyamine profiles of seedlings of nine cultivars of *Lactuca sativa* L. in response to salt stress during germination. *Plant Science*, *164*(4), 557–563. https://doi.org/10.1016/S0168-9452(03)00005-0

Zarza, X., Atanasov, K. E., Marco, F., Arbona, V., Carrasco, P., Kopka, J., Fotopoulos, V., Munnik, T., Gómez-Cadenas, A., Tiburcio, A. F., & Alcázar, R. (2017). *Polyamine oxidase 5* loss-of-function mutations in *Arabidopsis thaliana* trigger metabolic and transcriptional reprogramming and promote salt stress tolerance. *Plant Cell and Environment*, *40*(4), 527–542. https://doi.org/10.1111/pce.12714

Zhang, C., Atanasov, K. E., & Alcázar, R. (2023). Spermine inhibits PAMP-induced ROS and Ca^{2+} burst and reshapes the transcriptional landscape of PAMP-triggered immunity in Arabidopsis. *Journal of Experimental Botany*, *74*(1), 427–442. https://doi.org/10.1093/jxb/erac411

Zhang, J., Chen, Y., Lu, J., Zhang, Y., & Wen, C. K. (2020). Uncertainty of $EIN2^{Ser645/Ser924}$ inactivation by CTR1-mediated phosphorylation reveals the complexity of ethylene signaling. *Plant Communications*, *1*(3), 100046. https://doi.org/10.1016/j.xplc.2020.100046

Zhao, H., Yin, C. C., Ma, B., Chen, S. Y., & Zhang, J. S. (2021). Ethylene signaling in rice and *Arabidopsis*: new regulators and mechanisms. *Journal of Integrative Plant Biology*, *63*(1), 102–125. https://doi.org/10.1111/jipb.13028

Zhou, J., Pang, J., Tripathi, M., Ho, J. P., Widjaja, A. A., Shekeran, S. G., Cook, S. A., Suzuki, A., Diehl, A. M., Petretto, E., Singh, B. K., & Yen, P. M. (2022). Spermidine-mediated hypusination of translation factor EIF5A improves mitochondrial fatty acid oxidation and prevents non-alcoholic steatohepatitis progression. *Nature Communications*, *13*(1), 5202. https://doi.org/10.1038/s41467-022-32788-x

Zhu, X. F., Shi, Y. Z., Lei, G. J., Fry, S. C., Zhang, B. C., Zhou, Y. H., Braam, J., Jiang, T., Xu, X. Y., Mao, C. Z., Pan, Y. J., Yang, J. L., & Wu, P. (2012). *XTH31*, encoding an in vitro XEH/XET-active enzyme, regulates aluminum sensitivity by modulating in vivo XET action, cell wall xyloglucan content, and aluminum binding capacity in *Arabidopsis*. *Plant Cell*, *24*(11), 4731–4747. https://doi.org/10.1105/tpc.112.106039

Zhu, X. F., Wang, B., Song, W. F., Zheng, S. J., & Shen, R. F. (2016). Putrescine alleviates iron deficiency via NO-dependent reutilization of root cell-wall Fe in Arabidopsis. *Plant Physiology*, *170*(1), 558–567. https://doi.org/10.1104/pp.15.01617

Annexes

Supplementary Figures

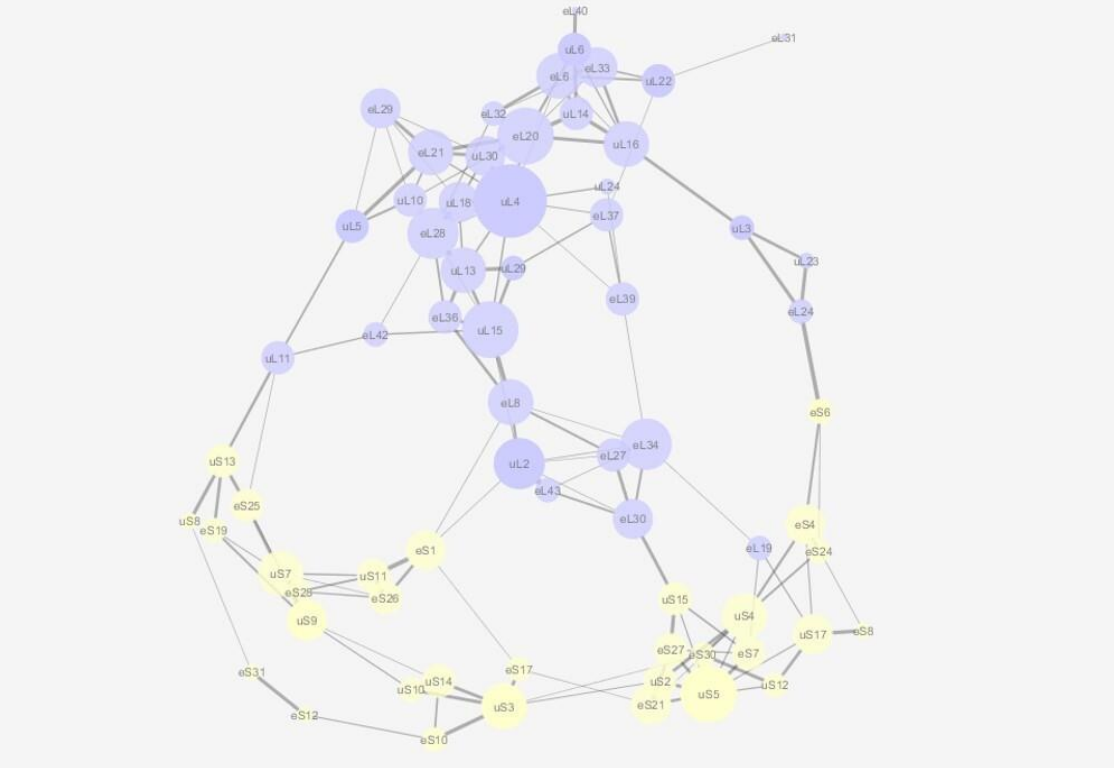

Figure S1. Ribosomal protein network built using the COSNet$_i$ workflow (https:// github. com/ MSeid elFed/ COSNet_i). The network was analyzed as undirected graph in Cytoscape. A larger node size indicates larger degree, the thickness of edges is defined as transit probability between nodes calculated based on the number of contacts between each protein pair. The network layout is edge-weighted spring-embedded to simulate a real structurally connected network with forces acting upon it.

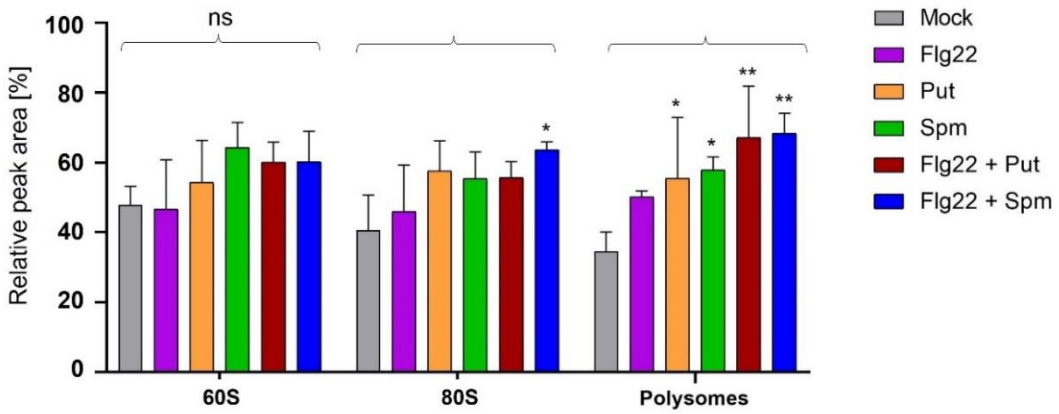

Figure S2. Quantification of polysome profiles in 100 mg of *A. thaliana* leaves collected from plants grown on soil for 5 weeks at 22ºC under 12 h light / 12 h dark cycles at 24 h of treatment (mock (H_2O), 100 µM Put, 100 µM Spm, 1 µM flg22, 1 µM flg22 + 100 µM Put, 1 µM flg22 + 100 µM Spm) as shown in **Figure 4**. The quantification process involved determining the relative areas beneath the A254 peaks corresponding to 60S, 80S, and the polysomes. The data are presented as mean ± SD, with $N = 3$ replicates. Statistical analysis was performed using a two-way ANOVA test against the mock treatment, denoted as follows: ⋆ $P \leq 0.05$, ⋆⋆ $P \leq 0.001$, ns = non-significant.

Supplementary Tables

Table S1. Summary information from whole genome sequencing of *spmi* mutants.

Mutant	Chromosome	Type	Count	Coverage	Frequency	Amino acid change
spmi - 2	1	SNV	**29**	29	100	At1g03060
spmi - 7	1	SNV	**13**	25	52	At1g03060
spmi - 8	1	SNV	**11**	26	42.31	At1g03060
spmi - 12	1	SNV	**19**	23	82.61	At1g03060
spmi - 2	1	SNV	**31**	31	100	At1g32750
spmi - 5	1	SNV	**28**	28	100	At1g32750
spmi - 7	1	SNV	**39**	39	100	At1g32750
spmi - 2	1	SNV	**36**	36	100	At1g45130
spmi - 5	1	SNV	**40**	40	100	At1g45130
spmi - 8	1	SNV	**22**	36	61.11	At1g45130
spmi - 6	1	SNV	**24**	24	100	At1g52150
spmi - 12	1	SNV	**28**	28	100	At1g52150
spmi - 19	1	SNV	**16**	30	53.33	At1g52150
spmi - 4	2	SNV	**40**	41	97.56	At2g28860
spmi - 8	2	SNV	**30**	30	100	At2g28860
spmi - 12	2	SNV	**13**	28	46.43	At2g28860
spmi - 6	2	SNV	**28**	28	100	At2g28860
spmi - 7	2	SNV	**16**	39	41.03	At2g38290
spmi - 12	2	SNV	**22**	50	44	At2g38290
spmi - 19	2	SNV	**24**	32	75	At2g38290
spmi - 4	3	SNV	**29**	46	63.04	At3g11910
spmi - 5	3	SNV	**21**	21	100	At3g11910
spmi - 7	3	SNV	**31**	31	100	At3g11910
spmi - 1	3	SNV	**10**	28	35.71	At3g43148
spmi - 1	3	SNV	**10**	28	35.71	At3g43148
spmi - 1	3	SNV	**10**	28	35.71	At3g43148
spmi - 1	3	SNV	**14**	35	40	At3g43148
spmi - 5	3	SNV	**12**	33	36.36	At3g43148
spmi - 6	3	SNV	**15**	30	50	At3g43148
spmi - 7	3	SNV	**11**	27	40.74	At3g43148
spmi - 16	3	SNV	**14**	35	40	At3g43148
spmi - 7	3	SNV	**15**	40	37.5	At3g45040
spmi - 8	3	SNV	**30**	30	100	At3g45040
spmi - 16	3	SNV	**21**	21	100	At3g45040
spmi - 1	3	SNV	**20**	27	74.07	At3g50380
spmi - 7	3	SNV	**11**	26	42.31	At3g50380
spmi - 16	3	SNV	**13**	23	56.52	At3g50380
spmi - 2	4	SNV	**31**	31	100	At4g00020
spmi - 5	4	SNV	**28**	28	100	At4g00020
spmi - 7	4	SNV	**22**	35	62.86	At4g00020
spmi - 16	4	SNV	**22**	22	100	At4g00020
spmi - 2	4	SNV	**32**	32	100	At4g00450
spmi - 5	4	SNV	**19**	19	100	At4g00450
spmi - 12	4	SNV	**30**	33	90.91	At4g00450
spmi - 16	4	SNV	**22**	22	100	At4g00450
spmi - 1	4	SNV	**14**	22	63.64	At4g09660
spmi - 8	4	SNV	**11**	27	40.74	At4g09660
spmi - 12	4	SNV	**14**	40	35	At4g09660
spmi - 1	4	SNV	**16**	29	55.17	At4g16340
spmi - 12	4	SNV	**25**	29	86.21	At4g16340
spmi - 16	4	SNV	**19**	19	100	At4g16340
spmi - 2	4	SNV	**10**	18	55.56	At4g27430
spmi - 7	4	SNV	**31**	31	100	At4g27430
spmi - 8	4	SNV	**15**	25	60	At4g27430
spmi - 2	4	SNV	**13**	29	44.83	At4g32700
spmi - 5	4	SNV	**25**	25	100	At4g32700
spmi - 6	4	SNV	**10**	28	35.71	At4g32700
spmi - 7	4	SNV	**32**	32	100	At4g32700
spmi - 12	4	SNV	**14**	34	41.18	At4g32700
spmi - 4	4	SNV	**42**	42	100	At4g35870
spmi - 5	4	SNV	**23**	23	100	At4g35870
spmi - 7	4	SNV	**27**	27	100	At4g35870
spmi - 2	5	SNV	**29**	29	100	At5g01050
spmi - 5	5	SNV	**33**	33	100	At5g01050
spmi - 12	5	SNV	**34**	34	100	At5g01050
spmi - 6	5	SNV	**13**	27	48.15	At5g28090
spmi - 16	5	SNV	**25**	25	100	At5g28090
spmi - 19	5	SNV	**19**	34	55.88	At5g28090
spmi - 1	5	SNV	**16**	33	48.48	At5g50170
spmi - 5	5	SNV	**21**	21	100	At5g50170
spmi - 7	5	SNV	**13**	36	36.11	At5g50170
spmi - 12	5	SNV	**16**	31	51.61	At5g50170
spmi - 5	5	SNV	**26**	26	100	At5g51200
spmi - 7	5	SNV	**18**	41	43.9	At5g51200
spmi - 8	5	SNV	**14**	28	50	At5g51200
spmi - 16	5	SNV	**21**	21	100	At5g51200

Table S2. List of primers used in this study for qRT-PCR analyses.

Primer name	Gene ID	Primer sequence
ACTIN2-F	At3g18780	5′-GATTCAGATGCCCAGAAGTCTTGT-3′
ACTIN2-R	At3g18780	5′-TGGATTCCAGCAGCTTCC-3′
bHLH100-F	At2g41240	5′-CTCCCACCAATCAAACGAAGAAG-3′
bHLH100-R	At2g41240	5′-TGTTTTGGTCGGTGTAAACGAG-3′
bHLH38-F	At3g56970	5′-ACGGTGCCGGAGATAACCTA-3′
bHLH38-R	At3g56970	5′-GTCGGTCACGTTCACTAGCA-3′
bHLH39-F	At3g56980	5′-CCGTTCATGTCTTCCTGCCT-3′
bHLH39-R	At3g56980	5′-GCCTTTGGTGGCTGCTTAAC-3′
CYP82C4-F	At4g31940	5′-CCTTACATGGGCCATTTCTC-3′
CYP82C4-R	At4g31940	5′-TCCTCGACGTTCCTGTCTCT-3′
F6'H1-F	At3g13610	5′-TGATATCTGCAGGAATGAAACG-3′
F6'H1-R	At3g13610	5′-GGGTAGTAGTTAAGGTTGACTC-3′
IMA2-F	At1g47395	5′-CGTTGCTAACTTGGTCATC-3′
IMA2-R	At1g47395	5′-AACACATGTCGCTCGAGAG-3′
IMA3-F	At2g30766	5′-GCTGAAGTTGTAGATCGTGC-3′
IMA3-R	At2g30766	5′-AGCTAGTCTCTCAACACTCG-3′

Table S3. List of *A. thaliana* accessions obtained from the Nottingham Arabidopsis Stock Center tested in this study to identify possible gene candidates responsible for Spm resistance and resulting no selected.

Nascode	Stock number	Locus as identified by SALK	Nascode	Stock number	Locus as identified by SALK	Nascode	Stock number	Locus as identified by SALK
652982	SALK_000441C	At5g43720	654856	SALK_119851C	At1g09480	657827	SALK_136526C	At2g31945
652988	SALK_002106C	At5g04930	654907	SALK_134114C	At1g24170	657888	SALK_022107C	At4g34680
652990	SALK_002483C	At4g25170	654919	SALK_137779C	At2g26980	657893	SALK_023296C	At3g28200
652995	SALK_003691C	At3g62830	654961	SALK_151571C	At2g19810	657918	SALK_041685C	At3g28890
652996	SALK_003891C	At1g54350	654978	SALK_004831C	At1g65845	657923	SALK_045608C	At5g43840
652998	SALK_004728C	At1g63050	655044	SALK_040805C	At5g24140	657928	SALK_048014C	At5g18130
653006	SALK_007197C	At3g49400	655103	SALK_078407C	At5g11210	658179	SALK_033785C	At4g34940
653007	SALK_007222C	At5g23020	655122	SALK_091124C	At3g07340	658190	SALK_037647C	At2g13960
653008	SALK_007247C	At1g20810	655181	SALK_134307C	At1g19320	658324	SALK_088182C	At5g14780
653009	SALK_007292C	At5g12920	655195	SALK_147451C	At3g46900	658374	SALK_114617C	At3g62280
653011	SALK_008037C	At1g04190	655209	SALK_000586C	At3g06880	658446	SALK_143445C	At3g51470
653015	SALK_008995C	At5g53930	655222	SALK_003079C	At4g01580	658486	SALK_078537C	At1g30360
653019	SALK_009706C	At5g08090	655229	SALK_003830C	At4g11910	658542	SALK_020112C	At1g68460
653021	SALK_009792C	At1g08080	655293	SALK_014839C	At1g02205	658597	SALK_030329C	At1g08250
653022	SALK_010330C	At3g50920	655339	SALK_021426C	At3g10720	658610	SALK_033902C	At1g13700
653024	SALK_010957C	At1g03890	655405	SALK_029626C	At1g25560	658624	SALK_038308C	At1g30520
653025	SALK_011296C	At3g06080	655442	SALK_037727C	At1g02340	658665	SALK_047922C	At3g17790
653027	SALK_011495C	At1g11130	655443	SALK_038088C	At3g12110	658997	SALK_114279C	At4g33260
653030	SALK_011908C	At1g03130	655461	SALK_040058C	At4g34135	659019	SALK_036380C	At4g01910
653046	SALK_015333C	At3g07470	655479	SALK_044730C	At1g14540	659025	SALK_139461C	At4g03540
653052	SALK_016312C	At4g14930	655542	SALK_057541C	At4g02130	659086	SALK_152044C	At2g29680
653061	SALK_018362C	At1g64530	655552	SALK_059044C	At1g72620	659210	SALK_109217C	At2g39330
653072	SALK_020125C	At3g02065	655606	SALK_072009C	At4g26080	659216	SALK_025338C	At2g40130
653077	SALK_020722C	At4g11240	655701	SALK_087921C	At4g21120	659303	SALK_010311C	At2g45210
653079	SALK_020839C	At1g15300	655724	SALK_091800C	At5g64550	659659	SALK_010277C	At2g37510
653086	SALK_022044C	At1g66960	655741	SALK_093534C	At2g40370	659733	SALK_024133C	At1g09080
653088	SALK_022312C	At3g11570	655742	SALK_093582C	At3g03870	659759	SALK_027248C	At3g56330
653090	SALK_022411C	At5g20540	655754	SALK_095643C	At1g32240	659778	SALK_029983C	At1g52565
653127	SALK_033434C	At4g27260	655888	SALK_120841C	At2g44580	659794	SALK_034700C	At5g28400
653138	SALK_035336C	At5g20250	655911	SALK_123643C	At5g64120	659877	SALK_053147C	At4g04510
653179	SALK_046877C	At4g28780	655989	SALK_137213C	At2g28200	659951	SALK_066703C	At3g51220
653202	SALK_051892C	At2g38080	656008	SALK_140204C	At1g05260	659952	SALK_066737C	At2g37025
653212	SALK_054337C	At1g53730	656019	SALK_141414C	At5g50915	660008	SALK_086630C	At3g50400
653213	SALK_054409C	At1g03457	656038	SALK_144487C	At2g38380	660064	SALK_101897C	At3g27510
653239	SALK_059815C	At4g32790	656084	SALK_152435C	At1g26790	660145	SALK_122700C	At3g50140
653275	SALK_067950C	At5g40450	656125	SALK_005724C	At1g29670	660146	SALK_122828C	At2g24240
653304	SALK_076651C	At1g52040	656144	SALK_008867C	At4g27440	660180	SALK_129915C	At5g48450
653369	SALK_092758C	At3g04030	656243	SALK_020482C	At5g01600	660187	SALK_131680C	At5g51850
653372	SALK_093385C	At3g52500	656245	SALK_020671C	At4g26670	660209	SALK_138430C	At5g46050
653435	SALK_111997C	At1g20850	656258	SALK_021999C	At4g39780	660266	SALK_151976C	At3g23250
653453	SALK_120599C	At1g24030	656322	SALK_028578C	At4g01950	660369	SALK_032836C	At3g25510
653462	SALK_123101C	At1g78670	656344	SALK_032946C	At1g03020	660409	SALK_045957C	At1g77000
653527	SALK_143928C	At2g29460	656365	SALK_036137C	At5g54190	660421	SALK_049763C	At5g27060
653529	SALK_144757C	At1g56240	656389	SALK_038952C	At5g65730	660432	SALK_054554C	At4g19690
653545	SALK_149747C	At1g17745	656408	SALK_042049C	At4g03270	660448	SALK_061428C	At3g26125
653556	SALK_152677C	At1g60190	656441	SALK_045370C	At5g67480	660487	SALK_076666C	At1g01520
653734	SALK_048968C	At4g01575	656472	SALK_048898C	At5g41040	660636	SALK_144144C	At1g78860
653819	SALK_021217C	At3g47640	656495	SALK_052951C	At2g46780	660656	SALK_149333C	At1g69040
653845	SALK_067751C	At1g30860	656498	SALK_053270C	At3g27200	660719	SALK_014743C	At3g60320
653859	SALK_008680C	At1g09230	656624	SALK_070770C	At1g64080	660759	SALK_022456C	At3g22970
653877	SALK_010192C	At1g48100	656626	SALK_070867C	At5g66630	660887	SALK_057463C	At1g53860
653906	SALK_025730C	At2g22470	656668	SALK_078808C	At3g48240	660921	SALK_065216C	At2g42170
653909	SALK_014557C	At2g41330	656678	SALK_080840C	At4g22010	660984	SALK_082545C	At1g19490
654009	SALK_026233C	At4g30850	656734	SALK_088500C	At1g23060	661012	SALK_090239C	At3g62090
654014	SALK_025682C	At1g51890	656775	SALK_094400C	At4g13340	661018	SALK_091887C	At5g47370
654015	SALK_140374C	At1g51940	656803	SALK_099500C	At1g14080	661033	SALK_097544C	At5g15500
654065	SALK_011077C	At5g15800	656818	SALK_102161C	At3g21080	661045	SALK_099662C	At4g02540
654076	SALK_015497C	At1g23480	656877	SALK_113143C	At1g61100	661153	SALK_132499C	At1g35140
654110	SALK_026798C	At4g16141	656917	SALK_120416C	At1g17060	661174	SALK_139786C	At2g22200
654116	SALK_028120C	At3g04140	656920	SALK_121097C	At2g44910	661186	SALK_143654C	At3g50650
654143	SALK_036551C	At5g46220	656950	SALK_125269C	At1g52000	661225	SALK_152540C	At1g50040
654181	SALK_046841C	At3g18660	657062	SALK_142672C	At5g59220	661305	SALK_003066C	At3g53460
654182	SALK_047015C	At2g32880	657200	SALK_046002C	At2g39870	661327	SALK_004337C	At1g11210
654245	SALK_069675C	At2g23690	657248	SALK_085727C	At4g12470	661363	SALK_006260C	At1g69310
654277	SALK_080024C	At5g62920	657290	SALK_125259C	At3g63450	661415	SALK_008594C	At4g02100
654280	SALK_082408C	At5g04770	657311	SALK_138692C	At3g47690	661513	SALK_012363C	At5g05840
654311	SALK_094838C	At1g05210	657413	SALK_090249C	At3g19680	661978	SALK_029403C	At1g48260
654355	SALK_110128C	At1g04770	657421	SALK_096499C	At2g16660	662312	SALK_045606C	At5g22920
654359	SALK_113348C	At4g39950	657422	SALK_098383C	At3g63380	662523	SALK_055373C	At3g50060
654417	SALK_135734C	At1g56010	657423	SALK_100838C	At4g36850	662681	SALK_061748C	At3g14200
654421	SALK_136393C	At5g54130	657474	SALK_003090C	At1g66400	662726	SALK_063746C	At5g03260
654452	SALK_149265C	At1g79160	657489	SALK_008497C	At1g80440	662926	SALK_072162C	At2g46530
654471	SALK_003421C	At3g56260	657530	SALK_019075C	At5g64190	663032	SALK_077717C	At4g16670
654573	SALK_029271C	At5g25110	657552	SALK_024228C	At2g46310	663085	SALK_080212C	At1g08340
654605	SALK_038930C	At1g55760	657571	SALK_030307C	At3g13000	663261	SALK_089158C	At5g50335
654675	SALK_059835C	At4g17460	657668	SALK_070180C	At3g56000	663388	SALK_094496C	At4g21230
654681	SALK_061645C	At1g23460	657695	SALK_079963C	At2g31360	663599	SALK_107203C	At4g27860
654771	SALK_089131C	At1g27020	657700	SALK_081488C	At1g70260	663882	SALK_123221C	At1g02470
654835	SALK_109611C	At5g56840	657733	SALK_094765C	At1g64950	664360	SALK_152055C	At3g61060
654848	SALK_117173C	At5g64230						

Table S4. Differentially expressed genes (fold change >2 or fold change < -2) in seedlings treated with 400 μM Spm compared to untreated seedlings. The table includes the gene name, the gene identifier (TAIR), fold change and *P* value.

Name	Gene ID	Fold change	FDR *P* value	Function
CYP71A13	AT2G30770	881.95	3.00E-02	Camalexin biosynthesis
PCR1	AT1G14880	592.85	8.06E-06	Plant cadmiun resistance
AT1G17820	AT1G17820	328.44	3.32E-04	Phosphate homeostasis
TAT3	AT2G24850	134.02	1.69E-04	Tyrosine aminotransferase
AT2G14247	AT2G14247	74.45	4.33E-36	Expressed protein
BHLH100	AT2G41240	50.62	6.54E-29	Fe deficiency responses
AT1G13608	AT1G13608	49.76	4.00E-02	Fe deficiency responses
NATA1	AT2G39030	40.74	0.04	Ornithine N-delta-acetyltransferase
WAK3	AT1G21240	39.7	1.27E-03	Cell wall-associated receptor kinase
ORG2/BHLH38	AT3G56970	29.64	7.67E-28	Transcription factor Fe deficiency responses
AT3G02400	AT3G02400	22.02	1.00E-02	Negative regulation of PEX11b.
IMA1	AT1G47400	20.65	2.33E-07	Fe deficiency responses
AT3G48640	AT3G48640	19.54	1.00E-02	Transmembrane protein
IPSP	AT5G04120	18.25	2.00E-02	Metal-independent phosphoserine phosphatase
IMA3	AT2G30766	15.58	1.25E-17	Fe deficiency responses
IMA6	AT1G07373	14.14	4.00E-02	Fe deficiency responses
IMA2	AT1G47395	13.5	8.19E-13	Fe deficiency responses
CWLP	AT3G22120	12.11	2.78E-03	Cell wall-plasma membrane linker protein
AT1G23110	AT1G23110	9.36	0.04	Fold protein
GGPPS1	AT4G36810	8.94	3.10E-03	Isoprenoid biosynthesis
IPS1_1	AT3G09922	8.62	4.00E-02	Induced by phosphate starvation
PPA3	AT2G46860	8.29	0.02	Pyrophosphorylase
AT2G27420	AT2G27420	7.98	8.22E-03	Protein degradation
ACD6	AT4G14400	7.84	3.94E-03	Defense response
AT4G22214	AT4G22214	7.17	0.02	Defense response
ROPGEF12	AT1G79860	6.57	0.01	Kinase
ORG3/BHLH39	AT3G56980	6.54	2.65E-13	Transcription factor Fe deficiency responses
AOX3	AT1G32350	6.3	2.87E-03	Alternative oxidase
ATGGPS8	AT3G20160	6.29	4.00E-02	Isoprenoid biosynthesis
ABCG40	AT1G15520	5.92	4.00E-02	ABC transporter
BHLH101	AT5G04150	5.37	1.96E-09	Fe deficiency responses
CYP82C4	AT4G31940	5	3.00E-02	Fe deficiency responses
PER24	AT2G39040	4.97	2.87E-03	Peroxidase
ATPEPC1	AT1G17710	4.84	0.02	Phosphate homeostasis
PS2_1	AT1G73010	4.77	1.32E-03	Phosphate homeostasis
AT2G27402	AT2G27402	4.62	1.00E-02	Plastid transcriptionally active protein
LLP	AT5G03350	4.56	0.03	Defense response
CSLG2	AT4G24000	4.55	4.00E-02	Cell wall cellulose synthase
AT5G05250	AT5G05250	4.26	2.21E-08	Hypothetical protein
JAL41	AT5G35940	3.92	5.00E-02	Mannose-binding lectin
CHI	AT2G43570	3.84	2.78E-03	Putative basic chitinase
EXT9	AT5G06630	3.8	0.02	Proline-rich extensin-like protein
AT3G59370	AT3G59370	3.76	0.02	Vacuolar calcium-binding protein-like protein
JAL8	AT1G52050	3.69	0.03	Mannose-binding lectin
AT5G54370	AT5G54370	3.54	3.94E-04	Late embryogenesis abundant
JAL10	AT1G52070	3.46	8.37E-03	Mannose-binding lectin
MSRB7	AT4G21830	3.44	5.52E-04	Methionine sulfoxide reductase
FRO2	AT1G01580	3.41	3.22E-05	Fe deficiency responses
MAM3	AT5G23020	3.15	2.78E-03	Biosynthesis of aliphatic glucosinolates
TGG4	AT1G47600	3.14	2.33E-03	Glucosinolate profile change
SAG13	AT2G29350	3.08	0.01	Defense response
RAP2-6	AT1G43160	3.08	5.00E-02	Ethylene response
RUBY	AT1G19900	3.06	5.00E-02	Cell wall modification
SQP2	AT5G24140	2.96	1.00E-02	Squalene monooxygenase
MDAR3	AT3G09940	2.94	5.52E-04	Fungal interaction
AT4G12520	AT4G12520	2.93	3.39E-03	Lipid-transfer protein / seed storage
AT4G29690	AT4G29690	2.71	4.00E-02	Alkaline-phosphatase
PER2_2	AT1G05250	2.65	5.00E-02	Lignification of cell wall
IRT1	AT4G19690	2.56	1.00E-02	Fe deficiency responses
TPS30	AT3G32030	2.56	0.02	Terpenoid synthesis
CEP2_2	AT3G48340	2.51	2.00E-02	Lateral root growth
MSL4	AT1G53470	2.43	4.00E-02	Mechanosensitive ion channel

BGLU21	AT1G66270	2.4	3.00E-02	Response to cold, auxin and methyl jasmonate treatments.
PAP14_2	AT5G53450	2.25	9.72E-07	Response to osmotic stress
ATPS3	AT3G47420	2.13	3.75E-03	Phosphate starvation
BGLU22	AT1G66280	2.12	1.08E-03	Beta-glucosidase
BTS	AT3G18290	2.09	2.52E-05	Fe deficiency responses
ACO5	AT1G77330	2.05	3.00E-02	Oxidase
PER33	AT3G49110	-2.2	9.72E-04	Involved in cell elongation
FLR1	AT3G12145	-2.33	1.18E-03	Floral transition at the meristem
NEET	AT5G51720	-2.36	3.39E-03	Plant development
AZI1	AT4G12470	-2.48	0.02	Involved in azelaic acid signal
F-ATMBP	AT1G52030	-2.7	2.00E-02	Involved in metabolizing glucosinolates
ZAT10	AT1G27730	-2.99	0.02	Salt tolerance
ATEXT4	AT1G76930	-3.02	8.19E-13	Enforce cell wall strength
PDF2.1	AT2G02120	-4.62	1.47E-05	Ammonium metabolism
PGLR	AT5G14650	-4.96	6.29E-04	Cell wall localized endo-polygalacturonase
PER15	AT2G18150	-5.18	4.00E-02	Peroxidase
RGF6	AT4G16515	-5.82	8.22E-03	Maintenance of the root stem cell
PER49	AT4G36430	-6.43	3.81E-06	Peroxidase
AT4G07820	AT4G07820	-6.99	3.94E-04	CAP protein
MYB15	AT3G23250	-7.39	0.02	Regulator of lignin biosynthesis
PI	AT5G20240	-8.25	3.84E-32	Required for the specification of petal and stamen identities.
AT1G78720	AT1G78720	-9.23	8.22E-03	SecY protein transport
PAR1	AT5G52390	-10.21	3.53E-04	PAR protein
HSP14.7	AT5G47600	-14.46	4.00E-02	Chaperone
AT5G22430	AT5G22430	-133.59	6.47E-03	Pollen allergen and extensin protein
ERF105	AT5G51190	-1015.5	0.02	Ethylene response
AT1G25055	AT1G25055	-1159.54	3.00E-02	F-box protein

Supplementary Information

Supplementary information can be found at:

https://drive.google.com/drive/folders/1hcOWCF5JAboNEFhXr_yIcObLmnj72smR?usp=sharing